MASS TRANSFER, CREEP AND STRESS DEVELOPMENT DURING THE DRYING OF RED OAK

by
Robert W. Rice

Dissertation submitted to the Faculty of the
Virginia Polytechnic Institute and State University
in partial fulfillment of the requirements for the degree of

DOCTOR OF PHILOSOPHY

in

Wood Science and Forest Products

APPROVED:

R. L. Youngs, Chairman

C. Skaar

F. M. Lamb

J. R. Loferski

W. C. Thomas

August, 1988

Blacksburg, Virginia

MASS TRANSFER, CREEP AND STRESS DEVELOPMENT
DURING THE DRYING OF RED OAK

by

Robert William Rice

Committee Co-Chairmen: R. L. Youngs and C. Skaar
Wood Science and Forest Products

(ABSTRACT)

The purpose of this research was to measure and simulate the major perpendicular to grain strain components and associated stresses which develop as the result of mass transfer and restraint of shrinkage in red oak. Particular emphasis was placed on the rheological or creep components of strain.

Mass transfer was measured during the first four days of drying under increasingly severe conditions. The resulting moisture gradient profiles were parabolic in shape under nearly all drying conditions. The pattern developed quickly and was modeled with reasonable accuracy using Fick's second law.

Three major strain components occur in drying. These are termed elastic strain, visco-elastic creep and "set" or mechano-sorptive creep. The magnitude and variation of each of these components was measured during the first four days of drying under increasingly severe conditions.

Using a slicing technique to cut very thin wafers of wood parallel to the surface, the elastic strain was shown to be quite small. The experiments led to the conclusion that the maximum stress develops within a few cell thicknesses of the surface.

Much of the experimental work centered on the measurement of the

rheological or creep components of strain. The magnitude of the visco-elastic creep was found to be about the same order of magnitude as the elastic strain and was clearly a function of the applied stress. The major strain component during drying was shown to be mechano-sorptive creep. This type of creep occurs in a number of polymeric materials undergoing diluent movement or temperature change. The maximum magnitude of the mechano-sorptive component was about 30 times larger than the maximum elastic strain. Mechno-sorptive creep was shown to be directly related to moisture loss and, to a lesser extent, a function of applied load.

Using relationships derived from the experimental data, a computerized simulation was developed to predict the development of stress and the probability of checking early in drying. The simulation makes use of data on elastic strain, mechano-sorptive creep and the elastic modulus. The concept worked well in this study, but its application is limited by the lack of strain data for the surface layers representing the outer few cell thicknesses where stress is greatest early in drying.

As an adjunct, acoustic response tests were performed on green samples stressed perpendicular to grain in flexure under third point loading conditions. The evidence indicates that the onset of surface failure can be predicted prior to the appearance of macroscopic checking. The acoustic response pattern is typical of that which occurs in brittle glassy polymers such as polystyrene.

ACKNOWLEDGEMENTS

I would like to begin by acknowledging the assistance and guidance provided by the members of my advisory committee whose names are listed on the title page of this dissertation. Each member in some way contributed to the planning, development, execution or analysis which comprised the phases of the project. A special debt of gratitude is owed to project co-chairman ; from whom advice and guidance were frequently sought and unfailingly given. Most importantly, I would like to acknowledge the help of my wife, , without her support and encouragement I would not have completed the project. Finally, many members of the University staff were generous and cooperative in providing advice and assistance as the work progressed. The assistance and encouragement of all these persons is gratefully acknowledged.

Table of Contents

List of Figures

List of Tables

INTRODUCTION

In terms of time and energy use, drying is the single most costly step in the manufacture of lumber. Because of this, a reduction in the drying time or an increase in the quality of the dried lumber offers the greatest potential for economic benefit. Unfortunately, a reduction in drying time often results in an increase of drying related defects such as surface checks, splits, and warp. Most of these defects are caused by drying stresses which develop from moisture gradients and restrained shrinkage within the wood.

The problem of drying degrade is particularly acute in the oaks (Quercus sp.) which are the species most used in the furniture and flooring industries. King (1975), found that 55 percent of the losses which occur in air dried red and white oaks in the Tennessee Valley are the result of drying degrade. Cuppett (1966), in a study of air drying losses, found that nearly 15 percent of red oak volume was lost to degrade during drying and nearly 80 percent of the total losses were due to checking and splitting. Finally, Gammon (1971), in an extensive study, found that 14 percent of the red oak lumber produced in eastern hardwood sawmills underwent a grade lowering during drying. The cause of the grade lowering in most cases was attributed to drying degrade.

In an effort to minimize drying related defects the kiln drying of wood is done according to "schedules" which consist of a series of increasingly severe temperature and relative humidity settings. Small sample boards are placed within the stack of lumber prior to the commencement of drying. The average moisture content of these boards is monitored during drying and serves as the basis for adjusting the sever-

ity of the drying conditions. Drying lumber using the established schedules is quite time consuming but if done properly the resulting lumber is usually uniformly dry with a fairly high level of quality.

It has been recognized for many years that a key to improved drying quality and a reduction of drying time lies in understanding and controlling internal stress development (Tiemann, 1919). However, despite decades of drying schedule refinement and computerized drying simulation, the basic relationships and interrelationships between the various drying parameters and stress development are not clear. Without a greater and more quantitative understanding of the nature of the moisture loss/stress development interaction further progress is limited. The current research has been undertaken in an attempt to characterize and simulate some of these relationships during the critical early stages of drying red oak lumber when surface checking begins.

Several experiments measuring elastic drying stresses and computerized drying simulations based on stress development have been reported. However, the reports contain very little basic information about the variation of drying conditions and internal stress development. In particular, almost no information was available regarding the perpendicular to grain rheological components of drying wood. As discussed in detail below, the rheological components represent the conformance of the wood to the internally developed stress. As such, their importance is that they function to reduce stress. A better understanding of them may lead to methods or procedures which will reduce drying degrade and/or drying time.

In view of the above, a hypothesis was developed to investigate the

relationship of the moisture gradients to the strain components. Specifically, the hypothesis stated that the potential for surface check occurrence in red oak under a defined set of drying conditions could be predicted using relationships among the strength, moisture gradient profile and strain characteristics of the material.

The paucity of available information required that the project be centered on the measurement of the basic moisture gradient and stress relationships which develop during drying. Particular emphasis was placed on rheological components of strain. The drying period chosen for study was the initial stage of drying where most degrade occurs. Following commercial drying practice, temperatures were kept at 110° F for all experiments.

An experimental design was developed (see Methods and Materials section) to measure the major moisture gradient and strain components during the chosen drying period. The variation of these components under different drying conditions was determined by changing the ambient relative humidity. Using data from these experiments a number of fundamental relationships between drying parameters and stress/strain development were determined.

After completing the experimental investigations, a computerized simulation was developed based on the experimental findings. The intent of the simulation is to predict stress and the liklihood of surface failure during the first four days of drying red oak.

As an adjunct to the project, acoustic response tests of green red oak during testing to failure perpendicular to the grain were performed. The purpose of these tests was to determine some of the acoustic charac-

teristics associated with surface failure during the drying of wood. The control of kiln drying using acoustic emissions appears to hold considerable promise and is an area of active research.

BACKGROUND

// The stresses which develop as a result of moisture gradients and restrained shrinkage are the result of several related mass transfer, rheological and strength factors as well as a variety of mechanisms.// Although each of the major factors and mechanisms will be discussed separately, a brief introduction will be given to acquaint the reader with the general concepts of stress development during drying.

A basic outline of how stresses develop during mass transfer has been described by McMillen (1955). McMillen limited his studies to strains which developed in the tangential direction based on the observation that nearly all drying related checking occurs on the tangential surfaces. Later studies by Youngs and Norris (1958), and Sales (1984) confirmed that the influence of radial and shear stresses on checking is minimal. Therefore, the following discussion refers only to stresses and strains developed perpendicular to the grain in the tangential direction.

Visualize the cross-section of a piece of wood during the first two days of drying (Fig. 1). \\ The outer surfaces of the wood rapidly begin to lose moisture and the surface fibers are approaching the equilibrium moisture content, which is assumed to be well below fiber saturation. Therefore, the fibers attempt to shrink. However, their shrinkage is restrained by the underlying wood which is at a higher moisture content and does not yet have the same shrinkage potential as the drier fibers nearer the surface. As a result of the moisture gradient and attendant differential shrinkage, the outer fibers are under a tensile stress.

Meanwhile, as a reaction, the inner fibers are undergoing compressive stresses.

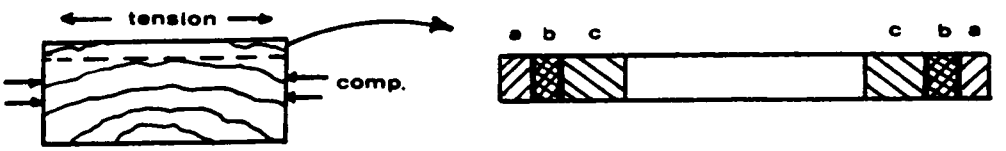

Figure 1. The major strain components early in drying as illustrated by a wafer sliced from the surface. Left: As drying proceeds, the surface undergoes tensile strain and the interior compressive strain. Right: The major components of strain (a) elastic, (b) visco-elastic creep, (c) mechano-sorptive creep. Observed shrinkage is not shown.

The tensile stress at the surface results in multiple strain components (Fig. 1.). The first is an elastic strain which is represented by the distance marked (a) in the figure. The second element is an elastic time dependent component termed visco-elastic creep and marked (b) in the figure (Leicester, 1971; Kawai, 1979). A third component, marked (c), is a stress relieving plastic deformation which is a function of stress and moisture change as the wood dries from the green condition. This component, variously termed casehardening (Roth, 1895), set (Tiem-

ann, 1919), plastic flow or mechano-sorptive creep (Grossman, 1976) causes the outer zone to maintain a dimension which is closer than expected to the green dimension after drying.

Although drying-related defects may occur at any time during the drying process, most happen during the early stages of drying (Vanek, 1987, Stamm, 1964). At this time the moisture gradient is quite steep and the stress relief due to plastic flow is small.

Each of the major factors leading to the moisture gradients and strains outlined above will now be discussed in detail.

A. Moisture Movement Within Wood

The major mechanisms responsible for the movement of moisture within wood are capillary flow and diffusion (Stamm, 1964). Capillary flow, which occurs primarily above fiber saturation, is responsible for the movement of liquid water from the cell lumens toward the surfaces of the wood. Diffusion is the movement of bound water and water vapor and occurs as the result of moisture concentration or related potential gradient within the wood (Siau, 1984). The differences in the moisture gradients produced by the two types of moisture movement are highlighted in Figure 2 taken from Hawley (1931). The figure on the left shows the moisture gradient pattern of a piece of wood in which drying has occurred only by diffusion above and below fiber saturation. The figure on the right shows the gradient when appreciable amounts of capillary flow occur above fiber saturation. The curve shape on the right approaches a parabola and is typical of the drying of wood (Stamm, 1946).

A number of models have been developed to explain the movement of

moisture above fiber saturation (Hart, 1965; Stevens, 1972; Wiley and Choong, 1975). Most of these models are derived from an article by Hawley (1931) who explained bulk moisture transport in terms of the effects of capillary action and the expansion of entrapped bubbles under the action of a total pressure gradient.

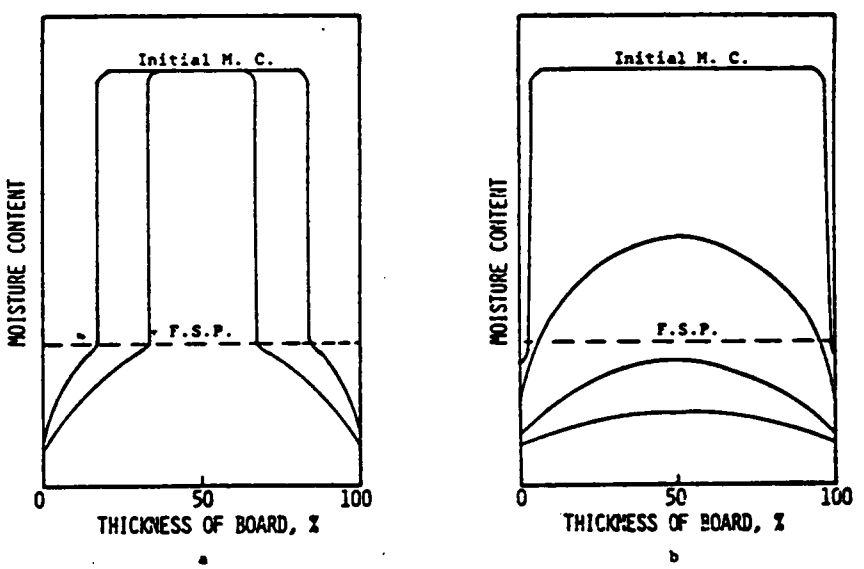

Figure 2. Extreme examples of moisture movement as discussed by Hawley (1931). A. Pure Diffusion B. Appreciable Free Water Flow (Adapted from Stevens, 1972).

Hawley's concepts were expanded in a model developed by C. Skaar (Figure 3) (Siau, 1984). The model consists of an exposed surface and a number of cells which are completely filled with water except for two bubbles having different radii and containing air and water vapor. It is assumed that drying takes place only from the upper surface of the

wood which is shown as a broken line in part (A) of the figure. As capillary water evaporates from the exposed cells into the air, menisci form on the air-water interface. Due to the relatively large radii, the capillary tension is small at this stage of the drying process. When the surface cells are empty, the evaporating surfaces recede towards the pit openings (Fig. 3B). The evaporating radii are then smaller and approach the radius of the large bubble. As the radii become smaller, the capillary tension in the cell system increases causing the pressure to drop and the bubbles to expand. Expansion occurs first in the large bubble since it is weaker than the small bubble and the bubble expands forcing the cell to empty (Fig. 3C). The models of Hart (1968), Stevens (1972), and Wiley (1975) attempt to introduce a more quantitative analysis of the changes in the bubble volumes, cell shapes and pressures during drying.

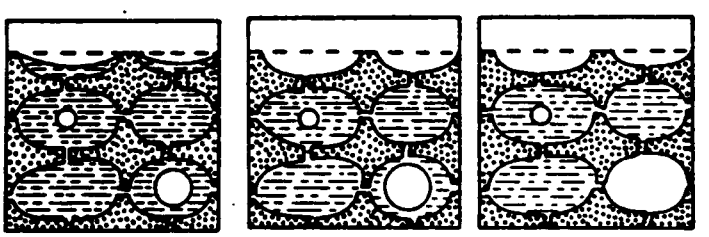

Figure 3. Diagram illustrating the mechanism of moisture movement above fiber saturation. See text for explanation. Taken from Siau (1984).

Below fiber saturation the movement of moisture is governed by the process of diffusion (Stamm, 1964). Diffusion is variously defined as molecular mass flow which results from the action of a moisture concentration (Siau, 1985), vapor pressure (Bramhall, 1976) or a density gradient (Wannier, 1966). Each of these driving "forces" relates directly to the partial pressure of the vapor. A variety of vapor pressure related units have been used to determine diffusion based mass transfer (Wengert, 1977).

Many equations have been developed to model the drying of capillary-porous bodies (Fortes and Okos, 1980). For modeling mass transfer in wood, two of the most frequently used methods result from equations developed by Luikov (1964) and Fick (1855).

Luikov (also spelled Lykov), after an extensive review of Soviet heat and mass transfer literature, developed coupled partial differential equations to describe heat and mass transfer in capillary-porous bodies. The coefficients in the equations are determined using the principles of irreversible thermodynamics and they have proven to be quite difficult to evaluate. Lewis et al. (1979) and Thomas et al. (1982), have applied Luikov's equations to the drying of wood with some success. Presently, the major obstacle to using these equations is that little information is available to determine how the coefficients vary with drying conditions.

The mainstay for the simulation of moisture movement in capillary-porous materials is a relationship known as Fick's law. In 1855, Fick postulated that diffusion could be mathematically modeled using an equation analogous to Fourier's heat conduction equation (Fick, 1855).

Fick's law for unsteady-state moisture transport is as follows:

$$\frac{\delta U}{\delta t} = \frac{\delta}{\delta x}\left[D_m \frac{\delta U}{\delta x}\right] \qquad \text{Eq. 1}$$

Where: U is the moisture concentration

t is the time

D_m is the transport or diffusion coefficient

x is the position within the drying wood.

Fick's law was first applied to the drying of wood by Tuttle (1925). Sherwood (1929) followed with a general theory of drying porous materials in which Fick's law was applied to the drying of a number of materials including hemlock slabs. Both Tuttle and Sherwood applied the law to the entire drying process both above and below fiber saturation. Although Hougen et al. (1940) later criticized the use of Fick's relationship at high moisture contents, Stamm has shown that, even though appreciable capillary flow exists, the drying of green wood often acts as if it were diffusion controlled within minutes after the commencement of drying (Stamm, 1964).

The relationship between vapor pressure and moisture movement is linear for pure solutions and the diffusion coefficient is probably constant (Hawley, 1931). However, because the water within the cell walls is chemically bound to the cell walls and to other water molecules, early researchers such as Martley (1926) recognized that pure diffusion does not occur in wood. To account for the decidedly nonlinear relationship between the flux and the moisture gradient of the wood the transport coefficient is often considered to be a function of

several variables. Generally, the functional relationship is related to moisture content, temperature and structural direction, and equations of the Arrhenius type have also been developed (Rosen, 1986; Stamm, 1964; Fortes and Okos, 1980). Skaar (1954), has analyzed a number of methods and assumptions which are used for determining Fick's transport coefficients in wood and Siau (1984) has tabulated values for the diffusion coefficient along and across the grain at different temperatures and moisture contents. In nearly all cases the magnitude of the coefficient in the tangential direction is between 10^{-4} and 10^{-8} cm^2/sec. for wood (Siau, 1984).

Two methods are commonly used to solve Fick's law. The first, giving analytical solutions based on classical Fourier analysis or Laplace transform techniques, tends to be somewhat cumbersome (Schaffner, 1981). The second method using implicit or explicit finite-difference techniques has been used frequently since the advent of digital computers (Lessard et al., 1982). The method may be described as follows (Carnahan et al., 1969):

Since the drying is symmetrical, Equation 1 is solved only for a single gradient of the drying board. The area is divided into a grid-like form as shown in Figure 4.

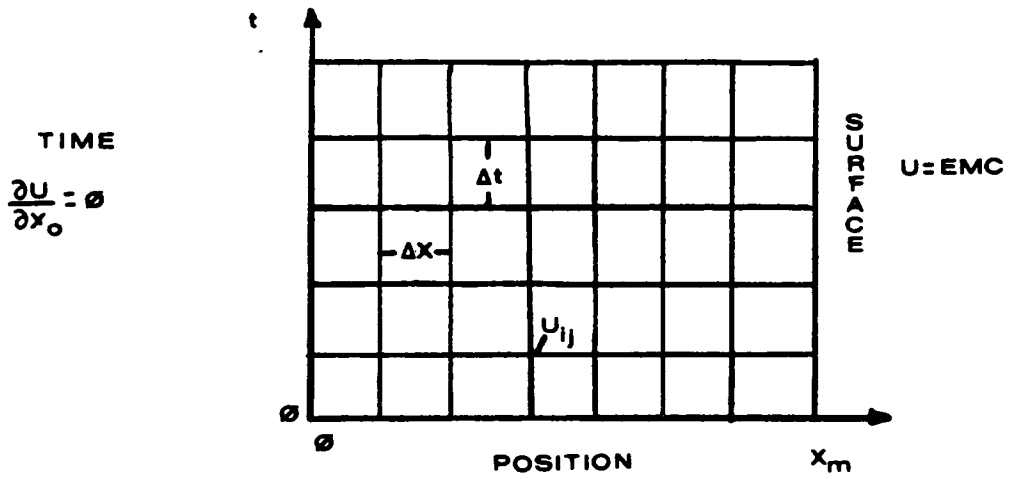

Figure 4. Grid used for the numerical solution of Fick's law. U represents the moisture content and t is time.

Using the Crank-Nicholson scheme, the derivatives may be represented as follows:

$$\frac{\delta U}{\delta t} = \frac{U'_i - U_i}{t} \qquad \text{Eq. 2}$$

Where the ' indicates the moisture content of time t + Δt. The right hand side of Equation 1 is represented using the following:

Eq. 3

$$\frac{\delta}{\delta x}\left[D_m \frac{\delta U}{\delta x}\right] = \frac{1}{2(\Delta x)^2}\left[(U'_{(i-1)} - U'_{(i)})\,\bar{D}_{(i-1,i)} + (U'_{(i+1)} - U'_{(i)})\,\bar{D}_{(i+1,i)} + (U_{(i+1)} - \bar{U}_{(i)})\,D_{(i-1,i)} + (U_{(i-1)} - U_{(i)})\,\bar{D}_{(i+1,i)}\right]$$

In this case, the D's represent the harmonic averages of the transport coefficients defined as:

$$\bar{D}_{(i-1,i)} = \frac{2D_{(i-1)} \cdot D_i}{D_{(i-1)} + \cdot D_i} = S \qquad \text{Eq. 4a}$$

And $$\bar{D}_{(i+1,i)} = \frac{2D_{(i+1)} \cdot D_i}{D_{(i+1)} + \cdot D_i} = B \qquad \text{Eq. 4b}$$

Equating Equations 2 and 3 and simplifying:

Eq. 5

$$- R \cdot S \cdot U'_{(i+1)} + U_i\,(2 + R \cdot S + R \cdot B) - R \cdot B \cdot U'_{(i+1)} = R \cdot S \cdot U_{i-1} + U_i \cdot (2 - R \cdot S - R \cdot B) + R \cdot B \cdot U_{(i+1)}$$

Where it has been assumed that D ' = D and $R = \frac{\Delta t}{2(\Delta x)^2}$

Equation 5 is for all interior nodes from 1 to M-1. For node zero, the equation becomes:

Eq. 6

$$-R \cdot U'_1 \ (S+B) + U'_o \ (2 + 2 \cdot R \cdot B) = R \cdot U_1 \ (S+B) + U_o \ (2-R \cdot S - R \cdot B)$$

Where it has been assumed that $U_{i-1} = U_{i+1}$ because of symmetry. Equations 5 and 6 are in a form where all of the values on the left are at time $t + \Delta t$. The equations form a system of the form:

$$\vec{A}\,\vec{X} = \vec{B} \qquad \text{Eq. 7}$$

Which is solved by inverting matrix A and multiplying by B to determine the moisture content values at $t + \Delta t$.

B. Stress Development During Drying

A general concept of how stresses develop inside wood as the result of moisture gradients and restrained shrinkage has been described above. A more detailed illustration of the strain components is shown in Figure 5. It is appropriate to discuss each of the strain components separately.

1. Unrestrained Shrinkage.

The inherent or unrestrained shrinkage of wood is the amount of shrinkage which would occur as a result of moisture loss in the absence of restraint or plastic flow. This situation may be approximated if the moisture gradients are minimal during drying such as in the case of thin wafers with large cross-sectional areas. Basic shrinkage (Fig. 5) is the unrestrained shrinkage which occurs if the shrinkage is deter-

mined between the green and oven-dry conditions and represents the maximum stress-free shrinkage which can occur. Unrestrained shrinkage is an important concept because deviations from the expected values indicate the development of one or more of the strain components shown in the figure.

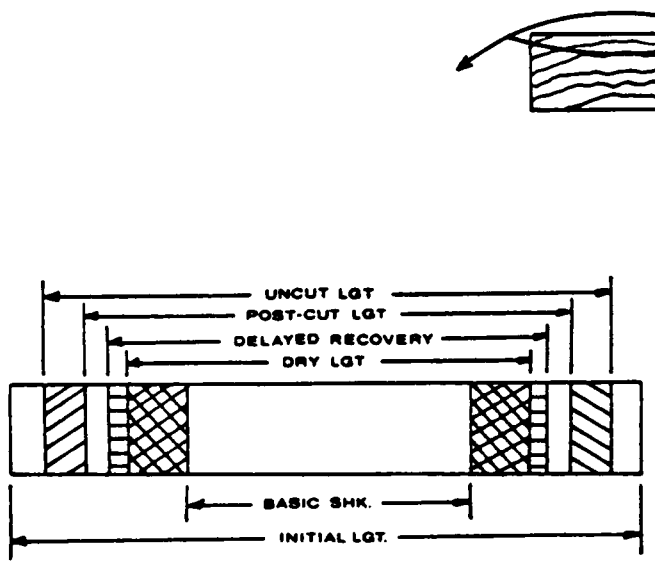

Figure 5. The components of strain which occur during drying as illustrated by a wafer cut from the surface. Basic shrinkage is the maximum shrinkage which would occur without restraint. Initial length is the green length prior to any shrinkage. Uncut length minus post-cut length is elastic strain. Post-cut length minus delayed recovery is the visco-elastic strain. Dry length minus basic shk is the mechano-sorptive strain.

The Unrestrained Fractional shrinkage of wood is expressed by the formula given by Panshin and DeZeeuw (1980):

$$shk = \frac{(\text{green lgt.}) - (\text{dry lgt.})}{\text{grn. lgt.}} \qquad \text{Eq. 7}$$

Where dry length is the length of the wood at its final moisture content. If the final moisture content is the oven-dry condition, the unrestrained shrinkage is basic shrinkage.

Shrinkage begins about the time the cell moisture content drops below fiber saturation and moisture loss begins to occur from the void spaces between the microfibrils within the cell walls. As the cell walls lose moisture, the amorphous regions of the cellulose molecules become more nearly parallel and closer together. As this occurs, the end-to-end distance of the fiber increases slightly and the thickness of the cell walls decreases (Jentzen, 1964; Stamm, 1964). Since the wood is anisotropic with respect to microfibril orientation, the shrinkage is also anisotropic, being greatest in the tangential direction (Panshin and DeZeeuw, 1980). There are a number of factors which affect unrestrained shrinkage significantly. These include the amount of wood substance present (density), the specimen geometry and the lignin content of the cell wall (Stamm, 1964). All of these items are major factors since they influence the amount of moisture which the cell walls may contain.

2. Observed shrinkage

The overall shrinkage of a board, measured across the tangential

surface, is the observed shrinkage. Unlike unrestrained shrinkage, observed shrinkage is subject to the strain components which result from moisture gradients and restraint of shrinkage. Kawai (1980) assumed the observed shrinkage of a board could be considered uniform and no appreciable "bulging" or concavity would exist when the difference in width between the center and surface of a board is measured. Weller (1987), suggests this assumption is not valid, but presents no evidence to support his contention. Regardless of the characteristics of the observed shrinkage, preliminary tests performed for this study showed that the observed shrinkage during the first four days of drying was negligible. One possible reason for this is that the average moisture content within .070 in. of the surface, for most of the test conditions, was well above fiber saturation even at the end of the four-day drying period. It is likely that any shrinkage would have been evident very near the surfaces and not readily measurable with the vernier calipers used for these tests.

3. Elastic strain

Most of the early studies regarding the development of drying stresses center on the measurement of elastic strain (McMillen, 1968; Ugolev, 1959). Elastic strain (EL-STR) may be defined as immediately recovered strain which occurs when a wafer is cut from a drying board as shown in Figure 5. Specifically, elastic strain is determined using the formula:

$$\text{EL-STR} = \frac{\text{(pre-cut lgt.)} - \text{(post-cut lgt.)}}{\text{initial lgt.}} \qquad \text{Eq. 8}$$

// If the wafer contracts when cut, the strain is assumed to be tensile and positive, whereas if the wafer elongates the strain is considered to be compressive and negative.//

The history of the method which is used to determine elastic strain begins with Tiemann (1919) who used a hypothetical slice analysis to describe drying strain developed perpendicular to the grain. Tiemann was followed by Peck (1940) who was the first to describe the development of stresses throughout the drying processes using what was to become the "slicing technique". Using one-inch thick quartersawn white pine boards, Peck marked the cross sections into six slices oriented parallel to the radial faces of the board. The slice lengths were measured before and after cutting and the difference in the lengths was taken to be a measure of the elastic strain. By repeating the process at various stages during drying, elastic strain development could be monitored. Subsequently, Peck applied the technique to an analysis of drying stresses in 8/4 magnolia and then 8/4 blackgum sapwood (1940).

Later, a more comprehensive study of this type was done using sweetgum heartwood by Loughborough and Smith (1946). Using the information from these strain tests, Reitz (1950) developed a new set of guidelines for the drying of wood and Torgeson (1951) published a series of schedules based on stress and strain development during drying.

Perhaps the most comprehensive studies of elastic strain development using the wafer slicing technique were done using red oak and then pine by McMillen (1955, 1956, 1968). McMillen studied the effects of drying time, temperature and relative humidity on strain development throughout the drying process using the slicing technique and slices which were

approximately .2 inches thick.

Other studies of elastic strain using the slicing technique during drying include the work of Ugolev (1959) who developed a finite element based elastic model of drying strain and Cech (1964) who studied stress development during the high temperature drying of pine.

All of the investigators cited above have concluded that "elastic tensile strain perpendicular to the grain occurs at the surface early in drying and that its magnitude is related to the moisture gradient in some way. As the surfaces develop tensile strains, the interior slices gradually begin to develop compressive strains. Although affected by temperature and moisture content, the magnitude of the elastic strain is generally related to the steepness of the moisture gradient" (Youngs, 1957).

Some idea of the magnitude of the elastic strain in red oak early in drying can be obtained by reviewing the bar graph adapted from McMillen (1955) and shown as Fig. 6.

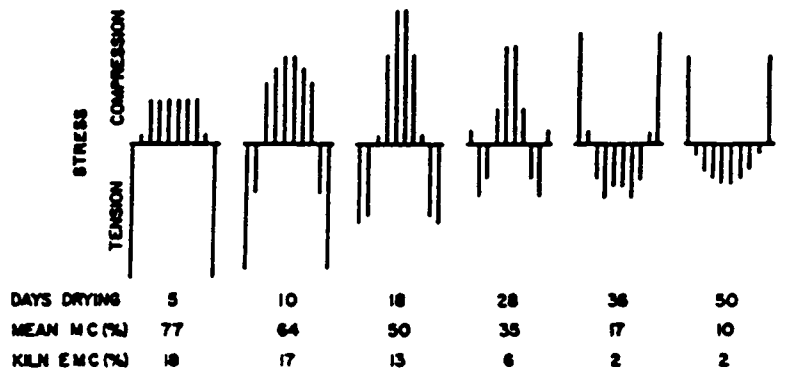

Figure 6. Bar graphs illustrating the general magnitudes of strain in red oak during drying. The length of each line is an indication of the strain magnitude and the longest lines represent strains of about .003 in/in. (from McMillen, 1955).

Creep Components During Drying

Creep is the time dependent deformation of a material. Two distinct types of creep which occur in wood have been identified and these are termed visco-elastic creep and mechano-sorptive creep (Bodig and Jayne, 1982; Grossman, 1976). Visco-elastic or recoverable creep is exemplified by wood deformation which occurs when a beam is conditioned to a specific moisture level, loaded, and the deflection over and above the initial elastic deflection is measured during a given time period as the beam is maintained at the same moisture content. Mechano-sorptive creep

is exemplified by the permanent deformation or bending which occurs when a loaded beam undergoes moisture change such as during drying.

The literature regarding creep of wood is vast and several reviews have been written describing the experimental findings and theories regarding the nature of the creep process (Schniewind, 1968; Grossman, 1976; Johnson, 1978). The major experimental findings may be summarized as follows:

1. The conditions which affect creep are loading, temperature, and moisture content (Hisada, 1980; Hunt, 1987).

2. Creep is nearly 100 percent recoverable under moisture cycling and 100 percent recoverable under oppositely applied load (Armstrong and Christensen, 1961).

3. Visco-elastic creep is nearly 100 percent recoverable after the removal of load if the recovery time is sufficient (Leicester, 1971; Miller, 1974).

4. Mechano-sorptive creep requires a moisture content change to develop (Armstrong, 1972).

5. The rate of change of mechano-sorptive creep is a function of the rate of change in moisture content. The final magnitude is unaffected by the rate of change of moisture content and is a direct function of the amount of moisture change which occurs (Armstrong, 1972; Szabo and Ifju, 1970).

6. There is a limit to the magnitude of creep and the limit is apparently related to the crystallite orientation; being reduced in the direction of alignment (Hunt, 1987).

7. Mechano-sorptive deformation is "permanent" only if the temper-

ature and moisture content do not change (Grossman, 1976).

8. Elastic strain and creep develop concurrently (McMillen, 1955; King, 1958; Sliker, 1978).

Nearly all of the theories regarding the nature of creep emphasize that the phenomenon occurs at the polymer rather than at the cellular level. A hypothesis that forms the basis for many of the explanations regarding the causes of mechano-sorptive creep is that the breaking of bonds between the water molecules and one of the polymeric constituents (usually cellulose) under a stress bias causes a "slippage" of one polymer past another (Szabo and Ifju, 1972). Although attractive and able to explain a number of the features listed above, the hypothesis becomes somewhat untenable because of the apparent recoverability of creep (Armstrong and Christensen, 1961; Grossman, 1976). Other theories, based on continuum mechanics (Ranta-Maunus, 1975), diffusion (Schaffer, 1972) or anatomy (Boyd, 1982), are useful only in a limited range or do not take into account some of the known aspects of creep (Grossman, 1976).

Qualitatively, perhaps the creep process can be most easily understood by using the tenets of polymer "rubberlike" elasticity and visco-elasticity. Polymer chemists suggest that polymer groups or "ensembles" as they occur in various fiber types can be characterized by their conformations and configurations (Morrison and Boyd, 1973). The extremes of the configurations range from a state of high enthalpy, measured by the alignment between molecules and high entropy measured by the "disorder" of the molecules. Conceptually, the polymer entropy and enthalpy represent opposite states. As an example, an ensemble in a

highly ordered, crystalline configuration has higher enthalpy and lower entropy than the same ensemble composed of randomly oriented polymers. The randomly oriented ensemble has higher entropy and lower enthalpy than the crystalline state.//

The general relationship between enthalpy and entropy may be described by the second law of thermodynamics which may be written in the following form (Daniels and Alberty, 1966):

$$\Delta G = \Delta H - T\Delta S \qquad \text{Eq. 9}$$

Where: G is the Gibbs free energy

H is the enthalpy

S is the entropy

T is the absolute temperature

The Gibbs free energy change is the "ability to do work" such as recover the original conformation or configuration of the polymer. The Gibbs energy always tends toward a minimum value for the given conditions. The enthalpy or "heat content" change is a measure of the polymer alignment. Highly crystalline or ordered polymers have higher enthalpy than those which are disordered. A change in entropy is assumed to correspond to conformational (stretching) changes or configurational (polymer rotation) changes. Although entropy and enthalpy changes are usually assumed to be in the realm of continuum mechanics, they are in fact statistically based (Wannier, 1966) and recovery of the original conformations and configurations must be understood as a stochastic process rather than an absolute process.

1/ In general, polymers tend to maximize their entropy by minimizing their end-to-end distance (Flory, 1953). In the presence of heat, most polymers contract to further reduce their end-to-end distance and often form a helical configuration (Wilkes, 1986).

Under stress, polymers tend to align in the direction of the stress, rotate to new configurations and develop new conformations (Morrison and Boyd, 1973; Aklonis et al., 1972; Hill, 1967). When all of the bonding sites in the amorphous areas are occupied by water molecules or bonded to matrix materials, an applied stress produces a strain which is essentially elastomeric, that is, entirely recoverable after the removal of stress as in an elastic deformation. In this case, entropy "wins" because there is little or no net displacement of the interleaving matrix materials or moisture and the polymers return to their original enthalpy and entropy positions.

The situation changes drastically if moisture is lost between the amorphous areas or there is a movement of the matrix materials (such as a softening due to approaching the glass transition temperature). This has the effect of freeing some bonding sites in the amorphous regions which increases the bonding potential between the polymers. The net result is that, under tensile stress, the enthalpy begins to dominate causing the alignment to become more permanent. If the moisture is lost in the amorphous areas, such as occurs in the drying of wood, a new equilibrium energy level with increased enthalpy and reduced entropy is achieved.[1] Macroscopically, the result is an apparent permanent deformation ("mechano-sorptive" creep) in the direction of any applied stress which can be almost completely recovered if moisture is reintroduced

into the amorphous areas (e.g.; by "moisture cycling") and the polymers attempt to return to their original conformations and configurations. If the moisture loss is the result of applied stress (i.e., the moisture is "squeezed out") it gradually rediffuses into the amorphous areas and the deformation is recovered, such as in the case of visco-elastic or recoverable creep.

The explanation outlined above is, of course, speculative and, due to the natural complexity of wood, it is necessarily qualitative. In practice, it is probable that lignin, which is a three-dimensional network polymer, forms covalent bonds with the cellulose molecules and increases the ability of the wood to conform to applied stress (Erins et al., 1976). Regardless of which polymers are primarily responsible, the natural conformational and configurational changes due to enthalpy and entropy seem to have been overlooked by many researchers in attempting to explain creep and particularly creep recovery.

C. The Strength of Wood Perpendicular to the Grain

Surface checks occur when drying stresses exceed the tensile strength of lumber perpendicular to the grain. Since the tensile strength of wood in this direction characteristically exhibits high variability (Barrett, 1974), it is important to discuss some of the major strength factors.

One of the major determinants of strength is related to the basic anatomy of the wood. Such items as the number of thin-walled early wood cells, the amount of dense latewood and the microfibril angle significantly affect strength. In a ring porous wood such as red oak, the variation can be particularly significant. In one study with red oak,

Maeglin (1976), reported that 58 percent of the variation in strength was the result of anatomical variation. The remaining 42 percent was attributable to site factors such as growing conditions.

Another pertinent factor was presented by Markwardt and Youngquist (1956) who showed that specimen geometry significantly affected the apparent strength of samples tested to failure perpendicular to the grain. No reasons for the link between geometry and strength were suggested. Barrett (1974), recognizing the relationship between geometry and strength, adapted the theory of Weibull which suggested a "weakest link" type of relationship between specimen geometry and strength. The evidence presented suggests that the probability of a weak link or material defect increases with the size. In other words, larger sized materials fail at lower stresses than smaller ones. Barrett considered this to be a volume related effect and developed a series of correction factors to be used for structural analysis.

Some evidence in support of a volume effect may be found by comparing the tensile strength perpendicular to grain in red oak at 80° F and 12 percent moisture content as found by Berry et al. (1983) and Youngs (1957). Berry et al., using thin samples with a volume of .183 cubic inches, found the maximum stress to be 2075 psi, while Youngs found the strength to be about 1018 psi with a sample volume of .5 cubic inches. As discussed below, the samples tested for use in this study had an average failure strength of 1362 psi (corrected to 80° F and 12 percent moisture content) and a volume of approximately .281 cubic inches.

The effects of temperature and moisture content on the strength of wood and on the modulus of elasticity are well known. Youngs (1957),

working with red oak stressed perpendicular to the grain and at a variety of moisture content and temperature levels, developed the following equation to relate strength and modulus to moisture content and temperature:

$$Y = A + BT + CM + EIM + FIM^2 \qquad \text{Eq. 10}$$

Where: Y is maximum load stress (p.s.i.) or modulus of elasticity.

M is the moisture content (8 to 18 percent)

T is the temperature (80 to 180° F)

A, B, C, D, E, and F are coefficients determined from a multiple regression analysis.

The strength of wood perpendicular to the grain as evidenced by short term tension tests, exhibits a slightly non-linear pattern in the elastic region and the overall stress/strain pattern shows little evidence of visco-elastic strain (Ivanov, 1941; Schaffer, 1972). There are at least two possible reasons for this pattern. First, under the action of increasing stress, microchecks or cell-level failures may be occurring which effectively reduce the cross-sectional area during the tests. The net effect is that the area bearing the load is decreasing during the test and the stress/strain pattern becomes non-linear. Second, the creep components develop simultaneously with elastic strain and may serve to cause the non-linear pattern (McMillen, 1955; Sliker, 1978). Most probably, both mechanisms interact simultaneously to cause the slightly non-linear curve.

D. The Acoustic Response of Wood.

The fact that materials emit vibrations or pressure waves during stressing has been known for many years. Since the first publication on the study of acoustic emissions (AE) in metals by Kaiser (1953), the method has been widely used as a non-destructive materials testing technique. The inherent appeal of the method has led to vast improvements in the equipment in a relatively short period of time. A general discussion on the applications and equipment of acoustic emission technology may be found in Pollock (1971).

Acoustic emissions in materials are usually generated by applying stress. The acoustic emissions which result are generally considered to be a release of strain energy within the material. In most cases, this strain energy is dissipated because of a local defect area or local "fast deformation" (microchecking) due to stress concentrations. Other known reasons for the production of acoustic emissions include material dislocations, phase changes or the growth of cracks (Qian and Zhu, 1987).

A typical AE system may be described in terms of the functions of the system components. Acoustic emissions are generally detected using a ceramic or quartz piezoelectric sensor, which is attached either directly to the surface being monitored or to a waveguide in contact with the material. The sensor converts the incoming signal to an electrical impulse. Next, the impulse is amplified and conditioned to remove unwanted, extraneous noise. Many systems in current use allow the amplified and conditioned signals produced by the stressed material to be filtered such that only those signals above a certain threshold

are registered. In this case, the signals crossing the threshold are termed "ringdown counts", "counts" or "events". The most common method of reporting acoustic emission activity is to describe the count rate, cumulative count rate, or event rate as a function of the stress applied to the material. Additional details of a typical acoustic emission detection system may be found in Honeycutt et al. (1985).

The application of the acoustic method to wood was first done by Porter et al. in 1972 who measured the cumulative count rate vs. load to predict failure in Douglas-fir finger joints. Noguchi et al. (1980) followed with a report in which the AE rate during drying was determined to be primarily a function of the ambient relative humidity. The monitored emissions from drying wood increased as relative humidity decreased and were suppressed as relative humidity was increased. Simultaneously, Skaar et al. (1980) suggested that the relationship between relative humidity and acoustic emissions could be used as a method to control kiln conditions through a feedback loop. The system was later tested using red oak (Honeycutt, et al., 1985).

The causes of acoustic emissions within wood are generally assumed to be the result of microchecks which form in or between cells. Sato et al. (1984) concluded from studies of wood in tension that two different types of emission rates were actually produced. Emission rates which showed a gradual increase with increasing load they termed "slow AE's" and rates which produced spikes in the emission spectrum were termed "fast AE's". Slow AE's were believed to correspond to microchecking and fast AE's to macrochecking. Noguchi et al. (1987) monitored the acoustic emissions from the cross-sectional surfaces of drying disks of

Zelkova serrata. Painted on the surface of the disks were conductive strips through which a voltage was monitored as the surface dried. When the disk cracked as the result of drying stresses, the strip broke and the rate of AE could be correlated with failure. Noguchi et al. concluded that checking could not be predicted by the level of AE, but the AE rate quite accurately predicted shrinkage of the material. To date, none of the studies outlined above, or others which were reviewed but not cited, have been able to characterize or isolate tangential surface failures in wood as a result of stress.

E. The Computerized Simulation of Drying Stresses.

It is the intent of this section to describe the chronological development of the models which have been used to quantify the stresses which develop in wood during drying. Some of these models are interpretations of experimental data (McMillen, 1955) while others use sophisticated mathematical techniques (Lewis, et al., 1982) to predict the stresses and strains during moisture movement in wood. Each of the models summarized below adds a new element or perspective to the accurate prediction of the stresses which develop during drying.

The models developed by McMillen (1955, 1956, 1968) were expository and resulted from using the slicing technique described above to monitor the development of elastic strain in samples which were drying under various temperature and relative humidity conditions. Once sawn, the wafers were dried and the moisture contents determined so that the elastic strains could be correlated with the moisture profiles. Some attempts were made to quantify mechano-sorptive creep by assuming that it could be represented as the difference between the dry width of the

outer and inner wafers. Both red oak and ponderosa pine were studied and the same methods of analysis were applied to each species.

McMillen's analysis of the data was in terms of a series of bar and cartesian coordinate graphs depicting strain in terms of position and time since the beginning of drying under different drying schedules. These graphs clearly show that the tangential surfaces of drying boards begin to develop tensile strains soon after the commencement of drying. The magnitude of the strains is dependent on the severity of the drying conditions as well as the time since the commencement of drying. McMillen's pioneering efforts also showed the development of compressive strains as well as the phenomenon of stress reversal during drying. There were no attempts to mathematically correlate the moisture gradients with the strains or to determine the stresses and moduli associated with the strains.

The experimental approach of McMillen was followed by a mathematical model developed by Youngs and Norris (1958). The basis of the model was a stress function which related stress to cross-sectional position. The basic model consisted of a parabola which was modified by a series of positionally dependent coefficients. The evaluation of these coefficients was the most crucial and difficult part of the model. The principle of least work, which states that stresses will adjust so as to minimize their energy, was used to solve for the coefficients at various positions in the cross-section of a drying board. Once the coefficients were determined, the stress function containing the coefficients was solved to give stress as a function of position. Similar methods were applied to determine the radial and shear stresses at various points in

the cross-section of a board during the early stages of drying.

The model of Youngs and Norris was intentionally limited to the first few days of drying under mild conditions. Neither stress reversal nor rheological components were considered. Because the model does not specifically relate moisture loss to the development of stress or strain, it is difficult to determine if the predictions correspond to the data presented by McMillen (1955). However, the calculations indicate that the magnitude of the tangential stresses are much greater than either the radial or shear stresses during drying.

Ugolev (1959) reported a series of experiments with "pine" from which a one-dimensional model of stress was developed. The model considers elastic and some aspects of plastic strain. The experimental approach is generally similar to the wafer slicing technique used by McMillen. Ugolev, recognizing the modulus of elasticity changes with moisture content, took the added precaution of determining the elastic modulus in bending of each sliced wafer. The details of mechano-sorptive creep determination are not clear in the report, but presumably the plastic component was determined as the difference between actual and unrestrained shrinkage.

The Ugolev model does not specifically relate moisture movement or drying conditions to stress development. In addition, the visco-elastic creep component was obscured by the experimental technique and overlooked. Although somewhat limited, the Ugolev experiments clearly show the magnitude of mechano-sorptive creep strain during drying is large in relation to the elastic component. His presentation of plastic flow as a stress relief mechanism appears to be correct.

From another series of experiments which are performed with birch, Ugolev (1976) purportedly developed a two-dimensional finite element model which calculates stresses during drying. Details of the model are lacking, but in one series of background experiments Ugolev determined that the coefficient of shrinkage does not change appreciably regardless of whether the wood is loaded or unloaded in tension perpendicular to the grain during drying. As discussed above, the unrestrained shrinkage is a datum. Deviations from the unrestrained shrinkage value indicate the development of one or more of the strain components illustrated in Figure 5. A significant change in the shrinkage coefficient could alter the basic concept of how stresses develop during drying.

Ashworth (1979) developed a one-dimensional model for the drying of "softwood". The model is one of the first reports to clearly couple moisture loss with strain development.

The moisture distribution in the Ashworth model is determined using a non-dimensional form of Fick's second law. The transport coefficient for the model is considered to be a function of both temperature and moisture content and based on an equation developed by Luikov (1966). Strain in the Ashworth model is considered to be both elastic and plastic. The observed shrinkage of the wood is also considered. All of the strain elements are coupled through the use of elastic/plastic parameters which supposedly result from the temperature or moisture distributions that develop during drying. For low strains, the model assumes only linear elastic strain and some shrinkage exists. As the strain increases, a pre-set yield point is reached where the plastic component begins to act to reduce the strain and attendant stress. By adjusting

the yield point and other model parameters, Ashworth was able to match, with reasonable accuracy, the curves reported by McMillen (1968) for ponderosa pine.

The model of Ashworth has no experimental basis or verification and elements such as visco-elastic creep are not considered. Constants which are used in the simulation are taken from the literature apparently without regard to species or drying conditions under which they are determined. In the final analysis, the simulation parameters were adjusted for convenience to fit reported stress data. Despite these shortcomings, the model represents a significant advance because it was among the first to clearly delineate the strain components and to directly couple moisture distribution with strain development.

The model developed by Kawai et al. (1979) and, later, Kawai (1980) represents a major advance in the determination of stresses during drying. The general experimental outline and approach to a computerized simulation have served as a paradigm for a number of other researchers. In addition, Kawai was the first to consider and measure all the major components of strain as they are currently understood.

The general scheme of the model was to determine the moisture distribution at some point during drying under specified conditions. Using this distribution and other drying parameters, the major stresses are calculated from the strain components and associated moduli. The calculations are done using relationships which have been developed from experiments relating the strains to moisture content or time.

The Kawai model assumes that moisture movement in the longitudinal direction gives rise to the strains shown in Figure 7.

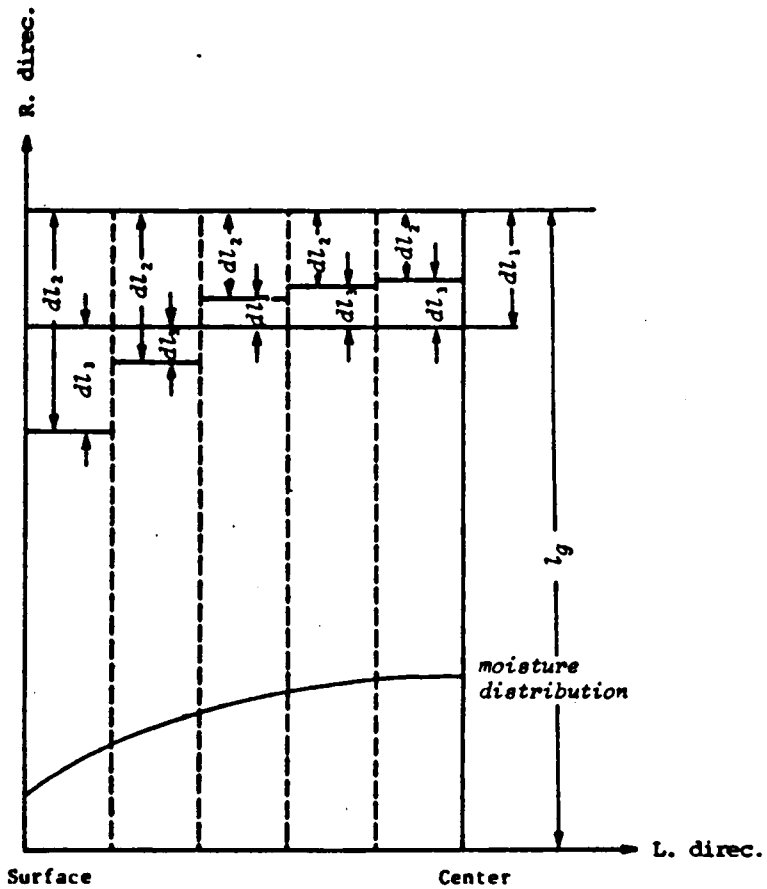

Figure 7. The strain components during drying, as defined by Kawai. The maximum possible strain is dl_2/l_g. The observed strain is dl_1/l_g and the total strain is dl_3/l_g.

For visco-elastic materials, the total strain may be considered to be the sum of the elastic and inelastic strains:

$$E^t = E^e + E^f \qquad \text{Eq. 11a}$$

Where E^t is the total strain, E^e is the elastic strain and E^f is the inelastic strain.

From Figure 7, the total strain from drying stress is dl_3/l_g or:

$$E^t = E^{BS} - E^{oBS} \qquad \text{Eq. 11b}$$

Where E^t is dl_3/l_g, E^{BS} is dl_2/l_g, and E^{oBS} is dl_1/lg_3.

Substituting 11b into 11a give Kawai's equation for drying stresses:

$$\bar{\nabla} = B^e\ Ee^{BS} - B^e\ E^{OS} - B^e\ E^F \qquad \text{Eq. 11c}$$

Where B^e is the modulus and $\bar{\nabla}$ is the stress.

Using these basic equations, Kawai et al. then developed an experimental plan where the components could be determined as functions of moisture content or time under specific drying conditions. The inelastic strain was assumed to be the result of both mechano-sorptive and visco-elastic creep strains which were measured using beams stressed parallel to the grain. Creep compliances were determined using a method developed by Takamura (1972). Basic or inherent shrinkage was measured using small samples under carefully controlled conditions. Elastic strain, which is implicit in the total strain term, was not measured directly but was determined from knowing the basic shrinkage, observed shrinkage, and inelastic strains in accord with Equation 11b.

Graphs of stress produced by the model agree well with the expected stress patterns. However, the criteria used to determine if a surface

check occurs are not clear. The creep components determined on using conditioned beams stressed parallel to the grain are not representative of those for lumber being dried.

Lessard et al. (1982) developed a one dimensional model for drying red oak which has both a theoretical and an experimental basis. The model assumes that the total strain is the sum of an elastic strain element and a plastic strain element. The determination of total strain at any given time is somewhat complex. First, the elastic strain is determined using equations based on the work of Youngs (1957). If the calculated strain does not exceed the elastic limit for the given moisture and temperature conditions, the strain is assumed to be entirely elastic. If the calculated elastic strain results in a stress which exceeds the strength of the wood, the next step is to calculate a stress relieving mechano-sorptive creep component. The determination of the magnitude of plastic flow at any given elastic strain level is based on an averaging procedure.

The determination of surface check occurrence is unique in the Lessard et al. model. The criteria of failure are not based on a single value of average strength, but rather on the basis of a linearized cumulative stress distribution. Using an assumed probability distribution of wood strength, the chance of failure increases cumulatively until the probability based failure prediction allows drying schedules to develop more realistically than when using a single valued failure criterion.

Most of the experimental basis of the Lessard et al. model is similar in detail to the wafer sawing experiments of McMillen (1955). In addition, they measured the amount of cup in drying lumber and deter-

mined a correction factor for cupping stress based on beam bending theory.

The graphs which compare the model predictions with experimental results show good agreement with McMillen's experimental data. However, the discussion given by the authors leaves the impression that they did not successfully correlate either temperature or moisture movement with stress or strain development. In addition, visco-elastic strain is not considered in the model.

Lesse (1982) and, later Lesse and Kingston (1982) developed what they termed an osmoelastic-plastic model. The one-dimensional model is based on an analogy in which the authors consider osmotic stress (shrinkage or swelling) to be equivalent to thermal stress. The thermal stress equations, which are developed from energy and momentum balances, are then interpreted in terms of moisture loss or gain. The resulting osmotic stress is responsible for the development of elastic, plastic and shrinkage strains during drying.

The Lesse and Kingston model is purely a theoretical approach to the computation of stress in terms of thermal conditions and moisture gradients. Some attempts are made to compare the model output to the data for oak reported by McMillen (1955). By adjusting the yield point considerably, moderate success was achieved.

Comini and Lewis (1976) developed a two-dimensional model to describe heat and mass transfer in porous media such as brick. The importance of the model results from its use as the basis of a series of studies in which moisture and temperature dependent stresses in other porous materials such as wood were calculated. In order to determine

the moisture distribution within the porous material, Comini and Lewis used the coupled heat and mass transfer equations developed by Luikov (1974). The solution of these equations was done using the finite element method.

The first expansion of the Comini and Lewis model was done by Lewis et al. (1979) who developed what they termed an elastoviscoplastic model. A constitutive equation with several elements was developed to define drying strains. Below a predefined stress/strain level, no plastic flow occurs. Above the level, a flow function begins to act causing plastic flow and a reduction of stress.

In 1980, Morgan et al. applied the model to a case in which a timber was drying under isothermal and purely elastic conditions. Values for the various model constants were compiled from reported drying studies on different softwood species.

Finally, Morgan et al. (1982) applied the heat and mass transfer model as well as the elastoviscoplastic model to the study of stress reversal in timber. The final model was used to investigate stress reversal as affected by moisture loss rate and the variation of model parameters with moisture content. After considerable adjustment of the model parameters, the curves presented show the general moisture distributions and overall patterns of stress and strain which are expected during drying.

The use of the coupled heat and mass transfer equations of Luikov represented a major advance in the determination of the moisture distributions. However, the model is difficult to evaluate because a number of details regarding the plastic flow function and other parameters

are missing. Further, since there is no experimental basis or verification, it is not possible to predict the accuracy of the model under actual drying conditions for a particular species.

Oliver (1987) developed a one-dimensional model for moisture loss and concurrent strain development in Eucalyptus. Moisture movement in the Oliver model is calculated using Fick's second law. The solution of this equation is exact and based on the solution of a semi-infinite plate given by Carslaw and Jaeger (1959). The transport coefficient in the model is considered to be constant. There is no direct consideration of temperature in the model.

The total strain which results from moisture loss during drying is based on the model of Leicester (1971) and consists of elastic, visco-elastic, mechano-sorptive and shrinkage strain components. The elastic and visco-elastic creep strains have linear as well as non-linear components.

Most of the input data used in the model is taken from beam tests under constant, longitudinal loading conditions. These data are then multiplied by various constants taken from the literature to simulate strains in the radial or tangential directions. Of particular interest is the manner in which the stress is calculated from the mechano-sorptive creep strain. Oliver uses the following formula developed by Leicester (1971) and discussed in some detail by Grossman (1971):

$$\nabla = E_g/u \; (\Delta e)/(\Delta m) \qquad \text{Eq. 12}$$

Where ∇ is the stress, E_g is the green modulus, $\Delta e/\Delta m$ is the

slope of the mechano-sorptive strain/moisture content curve and u is .6 for wood in tension.

The Oliver model is somewhat simplistic and the use of longitudinally loaded beams as a basis does not represent the same conditions which occur in drying. However, the model clearly differentiates and computes values for each of the major strain components in a manner similar to that of Kawai (1980). In this respect, the model becomes one in which the contributions of each of the major and minor strain components may be evaluated under varying conditions. In addition, Oliver is one of the few who clearly defines a modulus for mechano-sorptive creep strain.

Objectives and Scope of the Project

A. Objectives

The general hypothesis for the project was stated in the Introduction. Because the project involved a number of distinct facets, specific objectives were developed. The objectives were as follows:

1. Determine the magnitude and variation of the elastic strain in red oak perpendicular to the grain and its relationship to various drying parameters.

2. Characterize and determine the magnitude of mechano-sorptive creep early in the drying process and its relationship to various drying parameters.

3. Characterize and determine the magnitude of visco-elastic creep early in the drying process and its relationship to various drying parameters.

4. Determine the magnitude of the unrestrained shrinkage which occurs in the tangential direction in red oak during drying.

5. Determine a sampling distribution of failure stress in the tangential direction perpendicular to the grain under a specific set of drying conditions. Using the sampling distribution, develop failure criteria for a computerized simulation.

6. Develop a computerized simulation which uses the measured strain components and their relationships to various drying parameters to predict the likelihood of surface checking early in the drying process.

7. Measure the acoustic response of red oak wafers undergoing surface failure.

B. Scope of the project

The overall project was composed of two major subdivisions. The experimental subdivision was designed to investigate the relationships between drying stresses, moisture movement, and strength during the first four days of drying red oak (Quercus, spp.). The measurement of acoustic response was also a part of this portion of the study. The second subdivision, which consisted of a computerized simulation, was designed to incorporate the relationship between moisture gradients, strain and strength which were determined from the experiments.

The experimental portion of the study may be further subdivided into seven distinct phases. The experiments in each phase were designed to measure a particular aspect of moisture loss, strain, strength or acoustic response. First, one dimensional moisture gradients during the first four days of drying were determined using a wafer sawing technique. The experiments were repeated at three relative humidity levels. During the second phase, samples were prepared and the wafer sawing technique was employed to determine elastic strain and mechano-sorptive creep during the first four days of drying. The third phase was to measure the basic or inherent shrinkage of the red oak. Small samples were carefully measured and weighed while drying under controlled conditions. Fourth, mechano-sorptive creep as a function of load and moisture content was measured by drying small green wafers at several relative humidity and load levels. During the fifth phase, the visco-elastic component of creep was determined by measuring the deformation of conditioned wafers at several relative humidity and load levels. Next, the approximate strength distribution of green red oak was deter-

mined by measuring the load-deflection characteristics and failure stress of small wafers at 110° F. The final portion of the experimental phase was to measure the acoustic response of small green wafers stressed to failure perpendicular to the grain under third point loading conditions.

The next phase of the project called for the development of a computerized simulation. To obtain information which forms the basis of the simulation, the data from the first six experimental phases were analyzed using standard statistical methods. From this analysis a number of relationships between the moisture content, time, strength, and load level were determined. These relationships, when combined, form a model which predicts the moisture gradients, stress development and probability of failure during the first four days of drying. The computerized simulation is based on this model. The general design of the project is shown as Figure 8.

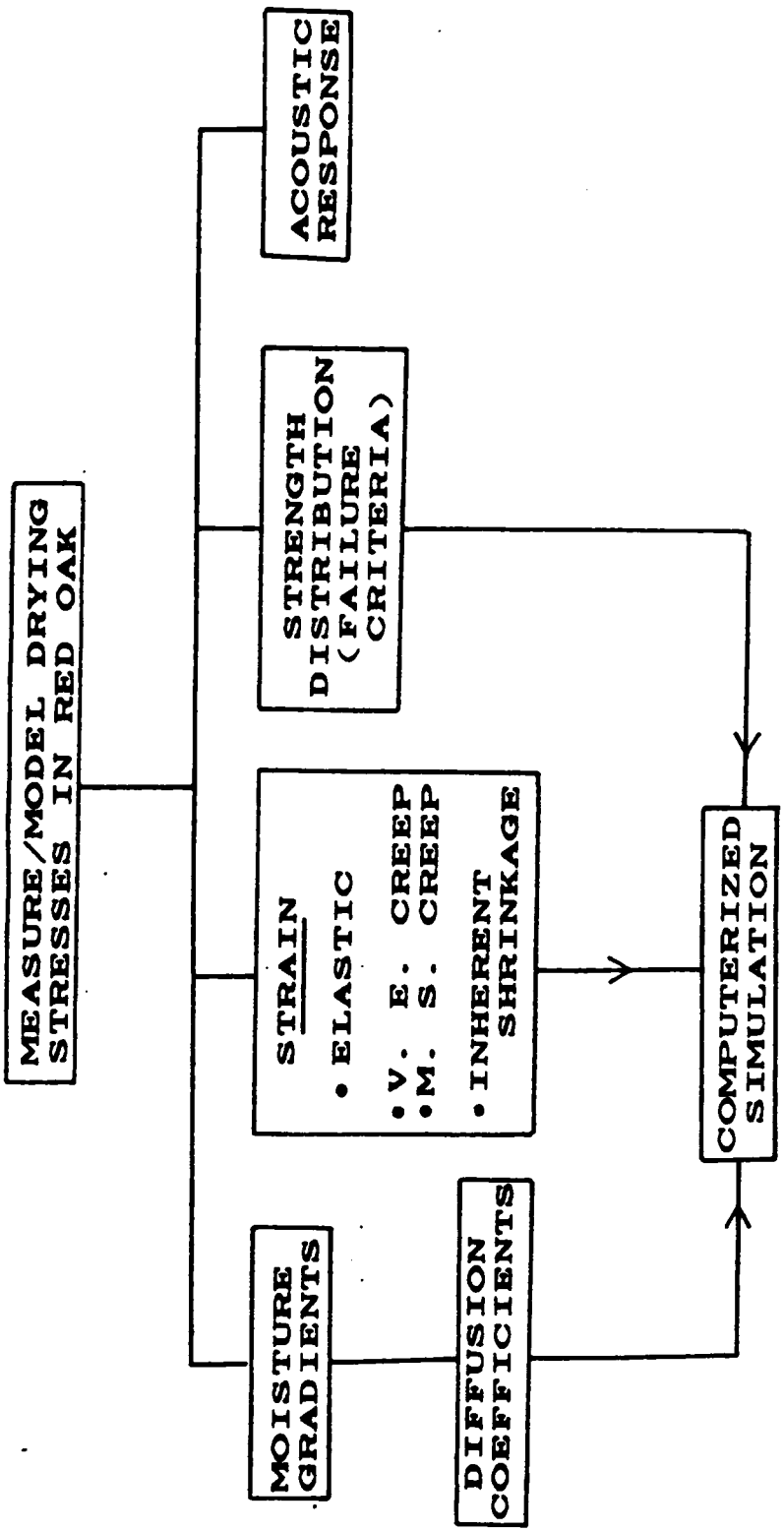

Figure 8. General Outline of the Project

METHODS AND MATERIALS

The general objectives and the scope of the project were discussed in the previous section. It is of interest to discuss the specific methods and materials for each project phase separately.

A. Choice and Preparation of the Material

In order to minimize material variation a single log of red oak (Quercus, sp.) was used to provide the material for all experiments. It was felled in Montgomery County, Virginia, in the fall of 1987 and purchased from a commercial sawmill approximately one week later. The log was a butt log with very few defects (NHLA grade 1) and little taper. Before sawing, the log had a diameter of 23 inches at the upper and 31 inches at the lower end. The lower end had a small area of eccentricity or "butt swell" causing some waviness in the growth rings near the lower end of the log. The number of rings per inch was approximately 4-6, the green moisture content of the log was 90.7 percent (avg. of 6 readings) and the dry density of the wood was .531 (avg. of 14 readings).

The log was sawn into planks using a 52 inch circular saw at Virginia Tech. The cutting diagram is shown in Figure 9.

The planks were sawn from the heartwood as far distant from the pith of the tree as possible to minimize ring curvature. Care was taken to rough-saw the planks with a ring angle as close to zero degrees as possible. Immediately after sawing, the wane was removed from the planks using a Cornell two-saw edger. The size of the rough cut planks was approximately 6.25 inches (tangential) by 1.75 inches (radial) by 12 feet long. The planks were numbered with an indelible marker immediately after sawing.

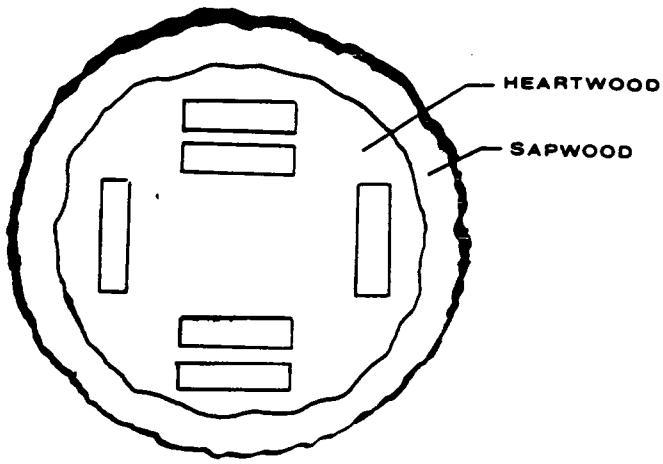

Figure 9. Cross-section of a log showing the relative positions from which the test specimens were taken. The heartwood diameter was about 25 inches at the lower end of the log.

After rough sawing and edging, the planks were planed on both sides to a thickness of 1.5 inches and re-marked with their identifying number. Before and after planing, the planks were wrapped in polyethylene to prevent drying.

The breakdown of the planks into the quantities needed to perform the various experiments was the next operation. Several of the planks contained appreciable amounts of sapwood. Since only heartwood was used for the experiments, the planks were cross-cut to remove the sapwood. The moisture gradient and elastic recovery tests each required 12 pieces of wood 18 inches long. The 12 pieces for each type of test were further subdivided into three groups of four pieces; with each group of four pieces representing an experiment at a particular drying condition.

The pieces were chosen from the planks such that the pieces in each of the three groups were from different planks. The basic shrinkage, visco-elastic creep, mechano-sorptive creep, strength distribution and acoustic response tests each used less than 30 inches of wood. The material was taken at random in 6-10 inch increments from the planks and distributed such that each test used material from at least two different planks. All of the material was trimmed to a width of six inches using a jointer, labeled with the plank number and wrapped in a double thickness of polyethylene. The wrapped material was kept in an environmental chamber at a temperature of 35-40° F until ready for use.

B. Moisture Gradient Tests.

1. Conditions for the Tests and Equipment

Moisture gradients were determined daily for the first four days of drying. The tests were conducted at relative humidity levels of 85, 60, and 35 percent corresponding to equilibrium moisture content values of 18.5, 11.5 and 7.3 percent. The estimated variation in the relative humidity was $\pm$ 2 percent. Temperatures were maintained at 110° F for all tests with an estimated variability of $\pm$ 2 degrees F.

The apparatus in which the tests were conducted was an Aminco environmental chamber having a capacity of approximately nine cubic feet. The interior of the chamber was fitted with wire mesh racks upon which samples were placed. Air velocity in the chamber was measured at approximately 150 feet/minute using an air velocity indicator (Bacharach Instrument Co.). The temperature was monitored using a recently calibrated mercury thermometer and the relative humidity was determined using a hygrothermograph (Bacharach Instrument Co.) as well as a

recently calibrated hygrometer.

2. Moisture Gradient Sample Preparation

After establishing the chamber relative humidity level at one of the three conditions outlined above, four 18-inch long samples were removed from cold storage and prepared for use. Preparation involved trimming approximately one inch from each end of the piece then removing an additional 1/2 inch thick moisture content sample. The ends and radial surfaces of each piece were coated with aluminized varnish to minimize moisture loss. Thin strips of plywood were then tacked to the coated areas to further seal the surfaces. All four pieces were placed on a rack in the environmental chamber as shown in Figure 10.

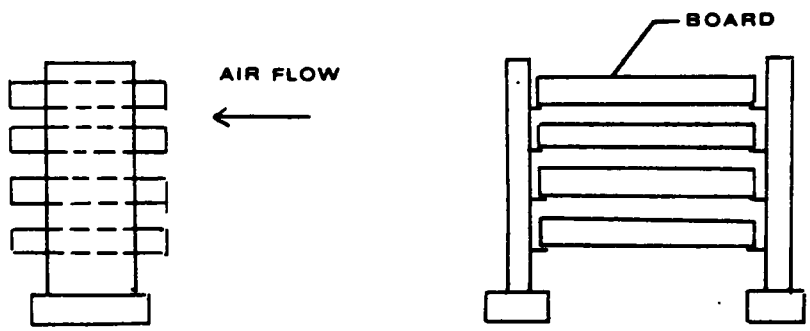

Figure 10. Rack used for holding the boards in the drying chamber. Left: side view. Right: front view. The wood rested on pins projecting from the side supports. As successive sections were cut, the side supports were moved inward. The spacing between the boards was about 1/2 inch.

3. Moisture Gradient Test Procedure

At the end of a 24 hour drying period the samples were removed from the rack and a four inch section was bandsawn from the end of each piece as shown in Figure 11. The remainder of the sample was resealed and returned to the drying chamber. The four inch sections were trimmed and each was bandsawn into a 3/4 inch moisture content sample and three one-inch moisture gradient samples (Fig. 11). The moisture content samples were labeled, weighed, and placed in an oven at 212° F to dry. All of the one inch samples were labeled, wrapped in polyethylene and placed in a "holding oven" which was maintained at 110° F until ready for use. After the completion of this step there were 12 moisture gradient samples and four moisture content samples.

Moisture gradient wafers were prepared following the method of McMillen (1955). Eight wafers were sawn from each of the samples using a bandsaw. The wafers were sawn from alternate sides of the sample, then weighed to the nearest milligram. Next, their thicknesses were measured using a dial caliper (.001 inch accuracy). Finally, to establish the kerf size, the thickness of the sample was measured before and after removing each wafer. All measured data were recorded. The average wafer thickness was determined to be approximately .070 inch and the saw kerf about .030 inch.

After cutting, labeling and weighing, the wafers were placed in an oven at 212° F for 24 hours to dry, then reweighed. The recorded weights were used to determine the average moisture contents of the wafers at the time of test.

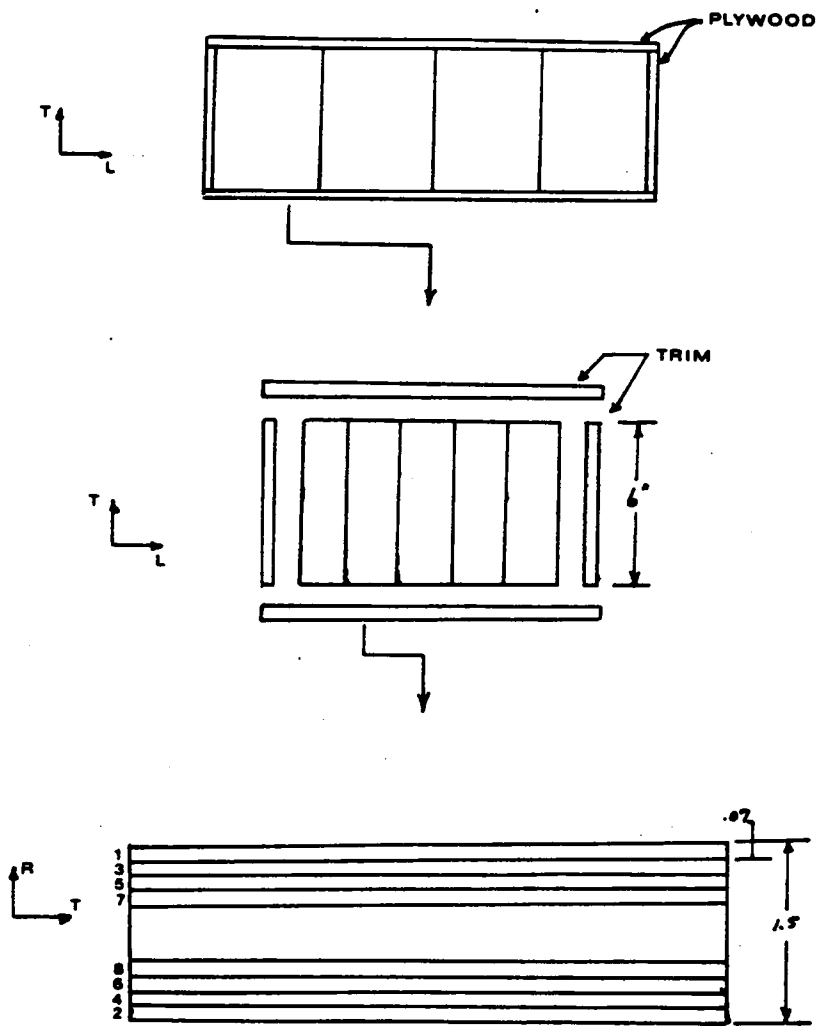

Figure 11. Cutting diagram for the moisture gradient and wafer slicing tests. Top: Each day a four inch section was cut from each board and trimmed (middle) to remove waste. From the four inch section, a moisture content sample and four additional samples were cut. Bottom: The four samples were sliced into wafers measuring about .07 inch thick. The small numbers refer to the order in which the samples were cut. For the wafer slicing tests no side trimming was done.

The wafer slicing and associated measurements shown in Figure 11 were repeated each day for a four day period. Next, the environmental conditions were changed and the entire process was repeated at the new relative humidity level. In summary, 96 wafers were sawn each day for a four day period at a particular relative humidity level. Tests were done at three levels of relative humidity giving a total of 1152 wafers.

C. Strength Testing

1. Conditions for the Tests and Equipment.

Eighty-three green wafers were tested to failure in tension perpendicular to the grain for this series of tests. The tests were conducted in circulating air which was heated to 110° F.

The perpendicular to grain tension tests were done using an Instron model TMML testing machine. The machine was fitted with a box around the test grip area so the heated air could be circulated around the sample. The load level was measured using a factory supplied load cell with a 100 kilogram capacity. Calibration of the cell was done before testing and periodically during the tests using calibrated weights.

Sample extension was measured using a Riehle snap-on type extensometer fitted with a Hewlett-Packard model 7CDT displacement transducer. The gage length between the knife edges was 2 inches. Calibration of the gage was done using a micrometer standard.

Curves of load versus deflection were recorded using a Hewlett-Packard X-Y recorder.

2. Sample preparation

Green red oak wafers measuring 6 inches (tangential) by 3/4-inch (long) by 1/4-inch thick were used for the tests. The gage length area

was machined to approximately $\frac{1}{2}$ inch in width as shown in Figure 12. The wafers were sawn such that the ring angle was approximately zero. After sawing and machining, the samples were wrapped in a double layer of polyethylene and heated to 110° F in a holding oven prior to testing.

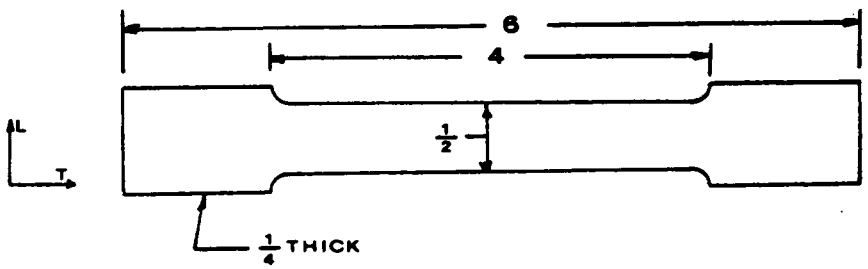

Figure 12. Illustration of the wafer configuration used for the strength tests. All dimension in inches.

3. Test Procedure

A sample was removed from the holding oven and mounted in the testing machine grips. Sample alignment was done using gages designed for the purpose. Next, the extensometer was mounted on the specimen and tightened to a specific preload level to insure the knife edges would not slip during testing. In addition, the extensometer was supported so as not to induce bending moments in the sample.

Mounting of the sample required approximately 1.5 minutes to complete. After mounting, the warm air chamber around the grips was tightly closed and the sample was allowed to warm for about 2 minutes before testing. At the end of the waiting period, the sample was tested in tension at a rate of 0.1 cm per minute until failure. Graphs of load versus deflection were made during each test.

D. Unrestrained Shrinkage Measurements

1. Conditions for the Tests and Equipment.

The unrestrained shrinkage measurements were conducted using small samples conditioned at the EMC values shown in Table 1. All conditioning was done under desorption conditions and at a dry bulb temperature of 110° F.

The tests were conducted in the same Aminco chamber used in previous tests. The control of relative humidity was done using the dew point temperature of the water bath which was monitored with a Bristol chart recorder. Confirming measurements were made using a calibrated hygrometer.

Shrinkage of each samples was measured with a dial indicator (0.001 in. accuracy) which was calibrated prior to use with precision micrometer standards. The indicator was mounted in a stand which had a 0.0250 inch diameter post protruding from its base. The shaft of the dial indicator had a diameter of 0.125 inches. Measurements were done by placing the samples between the two posts.

Table 1. Conditions for the unrestrained shrinkage tests.

Level	EMC	RH (%)
1	18.0	85
2	12.0	70
3	9.9	60
4	9.2	55
5	7.5	40
6	7.0	35

Samples were weighed to the nearest milligram and shielded during all measurements to eliminate disturbances caused by air currents.

2. Sample Preparation

The samples were prepared from green wood using a bandsaw. The sample dimensions were chosen so as to minimize the gradients which lead to restrained shrinkage. Each of the 19 samples measured approximately 1x1x1/4 inches in the radial, tangential, and longitudinal directions. Care was taken to orient the samples such that the growth rings were as nearly parallel to the tangential surfaces as possible. After sawing, the samples were marked with two "measuring points" on each radial and tangential surface. The measuring points were used to insure that the shrinkage measurements were always taken at the same locations.

3. Test Procedure

The tests were conducted by measuring and weighing the samples in the green condition and then placing them on a coarse wire mesh rack in the conditioning chamber which had equilibrated to the first EMC condition (Table 1). The samples were reweighed daily until the weight of each sample changed less than 0.02 gram between readings. Once the weight was stable, the samples were measured in both the radial and tangential directions at the measuring points. After measuring, the samples were returned to the chamber and the conditions were gradually changed to the next level. After conditioning and measuring the samples at the last level, they were dried at 212° F for 24 hours and final weights and measurements were taken. All measured data were recorded for later analysis.

E. Elastic Strain and Mechano-sorptive Creep Tests Using Sliced Wafers.

1. Conditions for the Tests and Equipment.

Elastic strain and mechano-sorptive creep were determined daily for the first four days of drying. The conditions under which elastic strain and set developed were identical to those used in the moisture gradient tests.

2. Elastic Strain Sample Preparation.

After establishing the chamber conditions at one of the three relative humidity levels, four 18-inch long samples were removed from cold storage and prepared for use. Preparation involved trimming approximately one inch from each end of the piece, then removing a green moisture content sample. The ends of each piece were coated with aluminized varnish and thin strips of plywood were tacked to the coated areas to further seal the surfaces. All four pieces were placed on a rack in the environmental chamber as shown in Figure 11.

At the end of a 24 hour period, the samples were removed from the rack and a four inch section was bandsawn from the end of each piece as shown in Figure 11. The remainder of the sample was resealed and returned to the drying chamber. The four inch sections were trimmed and each was then bandsawn into a 3/4 inch moisture content sample and three one-inch moisture gradient samples (Fig. 11). The moisture content samples were labeled, weighed, and placed in an oven at 212° F to dry. All of the one inch samples were labeled, wrapped in polyethylene and placed in a "holding oven" which was maintained at 110° F until ready for use. After the completion of this step, there were 12 elastic

strain samples and four moisture content samples.

3. Elastic Strain Test Procedure.

Elastic strain wafers were prepared following the concepts used by McMillen (1955). Eight wafers were sawn from each of the samples using a bandsaw. The elastic strain could readily be determined by measuring the overall sample size in the tangential direction before sawing and the wafer size in the tangential direction immediately after sawing. Preliminary testing revealed that the overall shrinkage of the samples in the tangential direction during the first four days of drying was negligible. However, consistent measurements of the sample widths were difficult to obtain. After experiencing this difficulty during the tests at the first relative humidity condition (85 percent) a method was developed to overcome the problem. Small holes (.062 in. dia. X 1/2 in. deep) were drilled a fixed distance apart in the green sample (Fig. 13). The hole spacing was then measured using a dial caliper (.001 in. accuracy) fitted with special conically tapered points which centered on the hole diameter.

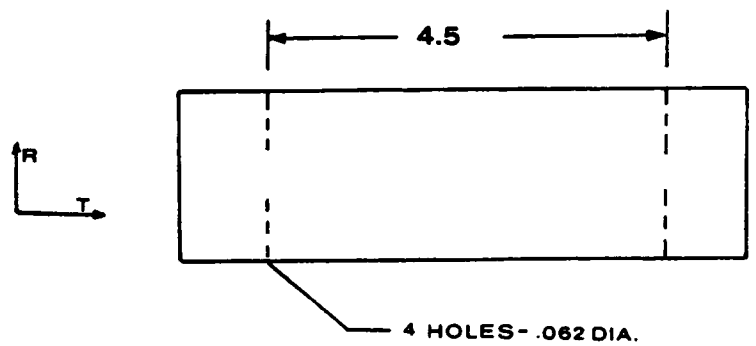

Figure 13. Hole drilling diagram for the samples. The hole positions were determined using a fixture so that each sample had the same gage length and hole placement.

The initial elastic recovery tests (85 percent RH) were done by measuring the overall block width before cutting and the end-to-end wafer width after cutting. All other tests were done by measuring the hole spacing in the sample, sawing a wafer from the sample, and then measuring the hole spacing in the wafer. The elastic recovery was taken as the difference between the before and after measurements. In all cases, the wafer was held so that any curvature or waviness was removed during the measurement. The wafers were sawn from alternate sides of the sample, measured, then weighed. The cutting area was heated using a high wattage bulb to prevent thermal contraction. All measured data were recorded. The average wafer thickness and saw kerf were assumed to be the same as in the moisture gradient tests.

4. Mechano-Sorptive Creep Test Procedure

The amount of mechano-sorptive creep which developed during drying was determined using the same wafers as were used for the elastic strain measurements. The sawn wafers were dried and the hole spacing measured in the dried condition. The unrestrained shrinkage values of the wafers were determined and the measured shrinkage was compared to unrestrained shrinkage. The difference between the two values was considered a measure of the mechano-sorptive creep which had developed at the moisture content of the wafer.

After cutting, the wafers were placed in special drying racks. The racks, shown schematically in Figure 14, were designed to hold the wafers flat so they would not curl during the drying process. If curling were not prevented, the hole spacing in the brittle wafers would be difficult to measure after drying.

The drying scheme for the wafers was a two step process. Immediately after sawing, the racked wafers were placed in an environmental chamber at 130° F and 30 percent relative humidity. After a 24 hour period, the racks were placed in an oven at 212° F for a second 24 hour period. At the end of this time the samples were removed from the racks and the hole spacing was re-measured.

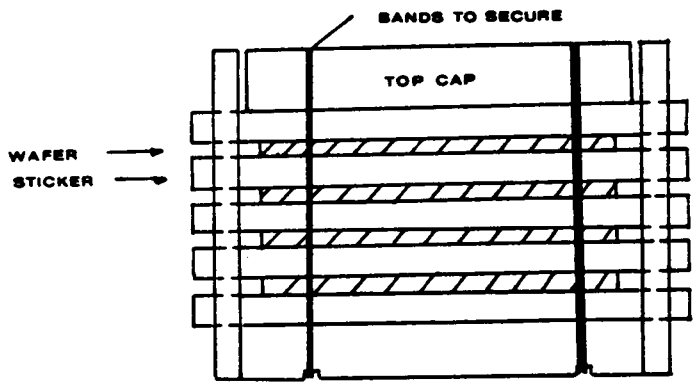

Figure 14. Schematic of the drying rack used to hold the wafers flat during drying. In practice, each rack held about 15 wafers.

5. Summary of samples

The removal of the four-inch sample and the subsequent wafer sawing steps and measurements were repeated each day for a four day period. Next, the environmental conditions were changed and the entire process was repeated at the new relative humidity level. In summary, a total of 96 wafers were sawn each day for a four day period at a particular relative humidity level. Tests were done at three levels of relative humidity. The total number of wafers was 1152.

F. Mechano-sorptive Creep Tests Using Loaded Wafers.

1. Conditions for the Tests and Equipment.

The tests were conducted by drying samples to one of three different relative humidity levels corresponding to EMC values of 18.5, 11.5, and 7.3 percent. The temperature was maintained at 110° F for all humidity levels. A minimum of 15 samples were tested at each relative humidity condition. At each level, the samples were loaded to one of three different load levels corresponding 10, 20, or 30 percent of the average failure stress which was assumed to be 775 psi at 110° F based on the results of strength tests performed for this study. At least five samples were tested at each load level and relative humidity condition.

The tests were done in a special chamber designed for the purpose (Figure 15). Conditioned air was supplied from an Aminco control unit into a manifold which circulated air around the samples. The air temperature and humidity within the chamber were monitored using two recently calibrated hygrometers and thermocouples. The estimated variation in the relative humidity levels was $\pm$ 2 percent and the temperature variation was estimated at $\pm$ 2.0 degrees F.

Sample extension and shrinkage during drying were monitored using strain gages mounted on 0.008 inch thick spring steel backings and wired in a full Wheatstone bridge configuration (Perry and Lissner, 1962). The gages were then mounted into "L" brackets as illustrated in Figure 15. Strain gage output was monitored by a Hewlett-Packard 3421 data acquisition system in conjunction with an HP model 75 computer. Excitation voltage for the gages was provided using a Heathkit precision power

supply. All monitoring equipment was tested and/or calibrated prior to use.

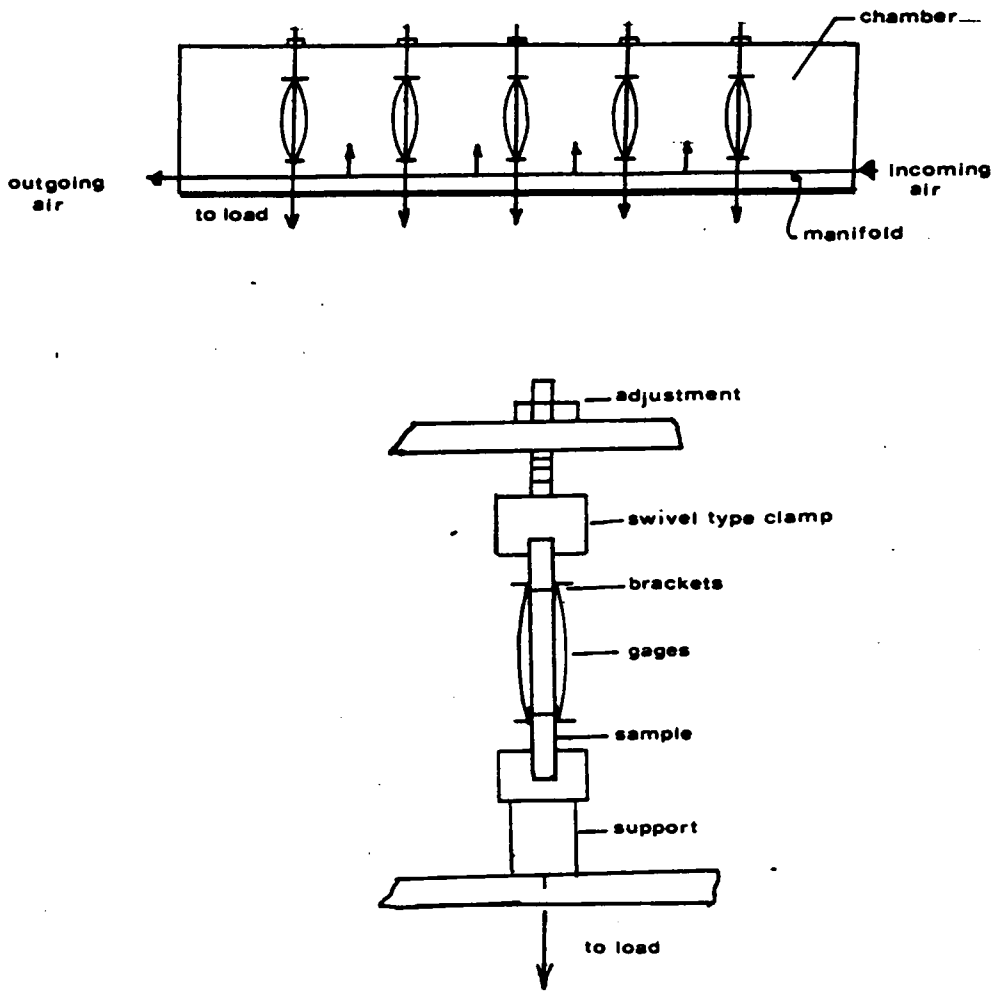

Figure 15. Creep test chamber and details of the sample fixturing for the tests. Top: Overall schematic of the chamber. The incoming conditioned air was directed around the samples using a manifold. Bottom: Details of the fixturing. The sample and brackets rested on a support until the adjusting nut at the top was turned to raise the sample and apply the load.

2. Sample Preparation

Green red oak wafers measuring 6 inches (tangential) by 1-inch (long) by 1/4 inch thick were used for the tests. The wafers were sawn such that the ring angle was approximately zero. After sawing, the samples were wrapped in a double layer of polyethylene and held in the room prior to use.

The green samples were weighed, then clamped on each end. "L" brackets were mounted using a gage that fixed the gage length at 3.4 inches as shown in Figure 15. Care was taken to insure all fixturing was aligned so as not to induce bending moments during testing. The samples and associated hardware were wrapped in plastic while awaiting test.

3. Test Procedure

Five samples were tested simultaneously at one of the three load levels outlined above. The samples were hung in the chamber and supported at the lower end (Fig. 15) while strain gages were affixed. Prior to the application of load, a series of "no-load" strain gage readings were taken at one minute intervals to establish the gage length precisely. The samples were then loaded by tightening the adjusting nut (Fig. 15) and thereby raising the sample and associated fixturing from its support.

The loaded samples were dried for approximately three days. Strain readings taken at one-minute intervals and then, at two-hour intervals for the remainder of the tests. At the end of the drying period, the strain was essentially constant. The load was removed and "recovery" strain gage readings taken. At the end of the test, the fixturing was

removed. Each sample was reweighed, dried and its moisture content determined. The mechano-sorptive creep was taken to be the difference between the actual shrinkage as measured by the difference between the no-load and post-recovery measurements and the unrestrained shrinkage. The mechano-sorptive creep measurements determined in this way also included a visco-elastic creep element which will be discussed below.

G. Visco-elastic Creep Using Loaded Wafers

1. Conditions for the Tests and Equipment.

The tests were conducted using samples which were conditioned to one of three different humidity levels corresponding to 18.5, 11.5, and 7.3 percent EMC. The temperature was maintained at 110° F for all humidity levels. At each level, the samples were loaded to one of three levels corresponding to 10, 20, or 30 percent of the average failure strength of red oak which was assumed to be 775 psi based on the results of tests performed for this study. Initial plans called for at least 5 samples to be tested at each load level and relative humidity condition. Due to difficulties with the experimental method, the plans were modified as discussed in the Results and Discussion Section.

The tests were done in the same chamber as the mechano-sorptive creep tests. The monitoring equipment and fixturing were also identical.

2. Sample Preparation.

The sample size and preliminary preparation were the same as in the mechano-sorptive creep tests. After cutting, the green wafers were conditioned at one of the three relative humidity levels for a two week period prior to use.

Immediately before testing, the samples were removed from the conditioning chamber, weighed, and wrapped in multiple layers of "Saran" wrap to prevent moisture gain during the tests. Once wrapped, the fixturing was applied as in the mechano-sorptive creep tests.

3. Test Procedure.

The basic test procedure was identical to that which was outlined for the mechano-sorptive creep tests discussed above.

Once loaded, the samples were strained for 2 or 3 days with strain readings taken at 2 hour intervals during that time. At the end of the period, the load was removed and "recovery" readings taken for about 10 minutes or until the readings were stable. At the end of the test, the fixturing was removed and the samples were reweighed, dried, and their final moisture contents determined.

H. Acoustic Response Tests.

1. Conditions for the Tests and Equipment

In order to determine the acoustic response at the surface of the red oak, green wafers were tested to failure under third point loading conditions as shown schematically in Figure 16.

During testing, the wood surface acoustic emissions were monitored using an Acoustic Emissions Technology Model 204B monitoring system with a lead-zirconate piezoelastic transducer and a resonant frequency of 175 kilohertz. The threshold voltage was set at about 1 volt (DC) and was adjustable between zero and 5 volts DC. Gain for all tests was set at 90 dB and the rate of emissions per 10 second period was monitored during loading.

Testing was done with green wafers under ambient conditions and

loaded using an Instron model TMML testing machine. The rate of loading was about 0.1 cm/min. for all tests.

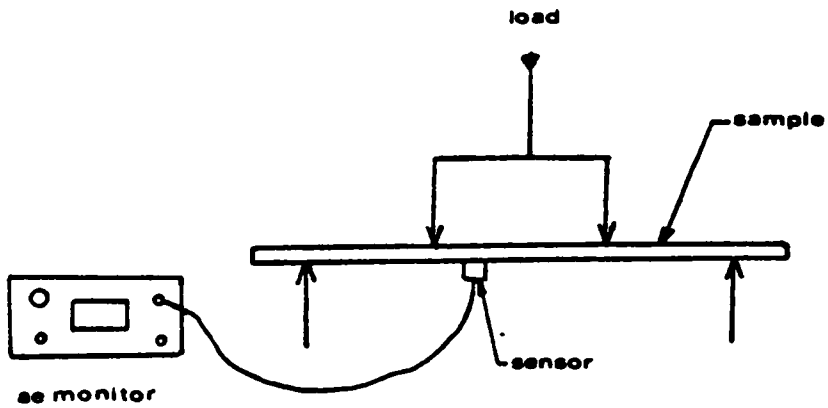

Figure 16. Schematic illustrating the set-up used for the acoustic tests. The sensor was attached to a thin, flat piece of spring steel which rested on the sample.

During testing, the acoustic emission rate, the time since the beginning of the test and the sample deflection were monitored using a Hewlett-Packard Model 3421 data acquisition system. Separately, a graph of load versus times since the beginning of the test was prepared using an X-Y recorder. Using time as the common basis, the information from both sources was correlated manually to produce graphs of load versus deflection and acoustic emission levels.

2. Sample Preparation.

Approximately 40 wafers, each measuring 1 inch along the grain by six inches in the tangential direction by 1/4-inch thick, were prepared from green oak. The ring angle was kept as close to zero degrees as

possible. Samples were wrapped in plastic and kept at room temperature prior to test.

3. Test Procedure

Samples were placed in the third point loading apparatus and the sensor was positioned as illustrated in Figure 16. A slight preload was applied prior to testing to remove the system "backlash". Once preloaded, the test was started and the samples were tested to failure while the acoustic emission rate, time, load, and deflection were recorded as described above.

RESULTS AND DISCUSSION

A. Moisture Gradient Tests

1. Moisture Gradient Test Results

The moisture content values for the 96 wafers sawn each day were grouped by position such that each of the eight positions within the drying board was represented by 12 wafers. The average moisture content of the 12 wafers was assumed to represent the moisture content at the center of the wafer for that day of drying. A schematic of the averaging process is shown in Figure 17.

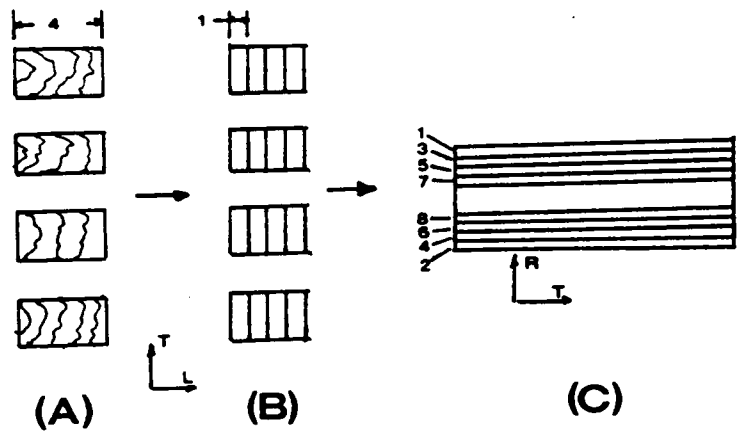

Figure 17. (A) Four 4-inch samples were taken from the 30-inch long boards shown in Figure 11. (B) Each 4-inch board was sawn into three 1-inch samples and a moisture content sample. (C) A cross-section of a one-inch sample. Eight wafers were sawn from the 12 samples. The 12 samples yielded 96 wafers/day.

Two additional data points were generated by assuming the moisture content at each surface was equal to the equilibrium moisture content for the given conditions. Using this information, graphs were prepared showing the moisture profiles for each day at each of the three relative humidity conditions. Composite graphs of this information with the data points connected by drawing a smooth curve are shown in Figures 18-20.

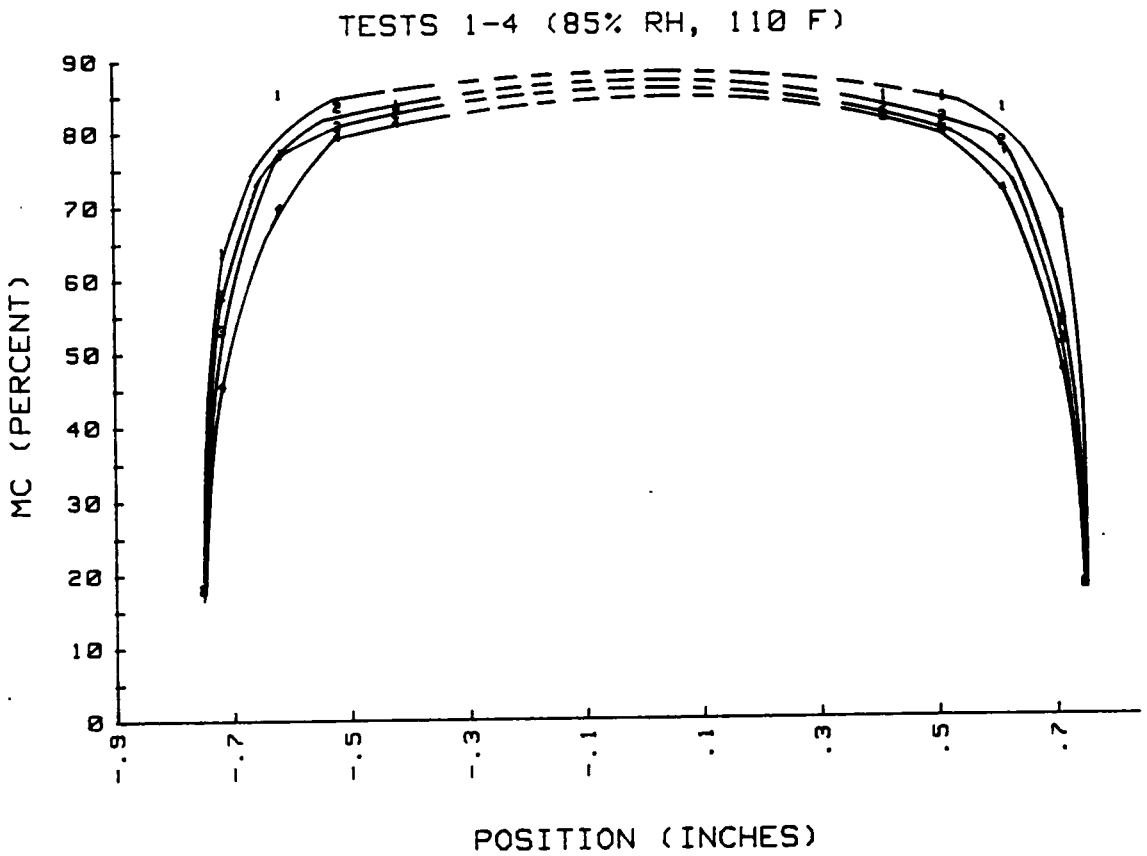

Figure 18. Moisture gradients developed during first four days of drying at 85 percent RH. Small numbers refer to number of days since drying began. The dashed lines are speculative.

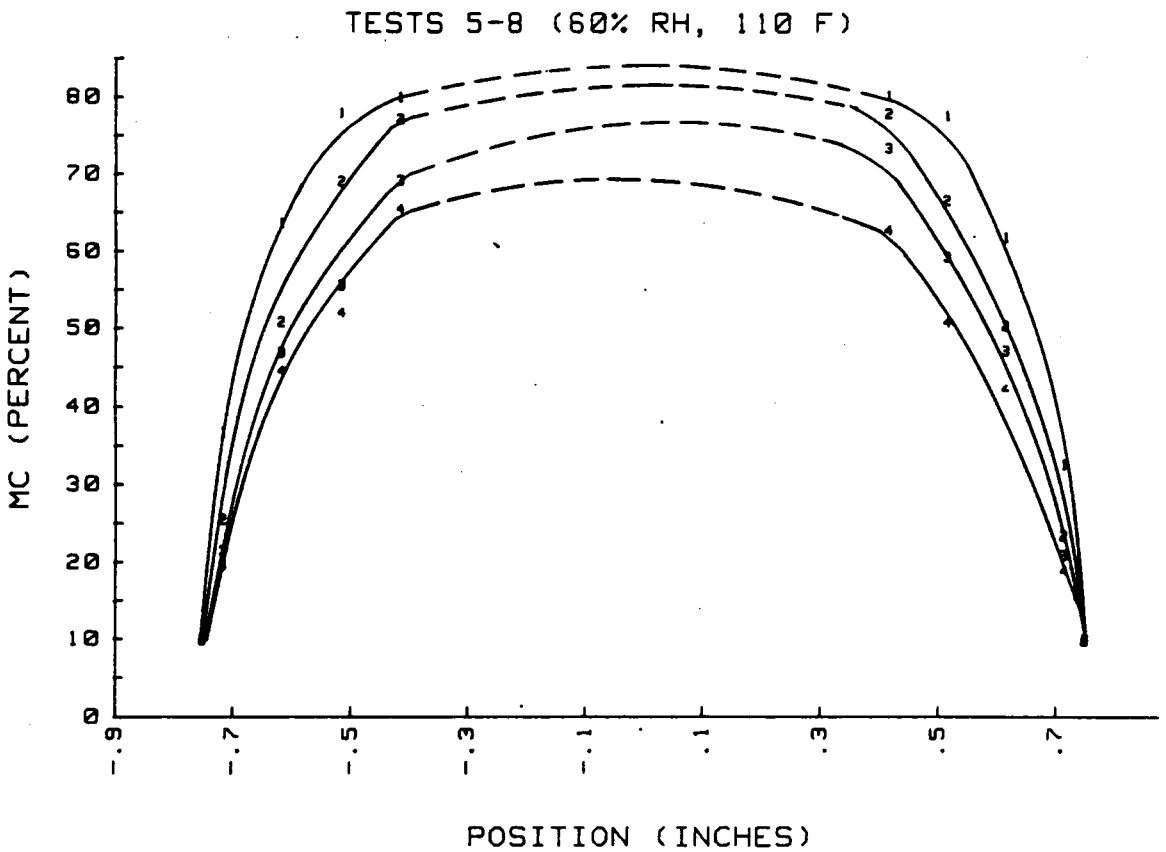

Figure 19. Moisture gradients developed during first four days of drying at 60 percent RH. Small numbers refer to number of days since drying began. The dashed lines are speculative.

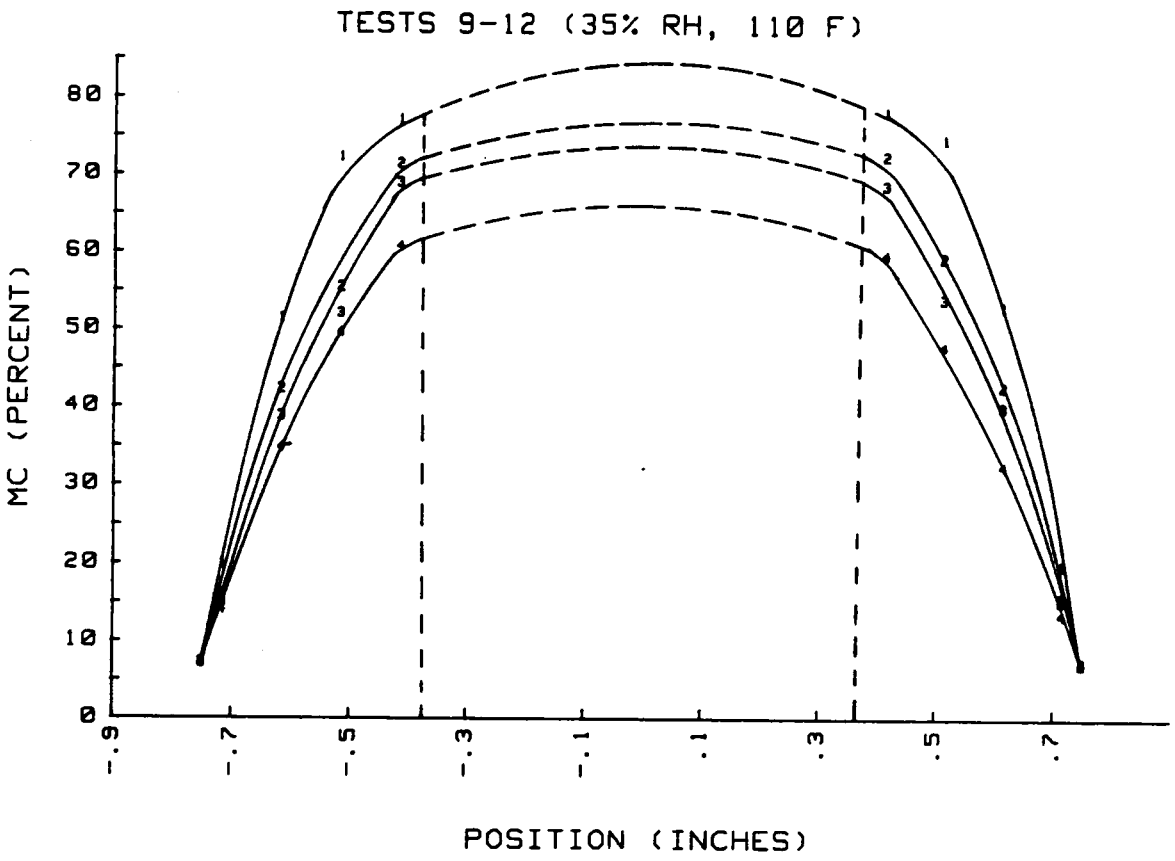

Figure 20. Moisture gradients developed during the first four days of drying at 35 percent RH. The small numbers refer to the number of days since the beginning of drying. The vertical dashed lines are the "zero" points for the equations in Table 2.

Once the moisture gradient profiles were established, equations of moisture content as a function of position were developed using a least squares polynominal regression procedure. Curves were fit to the bark side as well as the pith side resulting in two equations for each day of drying. For convenience in analysis, it was assumed the inside edge of the innermost wafer represented position zero. The equations are presented in Table 2.

To show the effect of drying conditions, composite graphs were prepared (Figs. 21-24). Each of the graphs illustrates the moisture gradient profile from each of the three relative humidity conditions superimposed on a single plot. Each of the four graphs represents one day of drying.

Table 2. Equations Determined from the Moisture Gradient Data

Day	RH (%)	Side	Equation	C.D. (R^2)
1	85	Pith	$MC = -10258X^3 + 5009.9X^2 - 662.8X + 102.9$	.928
		Bark	$MC = -9899.7X^3 + 4713.6X^2 - 599.2X + 100.12$	.963
2	85	Pith	$MC = -1033.4X^2 + 260.3X + 71.7$	.917
		Bark	$MC = -1105.3X^2 + 294.1X + 70.52$	.896
3	85	Pith	$MC = -1044.15X^2 + 262.9X + 71.08$	.939
		Bark	$MC = -1003.4X^2 + 246.2X + 72.72$	.920
4	85	Pith	$MC = -895.8X^2 + 197.2X + 73.74$	.958
		Bark	$MC = -860.7X^2 + 181.4X + 74.24$	.966
1	60	Pith	$MC = -830.6X^2 + 137.7X + 75.7$	.992
		Bark	$MC = -872.92X^2 + 161.5X + 74.3$	.981
2	60	Pith	$MC = -444X^2 - 18.6X + 78.66$	.998
		Bark	$MC = -505.5X^2 + 8.5 + 77.5$	.997
3	60	Pith	$MC = -342X^2 - 45.4X + 74.3$	.994
		Bark	$MC = -361.5X^2 - 22.63X + 68.96$	.988
4	60	Pith	$MC = -312.4X^2 - 26.5X + 62.9$	.990
		Bark	$MC = -326.06X^2 - 27.5X + 65.4$	.986
1	35	Pith	$MC = -685.6X^2 + 60.73X + 77$	.998
		Bark	$MC = -630.87X^2 + 43.5X + 76.82$	.999
2	35	Pith	$MC = -316.0X^2 - 67.94X + 75.04$	.998
		Bark	$MC = -264.95X^2 - 82.79X + 73.84$	.995
3	35	Pith	$MC = -243.58X^2 - 83.41X + 71.22$	.997
		Bark	$MC = -179.53X^2 - 109.06X + 72.2$	.996
4	35	Pith	$MC = -154.73X^2 - 95.43X + 63.3$	.999
		Bark	$MC = -218.2X^2 - 72.7X + 63.5$	.999

X = position (inches). The point X = 0 is shown in Figure 20.

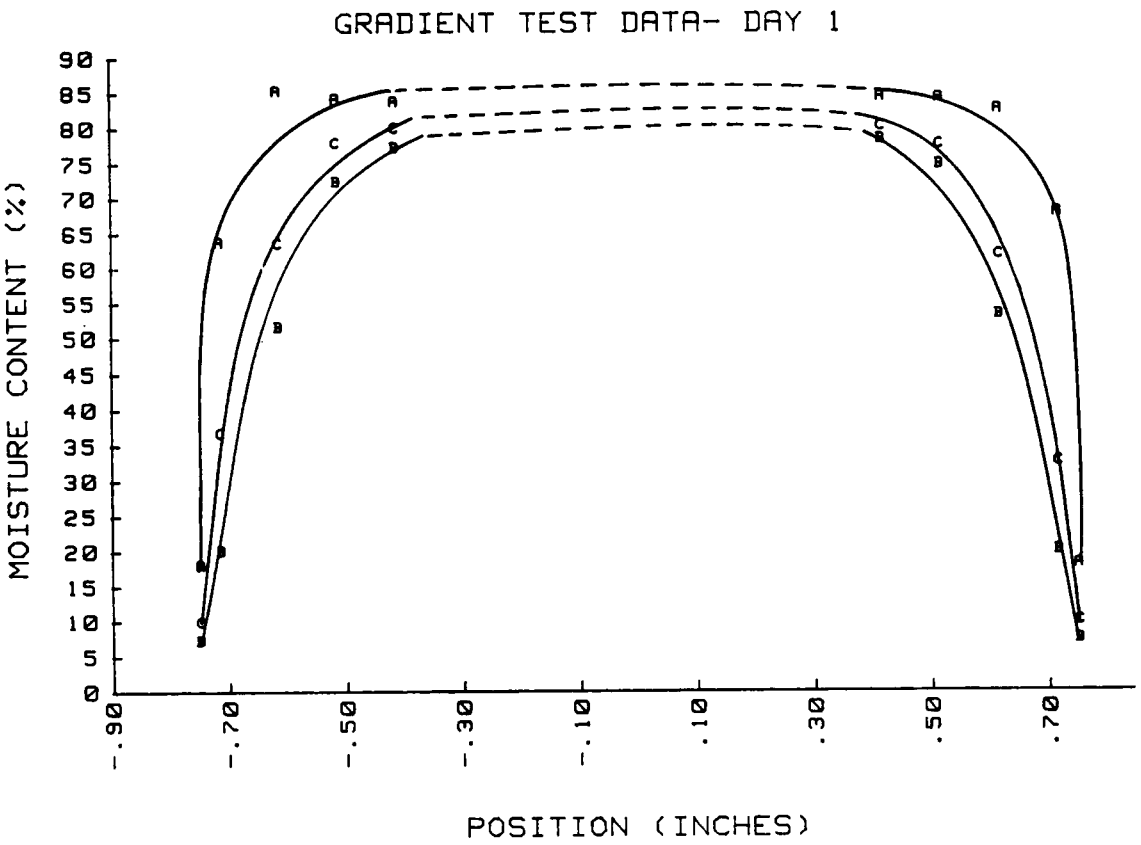

Figure 21. Composite graphs showing the moisture gradients for day 1 of drying at each RH condition. The outermost curve is the 85 percent RH condition and the innermost curve is the 35 percent RH condition.

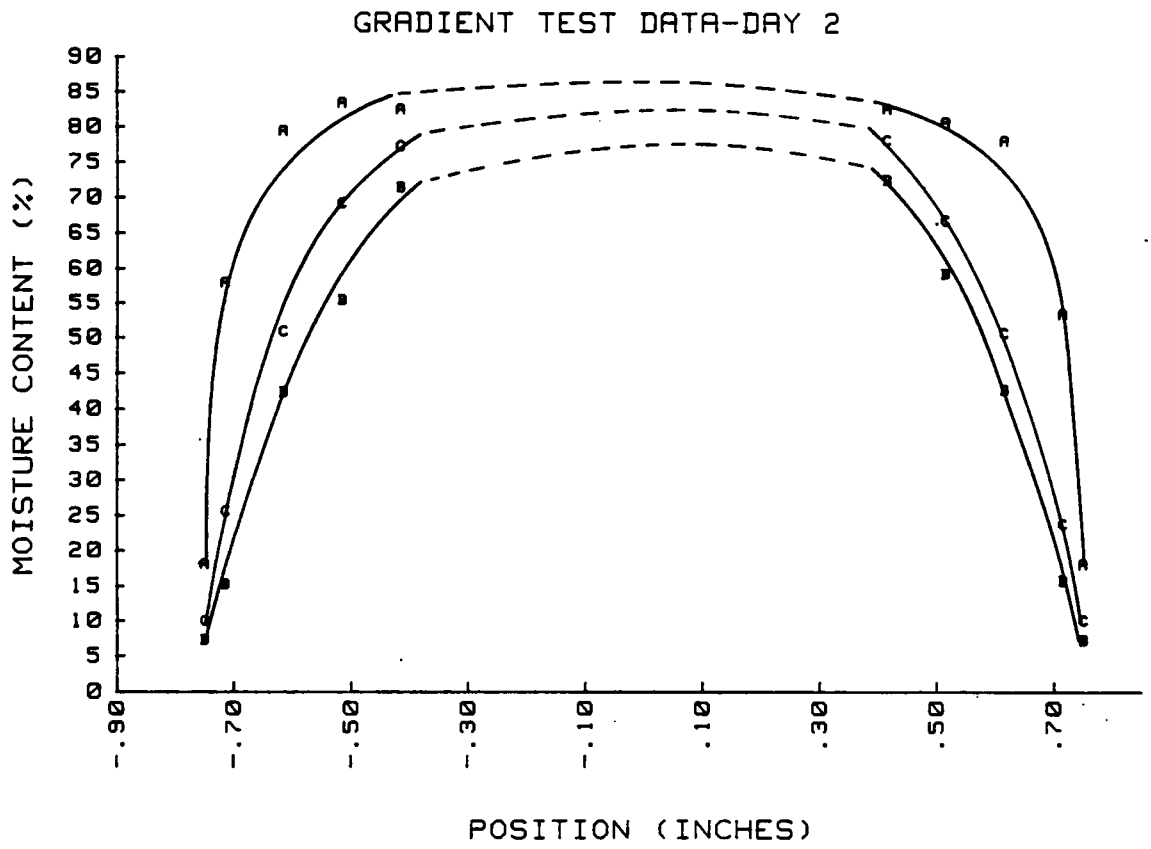

Figure 22. Composite graphs showing the moisture gradients for day 2 of drying at each RH condition. The outermost curve is the 85 percent RH condition and the innermost curve is the 35 percent RH condition.

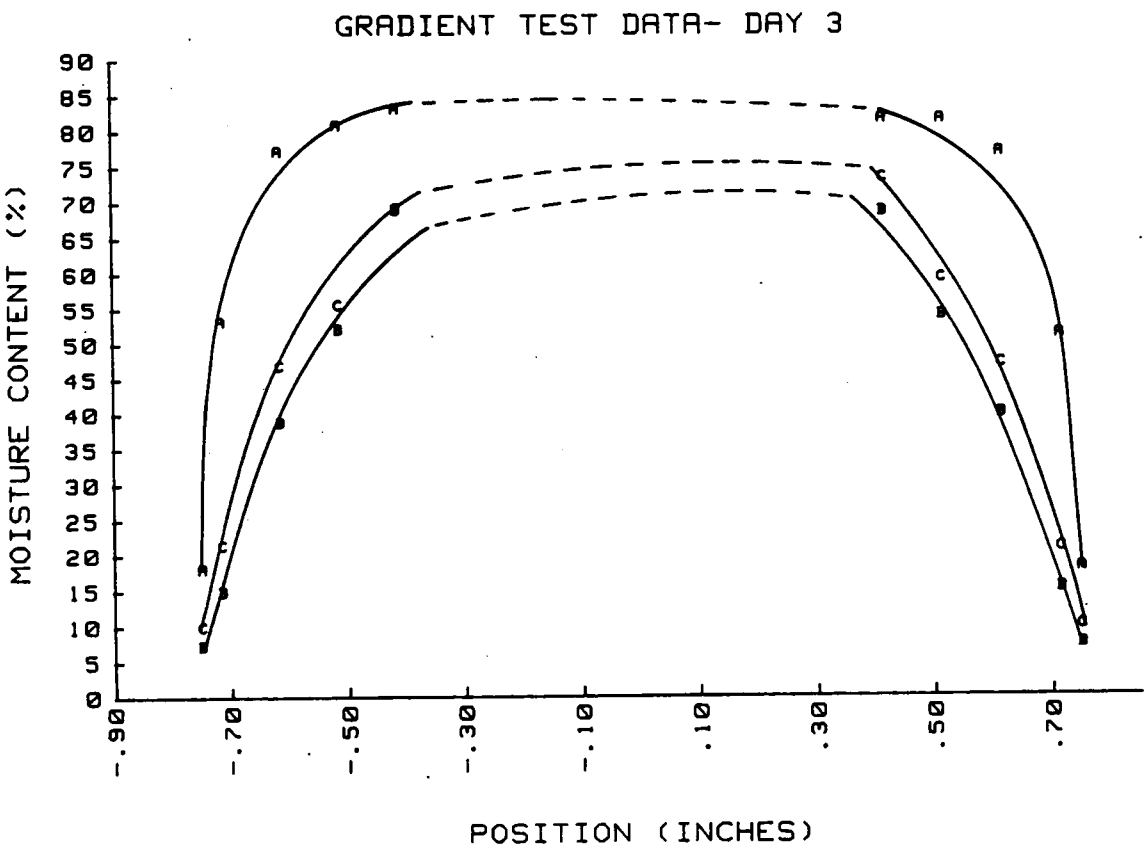

Figure 23. Composite graphs showing the moisture gradients for day 3 of drying at each RH condition. The outermost curve is the 85 percent RH condition and the innermost curve is the 35 percent RH condition.

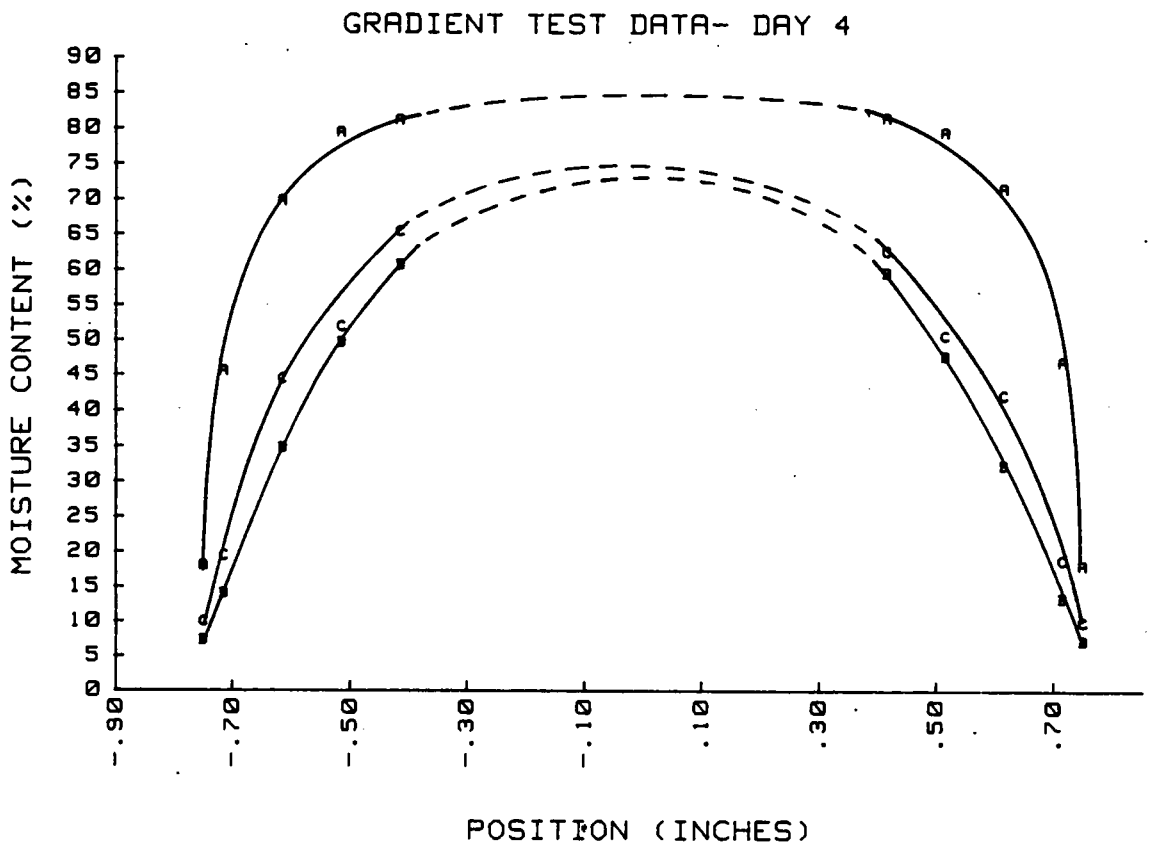

Figure 24. Composite graphs showing the moisture gradients for day 4 of drying at each RH condition. The outermost curve is the 85 percent RH condition. The innermost curve is the 35 percent RH condition.

2. Discussion of Moisture Gradient Results

One of the principal reasons for performing the moisture gradient tests was to determine the moisture profile to be modeled in the computerized simulation. In general, the profiles which occur in drying wood are parabolic in shape and represent appreciable amounts of both capillary flow and diffusion as discussed above. Little information was available in the literature to indicate how quickly the moisture profiles developed after the commencement of drying in red oak. Since this study was confined to the first four days of drying, and a major part of the research effort involved simulating the moisture profile in order to predict stress development, it was imperative to determine how quickly the parabolic profiles developed.

The central portions of the curves shown in Figures 18-21 are estimated due to the lack of data from the center of the board. The graphs clearly illustrate that continuous profile develops within the first 24 hours of drying. The profile appears to be confirmed by parabolic for nearly all the equations of Table 2. The single exception to the parabolic shape is curve for the first day of drying at the highest relative humidity condition. In this case the curve flattens considerably toward the center of the board indicating that little or no drying occurred.

The exception to the parabolic profile and the generally low moisture loss during the early stages of drying may be the result of the way in which the samples were handled. The samples were removed from the 40° F conditioning room, prepared as described above and placed in the drying oven while still cold. This practice was followed in order to prevent drying which may have occurred if the samples were allowed to

come to room temperature before preparation. Although effective in preventing drying of the samples during preparation, the initial period in the drying chamber probably resulted in little or no moisture loss since energy was expended in heating the samples and in removing condensate which developed when the cold samples were placed in the warm, humid drying chamber.

Although the shapes are generally parabolic, the profiles which develop from day to day under different relative humidity conditions are quite different. The two major effects are most clearly seen in Figures 21-24.

The first, and most obvious, effect is that the moisture loss is related directly to the relative humidity of the environment. Within the first 24 hours, appreciable drying has occurred at depths which are at least 0.350 inches inward from the surfaces. The moisture loss becomes more pronounced with each passing day and is always in proportion to the ambient relative humidity. The equilibrium moisture content, which determines the steepness of the moisture gradient is assumed to be "driving force" for moisture movement. It is evident, particularly in Figures 23 and 24, that more moisture loss has occurred at the 60 and 35 percent relative humidity levels. The result is that the profiles from the higher EMC condition are quite different due primarily to the lower moisture loss from the interior of the wood. In reviewing the graphs, it must be remembered that all the tests were done under isothermal conditions. The effect of temperature on moisture movement is pronounced and a general discussion may be found in Siau (1984).

A second, and less obvious effect, is the gradual drop and leveling

in each curve with each passing day. The overall drop and the leveling of the curves is indicative of the reduction of the moisture gradients and results from free water movement from within the wood. As the curves become less steep, the drying stress levels would tend to be reduced.

A major consequence of the parabolic shape is confirmation that the moisture profile during the early stages of drying was continuous. Therefore both pure diffusion and free water movement are occurring simultaneously (Fig. 1b). Moreover, the continuous pattern found early in drying provided evidence that the gradient portion of the computerized simulation could be modeled using Fick's second law.

3. Transport Coefficient Results

Although the solution of Fick's law provides a curve which has the same general shape as shown in Figures 18-20, the specific profile for a given situation is determined using a transport coefficient which is a function of one or more parameters. The use of Fick's law to simulate the moisture profile required that the variation of the transport coefficient with moisture content at all levels be known. Egner's method, described in detail below, was used to determine the transport coefficient for the entire range and the results at each of the three relative humidity levels are presented in Figure 25.

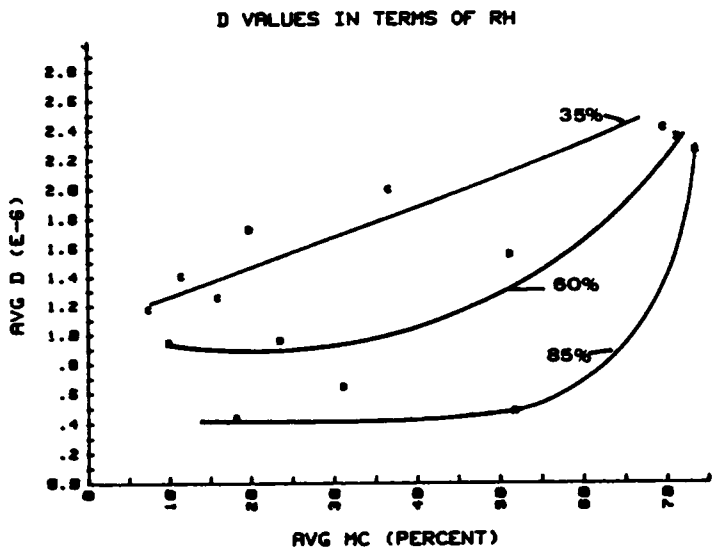

Figure 25. Average transport and moisture content values for each relative humidity condition. The units of D are cm^2/sec.

A review of the graph will indicate the magnitude of the transport coefficient does not change appreciably with relative humidity conditions. Therefore the data were combined and a composite graph prepared as shown in Figure 26.

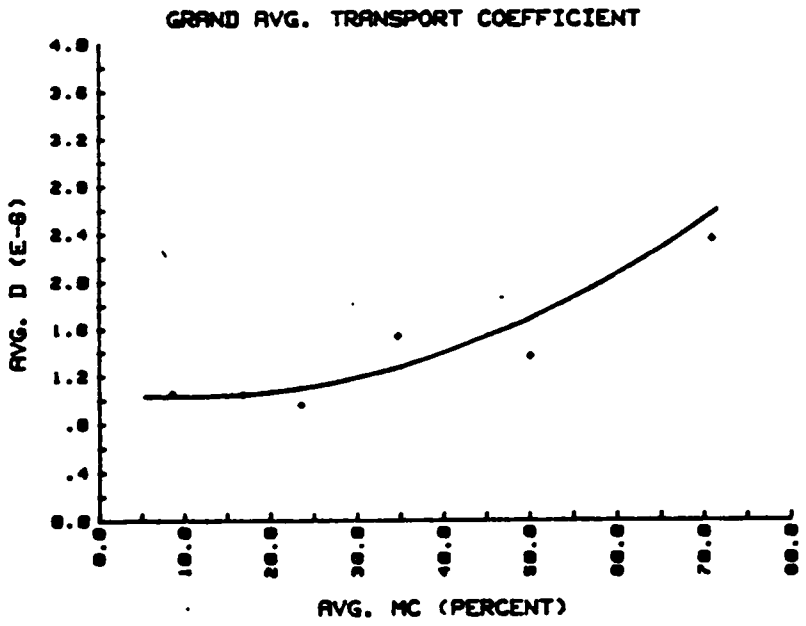

Figure 26. Grand average transport coefficient curve.

Using at least squares polynominal regression analysis, the data from Figure 27 were analyzed. The relationship which resulted is as follows:

Eq. 13

$$\overline{D} = .8X10^{-5}(MC)^3 - .54X10^{-3}(MC)^2 + .02(MC) + .84 \qquad R^2 = .895$$

Where MC is the moisture content, in percent.

4. Discussion of the Results.

Egner's method (1934) uses a form of Fick's first law to determine the unsteady state transport coefficients from moisture profiles such as those shown in Figures 18-21. The method is illustrated in Figure 27. Part (a) of the figure is a one-dimensional representation of the moisture profiles taken at two different times. The point zero represents the board center and (a) is the surface of the board.
The shaded area represents the integral:

$$\int_{\bullet}^{x} C dX \qquad \text{Eq. 14}$$

In part (b) of the figure, the difference integral representing the area between the two curves is shown. Dividing the integral by the time difference represents the moisture flux past point X in the given time period.

Part (c) of the curve represents the slope of the moisture gradient at point x. Using the information from parts (a) and (b) of the figure, the transport coefficient may be represented as the flux/gradient as shown in part (d).

Egner's method uses the cumulative flux from the center of the board and only the moisture contents from the eight slices taken from the surfaces inward were available from the moisture gradient tests. To overcome this difficulty, the data points were plotted and a smooth curve drawn to connect all of the data points. The moisture content at the center of the boards was inferred from the graphs and a linear extrapolation was performed from the innermost known data points to the assumed

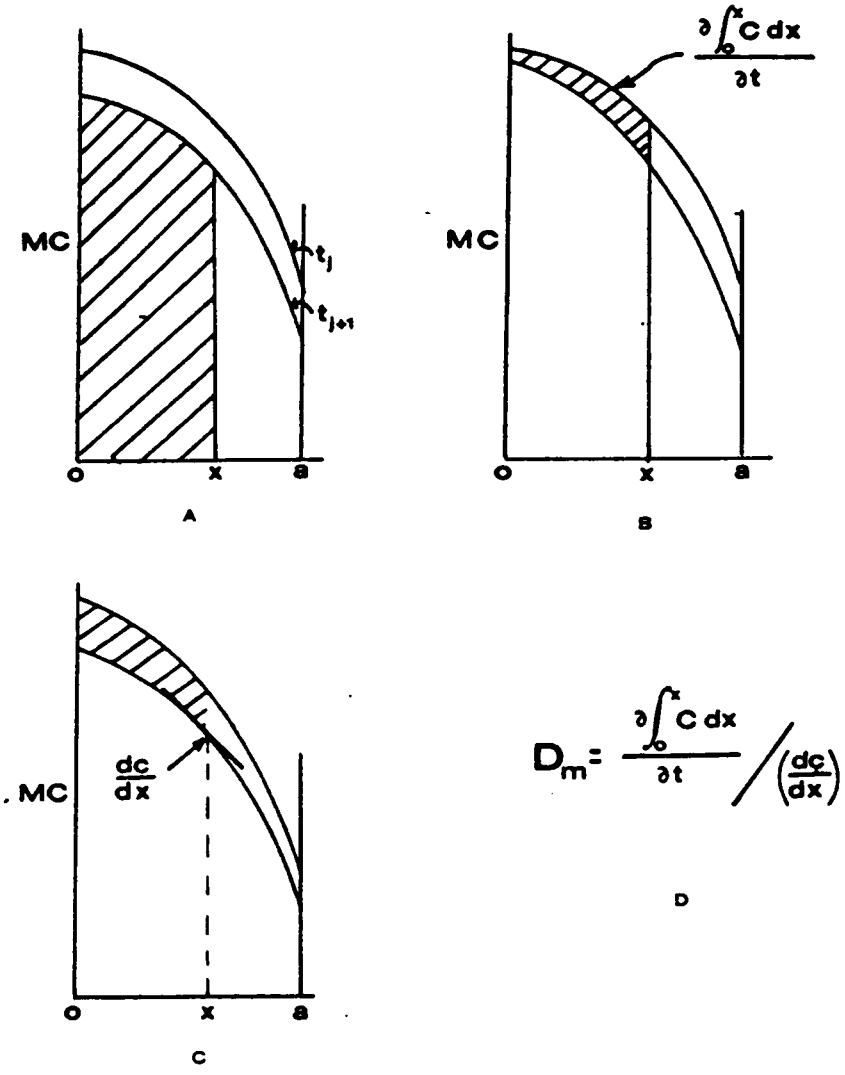

Figure 27. Diagrams illustrating Egner's method. (A) One-dimensional moisture gradient curves showing the gradient at two different times. (B) The flux as illustrated by the area between the two curves. (C) The slope of the gradient. In practice, an average slope was used. (D) The transport coefficient is given as Flux/gradient.

moisture content at the center of the boards.

To determine the transport coefficient for a given 24 hour period, the area between the linear portions was added to the area between the non-linear portions. The value of the gradient at a given value of x was an average of the gradient at t_j and the gradient at t_{j+1}.

The transport coefficients were determined for the drying curves representing days 1-2, 2-3, and 3-4 for each relative humidity condition. The positions at which the coefficients were determined correspond to centers of the wafers. For convenience in analysis and to reduce some of the variation in the data, average transport coefficients and moisture contents were determined for the following moisture content ranges: >60, 40-60, 30-40, 20-30, 10-20, and 0-10. The average moisture content and transport coefficients for each relative humidity condition are those plotted in Figure 25 and the combined average data from all relative humidity conditions are those illustrated in Figure 26.

The general shape of the curve shown in Figure 26 is indicative of the rate of moisture loss which is occurring at the various moisture content levels. Early in the drying process the curves are non-linear and represent a high rate of moisture loss. Much of this moisture loss is the result of free water movement early in drying (Kollman and Cote, 1968).

As the moisture content approaches the fiber saturation value at about 30 percent, the curve tends to level and the transport coefficient appears quite linear. The general pattern indicates the moisture loss rate is slowing and is most likely the result of the moisture loss mechanism being governed more strongly by diffusion.

The magnitudes of the measured transport coefficients are in general agreement with values reported in the literature (Siau, 1984). However, nearly all the transport coefficients reported in the literature are applied to either steady-state conditions or to moisture movement below fiber saturation. Very little information could be found which describes the magnitude of the transport coefficient above fiber saturation and no information could be found which reported values for the coefficient above fiber saturation early in drying. The only transport coefficient values above fiber saturation known to the author are those reported by Voight et al. (1940). Those curves are generally similar in shape to the curve shown in Figure 26.

B. Strength Tests

1. Results of the Strength Tests.

The primary use for the data obtained from the strength tests was to develop sampling distribution of failure stress. The intent was to use a relationship derived from the sampling distribution as the model for failure criteria in the computerized simulation.

A histogram of the measured failure strengths was prepared to determine the general shape of the measured sampling distribution. Subsequently, a three parameter Weibull curve was superimposed to indicate the general fit or lack of fit to the measured data. The result is shown in Figure 28.

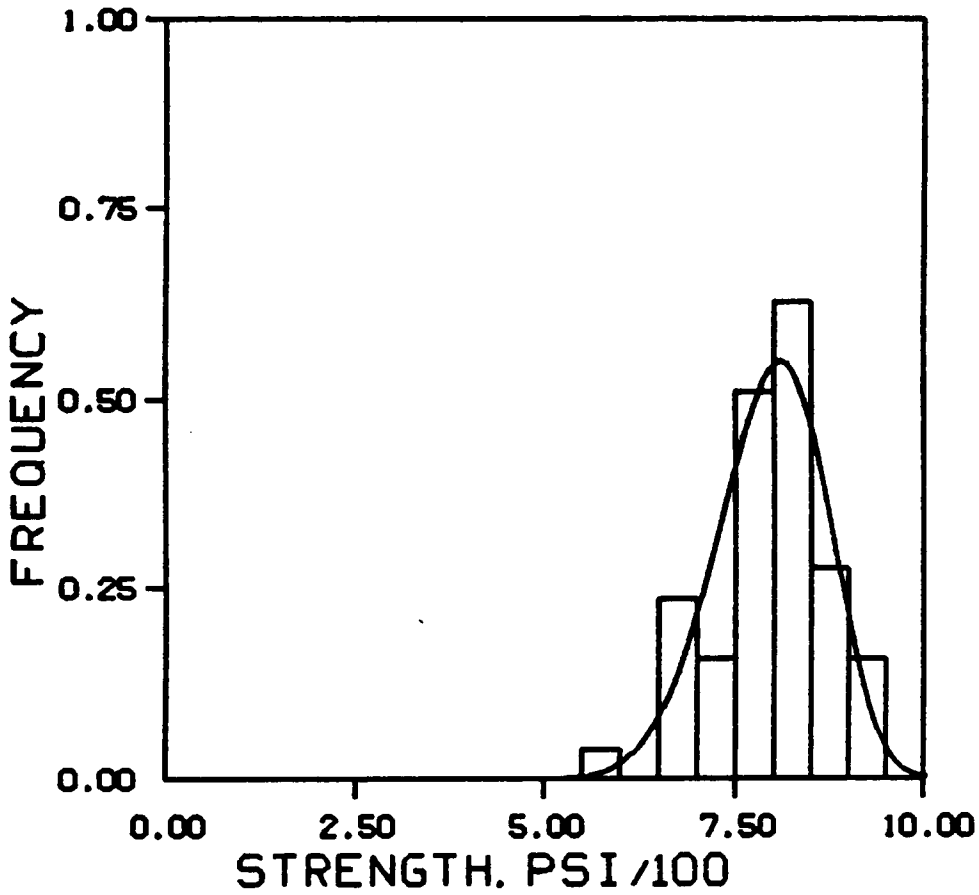

Figure 28. Histogram of the failure data with a Weibull curve superimposed.

To determine the failure criteria, a Weibull probability plot was prepared from the strength data. This correlates the measured strength

with the cumulative percentage of failure and provided the basis for a linear model of stress versus failure percentage (Figure 29).

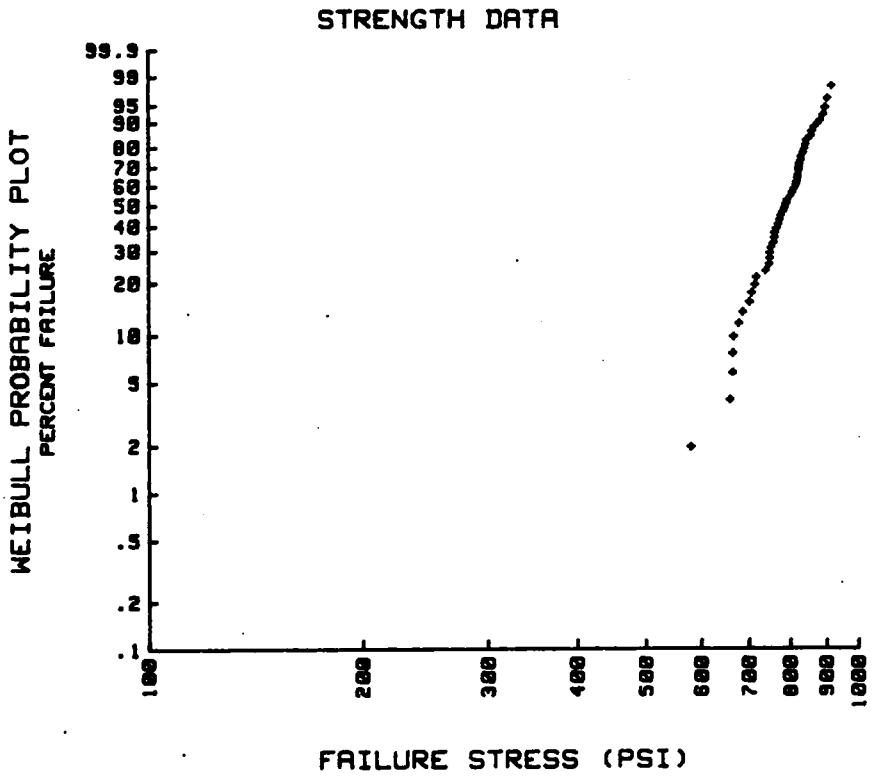

Figure 29. Weibull probability plot of the strength test data.

A regression analysis was performed using data taken from this plot to determine the relationship between the percentage of samples which failed and the failure stress. The failure criterion which resulted

from this analysis is shown as Equation 15.

$$prf = .216(stress)-116.47 \quad R^2 = .841 \qquad \text{Eq. 15}$$

$$540 < stress < 1000.0$$

Where prf is the probability of failure in percent and stress is the measured or calculated stress in psi.

2. Discussion of the Results.

Prior to determining the distribution of failure strength, samples which had failed at or near the grips and samples whose ring angle differed significantly from zero based on the visual examination were eliminated. Of the original 83 wafers, 51 remained after completion of this editing step.

The 51 wafers actually represented two different types of failures which were then separated into two groups for comparative analysis. Those samples which failed at the knife edges of the extensometer comprised the first group while samples which failed within the 2-inch gage length were placed in the second group.

The mean failure strength for the knife edge failures was 809 psi and the standard deviation was 76 psi. Those samples which failed within the gage length had a mean failure strength of 776.0 psi and a standard deviation of 67.

A paired "t-test" (Ott, 1983) was performed on the two groups of data in order to determine if the knife edge failures differed significantly in strength from those samples which failed within the gage length. The test results indicate the means of the data sets did not

differ significantly at the 5 percent level and therefore it is reasonable to assume the data sets are representative of the same population. Based on this result, the two data sets were combined and all further analysis was done using the combined data set.

An underlying assumption in the determination of equation 15 is that the data distribution follows a Weibull distribution. The histogram shown in Figure 28 generally approximates a skewed bell-shaped curve ... would be expected of a Weibull distribution, but the general shape ... a certain extent, on the choice of the cell size and to a ... on the sample size which was tested. To test the assump- ... Weibull distribution, a chi-square test was performed. The ... dicated that a three parameter Weibull curve was acceptable at ... level. As illustrated by the probability plot shown as Figure 29, ... data appears to be quite linear and the regression analysis performed shows a distinctly linear pattern.

C. Unrestrained Shrinkage Tests

1. Results of the Unrestrained Shrinkage Tests.

The moisture content and tangential shrinkage values taken were analyzed using a least squares linear regression analysis procedure (Ott, 1983). The resulting equation is as follows:

$$shk\ (\%) = -.3437*(MC) + 9.345 \quad R^2=.92 \qquad \text{Eq. 16}$$

Where: shk is the tangential shrinkage in percent and MC is the moisture content in percent.

The range of applicability for the equation is from zero to about 30 percent moisture content.

2. Discussion of the Results.

The initial plots of tangential shrinkage versus moisture content showed considerable variation and no strong mathematical relationship between the two variables could be found using linear or polynominal regression techniques. Because of this, an analysis was done to determine the sources of the variation. The result was that two primary causes were identified.

First, ten samples appeared to have non-zero ring angles when measured with respect to the tangential direction. Although in most cases the ring angle variation was estimated as being less than 20 degrees, the effect on shrinkage was significant and the variability in the data, as measured by the coefficient of variation, was decreased by approximately 50 percent when the data points were deleted from the analysis.

Once this source of variation was identified, the data was edited to remove the samples with non-zero ring angles. This severe step is perhaps best justified by a brief discussion of the end use of Equation 16. As illustrated by Figure 5, the value of mechano-sorptive creep is given by the distance between "dry lgt" and "basic shk" and the primary purpose of these experiments was to find a relationship between moisture content and shrinkage which could be used to establish a value for "basic shk" at any moisture content. The samples used to determine values for "dry lgt" were carefully chosen such that the ring angles were approximately zero. Therefore, deleting the non-zero ring angles

from the basic shrinkage data insured that the calculation of mechano-sorptive creep came from samples which had the same ring orientation.

The second source of variation centered on the data obtained at the highest humidity condition (85 percent RH). In general, the data variation was approximately double that of any other relative humidity level. Variation of shrinkage and moisture data at high relative humidity levels is quite a well known phenomenon in red oak and Stamm (1964) has suggested it is the result of two principal causes. First, at high humidity conditions, condensation is likely to occur in the microcapillaries and voids causing the moisture content to increase above the expected equilibrium moisture content value. The effect is not uniform and depends on the surface preparation and the anatomical structure of a particular sample. Second, in some cells, collapse may occur above fiber saturation due to capillary tension and cause the measured shrinkage values of the small samples to appear larger than expected.

The second editing step was to delete all data taken at the 85 percent relative humidity condition. The step, taken because of the advice of more experienced researchers, removed much of the variability while not drastically affecting the linearity of the shrinkage/moisture content relationship.

After the data were edited, graphs of shrinkage versus moisture content were prepared for each sample. Then a "fiber saturation point" for each sample was determined using a linear extrapolation. This point was added to the data set and included in the linear regression analysis leading to Equation 16. A graph of the data used in the final regression analysis is shown in Figure 30.

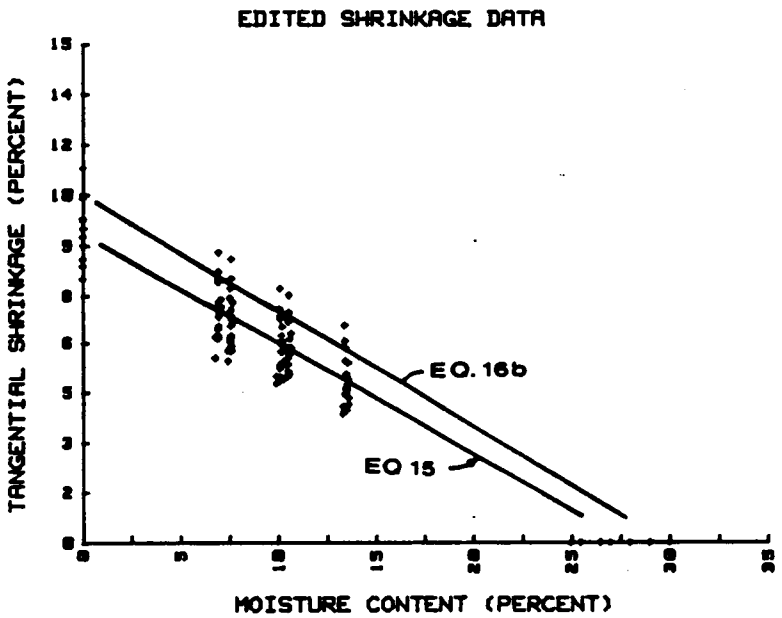

Figure 30. Graph of the edited shrinkage data used for analysis. The lines are a comparison between the Wood Handbook (USDA, 1987) equation and the results of these tests.

Despite the severe editing, the final relationship as expressed by Equation 16 seems to agree well with established values. The Wood Handbook (USDA, 1987) lists the range of values for the tangential shrinkage of various red oak species as between 8.6 and 11.3 percent. The average for the eight species listed is 10.07 percent which compares well with the value of 9.3 percent shown in the intercept of Equation 16.

Another comparison may be made using the following shrinkage formula taken from the Wood Handbook (USDA, 1987) which is used to calculate the percentage shrinkage at any moisture content less than 30 percent.

$$S = S_o\ (30-MC)/30 \qquad \text{Eq. 17a}$$

Using the average shrinkage value for S_o the formula becomes:

$$Shk\ (\%) = -.34(MC) + 10.07 \qquad \text{Eq. 17b}$$

A comparison of the lines represented by equations 16 and 17b is shown in Figure 30. The lines are in good agreement which indicates the experimental results are in general accord with previous research efforts.

D. Elastic Recovery Tests.

1. Results of the Tests

The results of the analysis of the elastic strain data are illustrated in the manner developed by McMillen (1955) and shown as Figures 31-37. In Figures 31-33, the data are graphed such that all the data from a given relative humidity level are shown on one graph. The num-

bers adjacent to each line represent positions from which the wafers were taken in the drying samples. Positions 1 and 2 represent the surfaces and positions 7 and 8 are the wafers in the interior as illustrated in Figure 17. In Figures 34-37 the data are grouped such that the elastic strain values from each position and from each relative humidity level are shown on a single graph. Figures 34-37 provide a ready comparison of the relative magnitudes of the strains at a given time during drying. A regression analysis was performed of the elastic strain data and other measured variables at each relative humidity level. The results are shown in Table 3.

Table 3. The equations of elastic strain as determined using a multiple linear regression analysis. EL-STR is the elastic strain in in/in; t is the time since the beginning of the drying, in hours; X is the distance from the surface in inches and ss is the mechano-sorptive strain in in/in.

Cond.	Equation	CD(R^2)
85	$EL\text{-}STR = .128X10^{-1} + .176X10^{-2}(X) - .113X10^{-4}(t) - .119X10^{-3}(MC) - .974X10^{-1}(SS)$	.954
60	$EL\text{-}STR = .628X10^{-2} - .734X10^{-2}(X) - .746X10^{-5}(t) - .389X10^{-4}(MC) - .569X10^{-1}(SS)$	.898
35	$EL\text{-}STR = .77X10^{-2} - .107X10^{-1}(X) + .252X10^{-5}(t) - .283X10^{-4}(MC) - .102(SS)$	.910

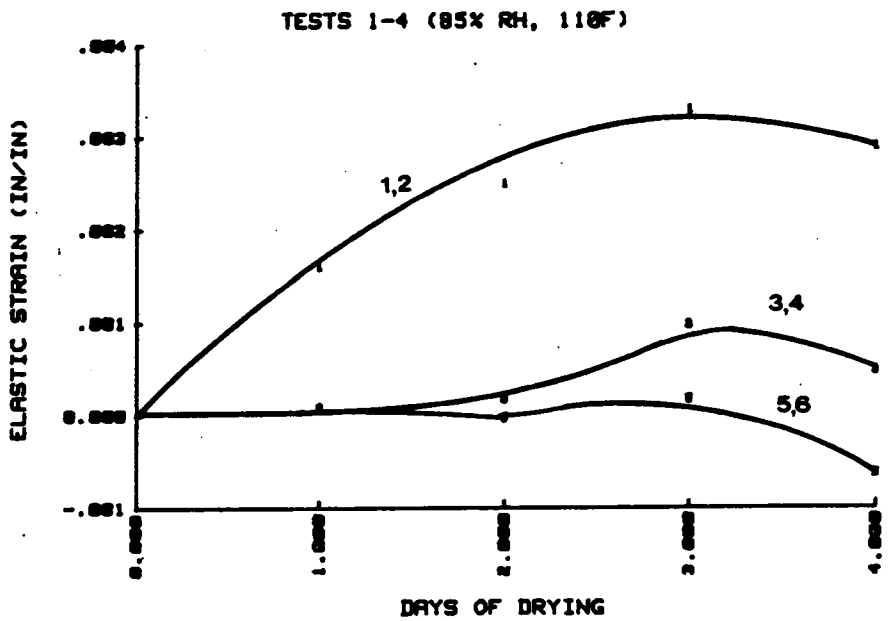

Figure 31. Elastic strain vs. time (85%). The small numbers next to the curves refer to positions.

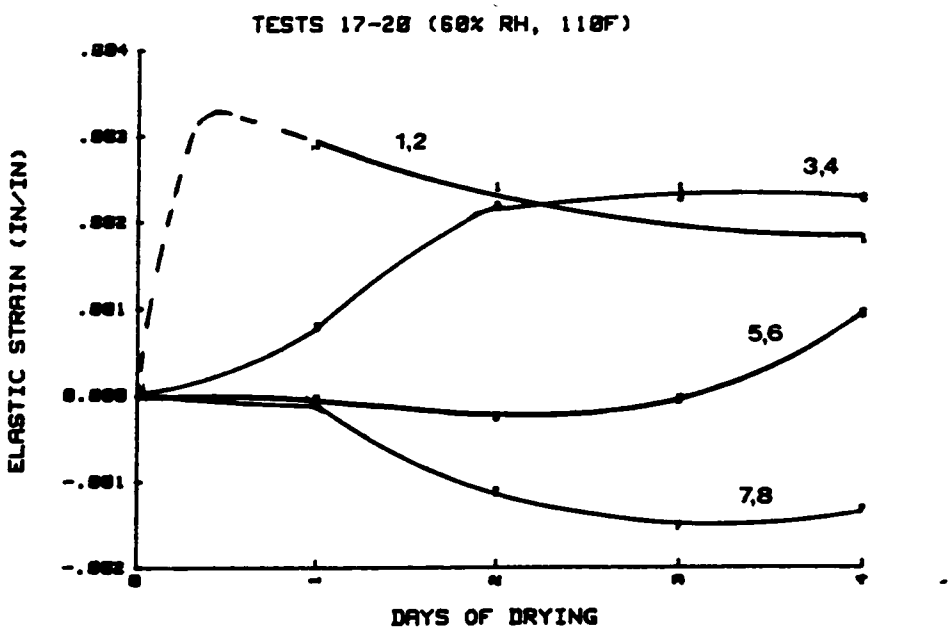

Figure 32. Elastic strain vs. time (60%). The small numbers next to the curves refer to positions. The dahsed line is speculative.

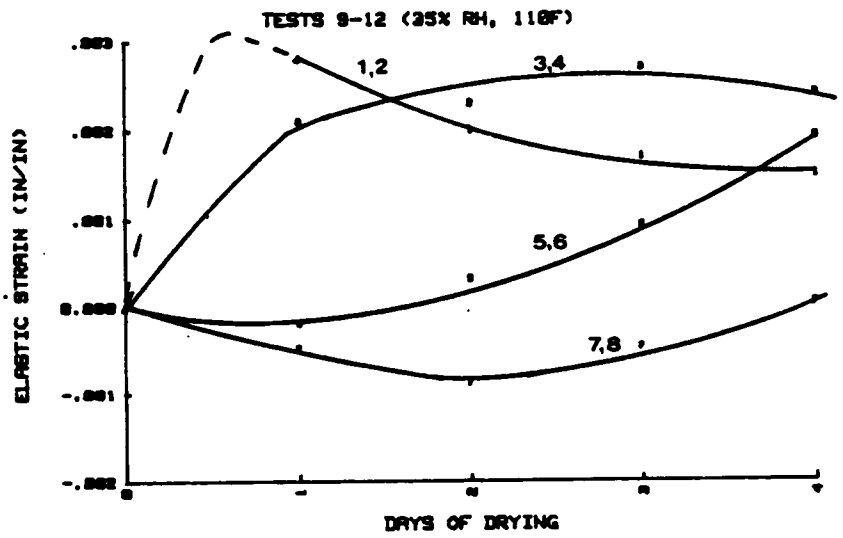

Figure 33. Elastic strain vs. time (35%). The small numbers next to the curves refer to positions. The dashed line is speculative.

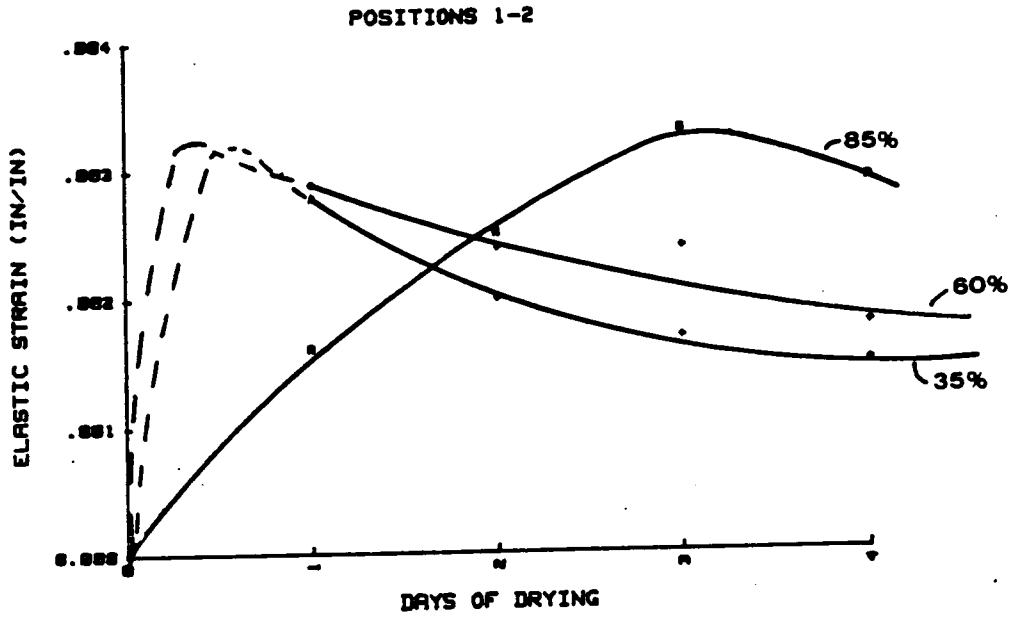

Figure 34. Composite graphs showing strain as a function of position at each RH condition (Pos. 1,2). The dashed lines are speculative.

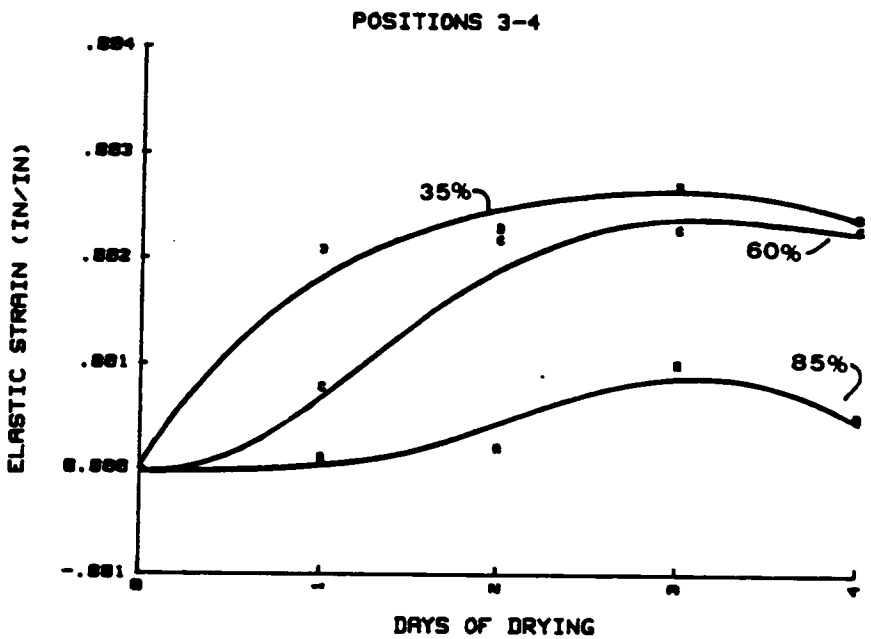

Figure 35. Composite graphs showing strain as a function of position at each RH condition (Pos. 3,4).

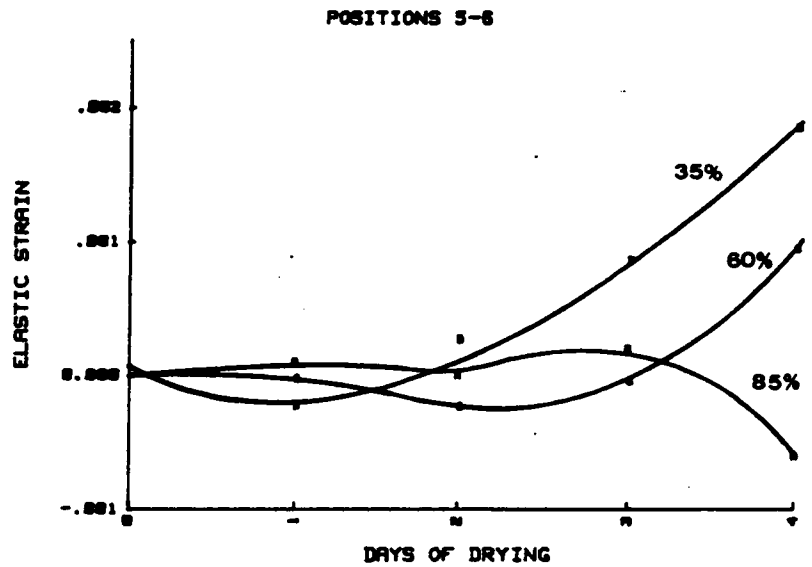

Figure 36. Composite graphs showing strain as a function of position at each RH condition (Pos. 5,6).

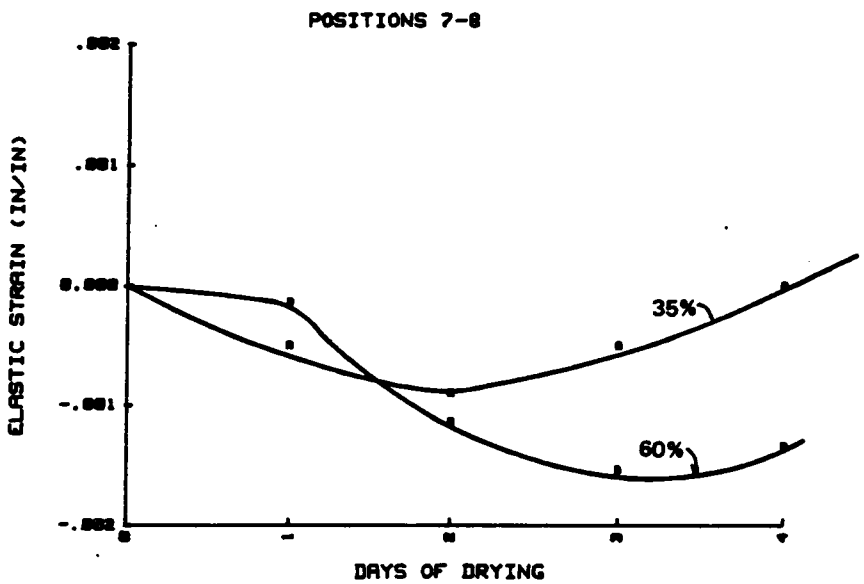

Figure 37. Composite graphs showing strain as a function of position at each RH condition (Pos. 7,8).

2. Discussion of the Results

Because of the variation in the elastic strain data, an averaging method was used for analysis. First, the data at each relative humidity level were grouped by position with the surface equilibrium moisture content representing point zero. Next, the elastic strain and moisture content of the 24 values representing each position were averaged. In the case of the data from the 85 percent RH condition, the innermost wafers (positions 7 and 8) were used as datums from which the elastic strains were measured. Therefore, no elastic strain data for these positions are shown in Figures 31 and 37. The result of the averaging process was one data point represented both the average moisture content and elastic strain value for each 24 hour period during the four days of the tests. The same data were also used to perform the regression analysis which led to the equations for elastic strain in Table 3.

The curves shown in Figures 31-37 illustrate that the surfaces reach a maximum tensile strain level quickly. At the 85 percent relative humidity level, the maximum of approximately .003 in/in occurs in about three days. For the 60 and 35 percent RH levels, the maximum tensile strains are achieved much sooner. Although the maximum tensile strain values for the 30 and 60 percent RH curves are shown as being speculative, it is quite likely that the strain peaked before the end of the first 24 hour period. Although no data are available to substantiate this, the measured values for the surface wafers at the 35 and 60 percent levels appear to be in a gradual decline after 1 day.

As drying proceeds, tensile strain development gradually moves inward in response to the change in the moisture content and the tensile

strain at the surface begins to decrease. The decrease occurs for several reasons. First, in response to moisture loss, mechano-sorptive creep strain begins to develop and acts to reduce the tensile stress. Another reason is that the moisture loss from within the wood tends to reduce the steepness of the moisture gradient near the surface. The tensile strains, which develop as the result of the gradient, will tend to be lowered as the gradient drops. Finally, as the wood dries, the stiffness increases (Youngs, 1957) and the elastic strain is proportionately decreased.

It is generally assumed that the magnitude of the elastic strain is closely related to the shrinkage of cells which are below fiber saturation. However, in reviewing the data leading to the curves which show tensile strains, it seems probable that only a small portion of the cells in a given wafer were at moisture contents less than the assumed fiber saturation level of about 30 percent. In a number of cases the average moisture contents are well above fiber saturation. As an example, the average moisture content [i.e.: (Average MC of surface wafers + EMC moisture content)/2)] of the surface wafers for the 85 percent relative humidity condition when the maximum surface tension developed (Fig. 31) was 35.6 percent. McMillen (1955) reported the same general trends with the thicker red oak wafers which he used to measure elastic recovery. There are at least two possible causes for this phenomenon. First, Stamm (1964) reported collapse due to capillary tension forces could cause abnormal shrinkage even when the majority of cells were above fiber saturation. The occurrence of collapse could result in tensile strains being applied to cells near the surface of the lumber.

Second, it is likely that some preferential drying occurs around the ray cells which are both large and prevalent in red oak. The preferential drying would cause local areas to be below fiber saturation and lead to the development of tensile strain.

The relative development of compressive strain in the interior of the wood is quite interesting. To maintain equilibrium, the sum of the compressive and tensile forces must be zero and, therefore, the tensile forces must be balanced by the compressive forces. In relative terms, the volume of wood which is near or below fiber saturation and under tensile stress is small compared to the volume of wood above fiber saturation and under compressive stress. Therefore, the compressive strains which were measured tend to be lower in magnitude and appear to develop much more slowly. In reviewing the graphs, it must be remembered that only the outer 1/2 inch from each surface of the 1.5 inch thick board was measured. Because of this, the areas under the curves are not equal.

The same general pattern which occurred with respect to relative humidity level in tensile strain was also in evidence with compressive strain. The maximum compressive strains (approximately .0012 in/in) developed much more quickly under the lower relative humidity conditions than with the less severe conditions.

The patterns shown for strain development in Figures 31-37 are similar in form to McMillen's (1955) curves. Except at the 85 percent level of relative humidity, the curves developed by McMillen and those developed as the result of this research are not directly comparable. After approximately three days of drying the magnitude of tensile strain

at the surface of McMillen's samples was almost .003 in/in and the compressive strain was nearly .001 in/in. Both of these values compare well with the results shown here.

E. Mechano-sorptive Creep Determined Using the Wafer Slicing Method.

1. Results of the Tests.

The mechano-sorptive creep values were plotted against the average moisture contents of the wafers for all data less than 32 percent moisture content. The results are illustrated in Figure 38.

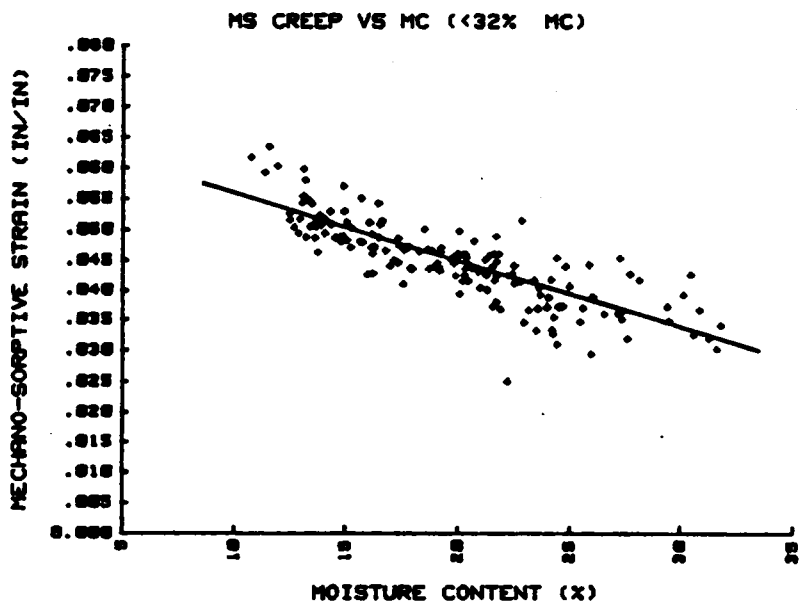

Figure 38. Mechano-sorptive creep is determined from the wafer slicing experiments.

In view of the apparent linear relationship between mechano-sorptive creep and moisture content, a least squares linear regression analysis (Ott, 1984) was performed using mechano-sorptive creep strain as the dependent variable and moisture content as the independent variable. The result was as follows:

$$MS\ creep = .66X10^{-1} - .112X10^{-2}\ MC \quad R^2 = .682 \quad Eq.\ 18$$

The initial graphs of mechano-sorptive creep strain above 32 percent moisture content showed considerable variation and no definite relationship to moisture content was evident. This was expected in light of the discussion of the mechanism of mechano-sorptive development given above. However, the elastic strain equations shown in Table 3 predicted a small dependence on mechano-sorptive creep at all moisture content levels (correlation coefficient between .17 and .36 for the three relative humidity conditions). Because of this, the average mechano-sorptive creep (by wafer position) was determined for the data above 32 percent. The average value at all levels was about .026 in/in as shown in Figure 39.

The mechano-sorptive creep values from all of the wafer slicing experiments ranged from approximately .026 in/in to .065 in/in.

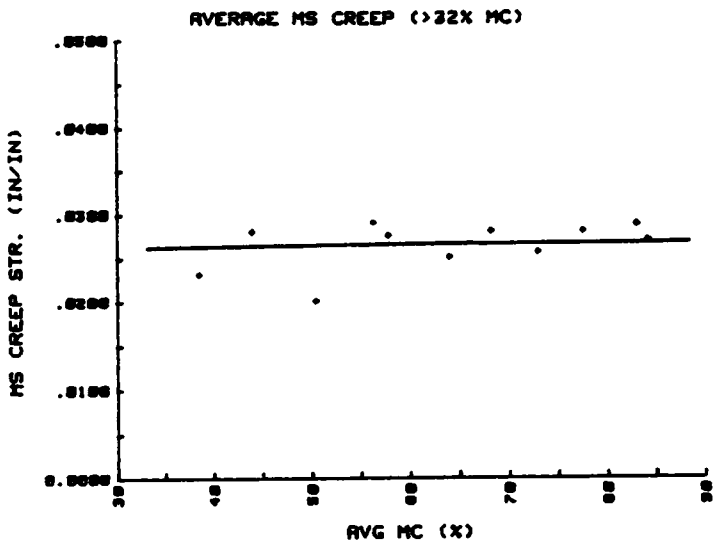

Figure 39. Average mechano-sorptive creep above 32 percent moisture content.

2. Discussion of the Results.

The mechano-sorptive creep values were determined using the following procedure. First, a value for the dry length (Figure 5) was determined for each wafer by measuring the hole spacing in the dried condition. Next, a value for the unrestrained shrinkage was determined using Equation 7. Finally, the value of the mechano-sorptive creep was determined as the difference between the measured shrinkage and the unrestrained shrinkage (Equation 16) assuming that no additional creep occurred after the wafers were sliced.

The plot of mechano-sorptive creep versus moisture content shown as Figure 38 shows considerable variation about the regression line for which there are probably several reasons. First, in some cases, the wafers developed a small amount of crook during drying to the oven dry condition. The net effect is that the measured values of shrinkage in the dry condition appeared to be greater than would be expected. Another possibility results from the basic wood structure. The moisture content for a given wafer was an average value for the wafer as a whole. However preferential drying, particularly around the ray areas may have occurred, resulting in localized areas of mechano-sorptive creep development. This may have affected the overall shrinkage and calculated creep strain values. If considerable preferential drying occurred, the shrinkage would be less than expected if little or no preferential drying occurred.

Perhaps the most important reason for the variation in the mechano-sorptive creep data is the effect of load. Fujita and Nakato (1965) have shown that the development of mechano-sorptive creep depends to a certain extent on the applied load. The mechano-sorptive creep values shown in Figure 38 are taken from many samples under different drying conditions and with different moisture gradient levels. These differences serve the same function as changing the load or strain level and as such may account for much of the observed variation.

The small but relatively constant value for mechano-sorptive creep above fiber saturation is not easily explained in light of the discussion regarding creep given in the background section. Despite precautions which were taken in drying the wafers, after slicing some creep

strain may have developed during the slow drying process to the oven-dry state. The development of some creep would be likely anytime that a moisture gradient developed during drying and the wafers were of sufficient width and thickness so that a small gradient might be expected. The fact that all the wafers were nearly the same size might account for the constancy of the average magnitude of the creep strain at .026 in/in.

Another possible reason could be creep which might result from preferential drying around the ray tissue of the type discussed above. The localized creep would cause the shrinkage to be less than expected and the calculated creep would be greater than zero. Since the local moisture loss would vary, the creep strain values would be expected to show considerable variation, but would always be greater than zero. The mechano-sorptive creep data showed evidence of this pattern before an average value was determined.

F. Mechano-sorptive Creep Determined Using the Loaded Wafer Method.

1. Results of the Tests

The second method used to determine the variation of mechano-sorptive creep with moisture content was to use wafers which were loaded to 10, 20, or 30 percent of nominal failure strain (assumed to be 775 psi based on strength tests performed for this study). The wafers were then dried to one of three equilibrium moisture content conditions. The results are illustrated in Figure 40.

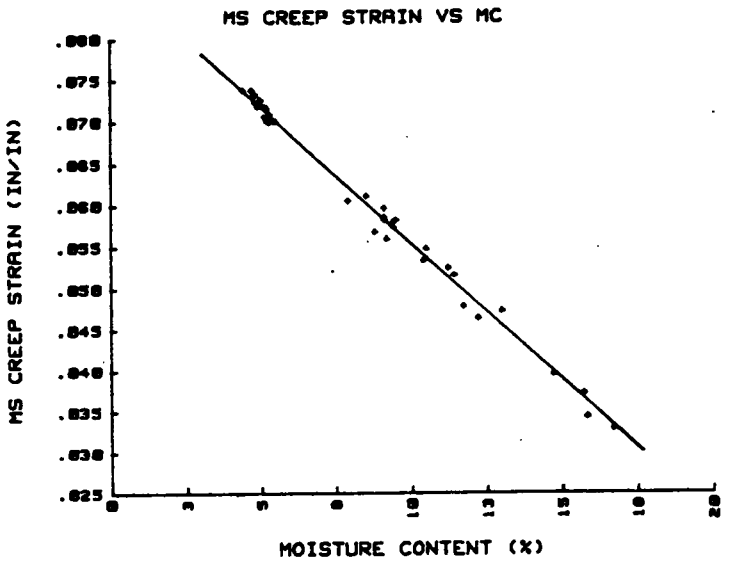

Figure 40. Mechano-sorptive creep versus final wafer moisture content as determined from the loaded wafer tests. All wafers began in the green condition.

A linear regression analysis using the method of least squares gave the following relationship:

Eq. 19

$$MS\ creep = .88X10^{-1} - .332X10^{-2}(MC) \quad R^2 = .992$$

Hunt (1987), has indicated that the amount of mechano-sorptive creep is a function of load as well as moisture content. To explore this possibility, the data were replotted with each load level being represented by a different symbol. The result is shown as Figure 41.

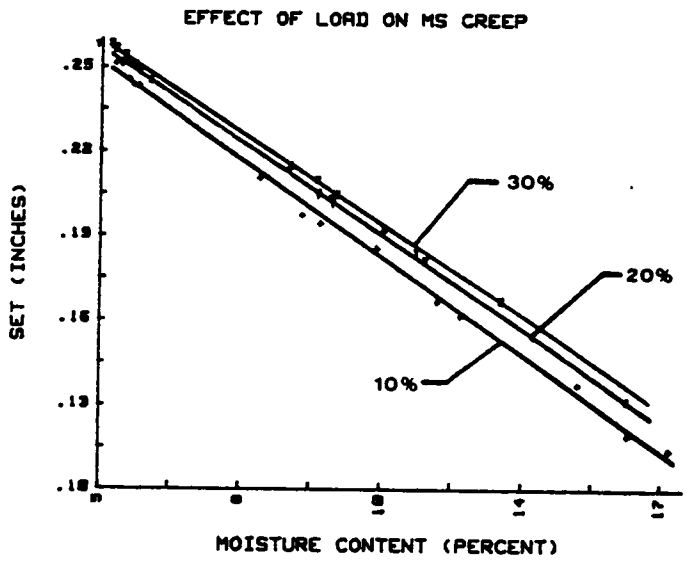

Figure 41. Effect of load on mechano-sorptive creep. Note that the ordinate value is set or total MS creep (over a 3.47 in. gage length).

2. Discussion of the Results.

The mechano-sorptive creep strain values illustrated in Figure 40 were determined using a multi-step procedure. The samples were loaded to a percentage of failure stress and allowed to dry until the strain readings were stable. The process required about 2.5 days of drying time. Next, the load was released and the samples were allowed to recover the elastic strain for approximately 5 minutes before a

measurement of the final dried length was taken. The shrinkage strain of the sample was calculated using the following formula:

$$\frac{\text{green unloaded length - final dry length}}{3.47} \qquad \text{Eq. 20}$$

Where the 3.47 was the known gage length in inches.

The difference between the value of shrinkage strain given by equation 20 and the inherent shrinkage given by equation 16 at the measured moisture content of the wafer was the calculated mechano-sorptive creep strain.

The mechano-sorptive creep values determined in this manner also contain a component of visco-elastic creep shown as the difference between the post-cut length and delayed recovery length in Figure 5. As discussed below, the magnitude of the visco-elastic creep component is small in both relative and absolute terms. Its inclusion in the mechano-sorptive creep calculations probably had little or no effect on the overall relationship.

The mechano-sorptive creep measured in this manner was clearly shown to be a function of moisture content. Unfortunately, in measuring creep in this manner, it was not possible to determine if any creep existed at moisture content levels above fiber saturation. In addition, to maintain conditions during the experiments, the equilibrium moisture content values were quite limited and ranged from approximately 5 to 18 percent. The end result is that the mechano-sorptive strain values determined by this method and the slicing method are not directly comparable because the moisture content values overlap only in a small area. However, a

graphical comparison is possible and a composite graph of the mechano-sorptive creep versus moisture content using the two methods as well as the average mechano-sorptive creep above 32 percent MC is shown in Figure 42. A polynominal regression analysis done on the entire data set shows the following relationship between mechano-sorptive creep and moisture content;

Eq. 21

$$MSCREEP = .816X10^{-1} - .274X10^{-2}(MC) + .458X10^{-4}(MC)^2 - .25X10^{-6}(MC)^3 + .081 \quad R^2 = .856$$

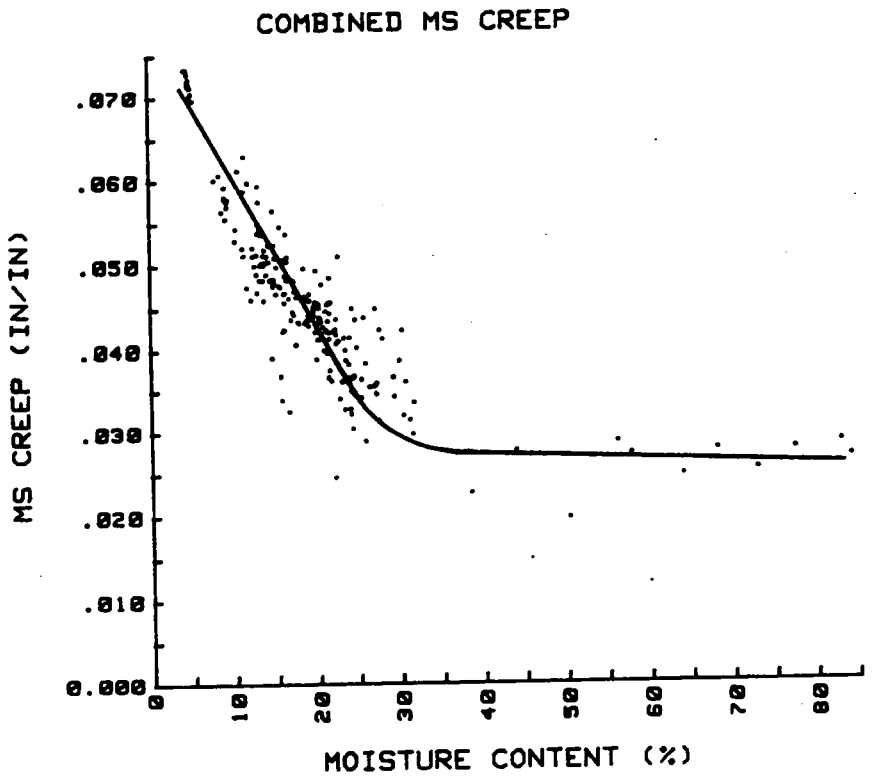

Figure 42. Graph of the combined mechano-sorptive creep from the wafer slicing and loaded wafer tests. The data above 32 percent MC are average values.

It is apparent from the figure that the relationship becomes non-linear at higher moisture contents. A similar relationship for makaba was reported by Hisada (1986).

The magnitude of the mechano-sorptive creep was surprising. The maximum value as illustrated by Figure 40 was approximately .075 in/in. Using the gage length of 3.4 inches, the dimensional increase over and above the unrestrained shrinkage length is approximately .250 inches, which represents a very substantial change. In view of the drying process as a whole, the maximum values represented in the figure probably represent the highest levels of mechano-sorptive creep which occur during drying. As McMillen (1955) points out, the magnitude of the mechano-sorptive creep is likely to decrease as the stresses reverse and become compressive. At the surfaces of the driest samples where the mechano-sorptive creep is a maximum, the stresses are beginning to reverse as illustrated in Figures 31-37.

The effect of load on creep seems to be small and slightly non-linear as illustrated in Figure 41. Although the comparisons may be suspect because of the differing conditions and species, Fujita and Nakato (1965) as well as Hisada (1986) have shown that the effect of load perpendicular to the grain of creep strain is nearly linear to approximately 40 percent of failure strain.

G. Visco-elastic Creep Tests Using Loaded Wafers.

1. Results of the Tests.

The second creep component which was measured was the visco-elastic creep. A graph comparing the magnitude of the visco-elastic strain at three different load levels is shown as Figure 43.

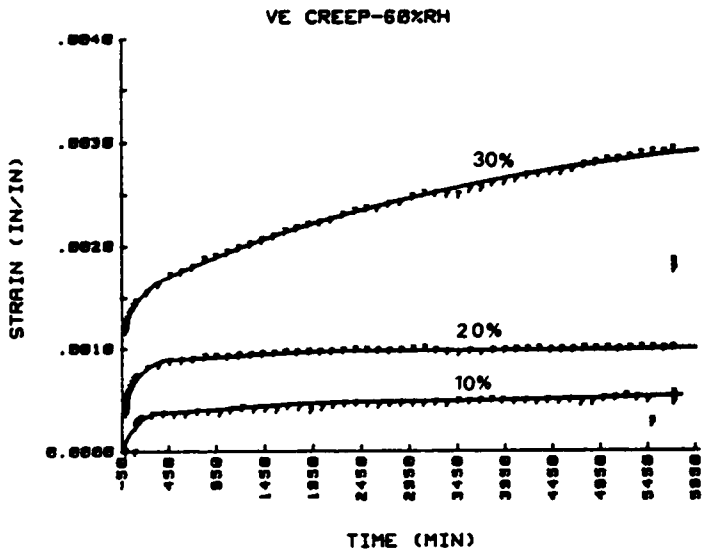

Figure 43. Typical visco-elastic creep patterns. The load levels are nominal percentages of failure stress.

The magnitudes of the visco-elastic creep strain shown on the graph are small and quite typical of those found for most of the tests. The average values of the creep from all tests measured when the creep was at its maximum level at each load level tested are shown in Table 4.

Table 4. Average visco-elastic creep magnitudes at different load levels.

Load level (% Max.Load)	10	20	30
Visco-elastic Creep (in/in)	.00026	.0007	.0010

2. Discussion of the Results

The experimental design called for the samples to be conditioned to one of the three relative humidity levels, loaded to a specified level and the deformation measured over a time period. Difficulties were experienced almost immediately because of a tendency for the samples to shrink after loading, possibly due to a loss of moisture. Although the small samples were conditioned for approximately 2 weeks prior to test, the problem reoccurred sporadically throughout the tests even when the gage lengths of the samples were wrapped with plastic wrap for the duration of the tests.

A further difficulty occurred at the highest relative humidity condition (85 percent). Both the temperature and relative humidity conditions within the chamber were difficult to maintain consistently for the 2-4 day period of the tests. As a result, and in view of the comparatively small magnitude of the visco-elastic creep component, the tests were suspended after completing the measurements at the 35 and 60 percent relative humidity levels. Although the tests could not be completed, there were two major reasons why this was not of great concern.

First, as outlined above, the mechano-sorptive creep calculations from the mechano-sorptive creep experiments using loaded wafers contained the element of visco-elastic creep. Because of the manner in which the experiments were designed, the visco-elastic strain component could not be isolated.

Second, when compared, the magnitude of the visco-elastic component is approximately equal to the elastic strain. This same general trend was also reported by Bello (1976) and Kawai (1980). However, when com-

pared to the mechano-sorptive creep component, the visco-elastic component appears to be insignificant. In general terms, the magnitude is less than 1/50 the value of the mechano-sorptive creep strain.

H. Acoustic Response Tests

1. Results of the Tests

As discussed in detail above, the acoustic response and load/deflection characteristics were measured separately and composite graphs were prepared from the data. A typical example of a composite plot is shown in Figure 44.

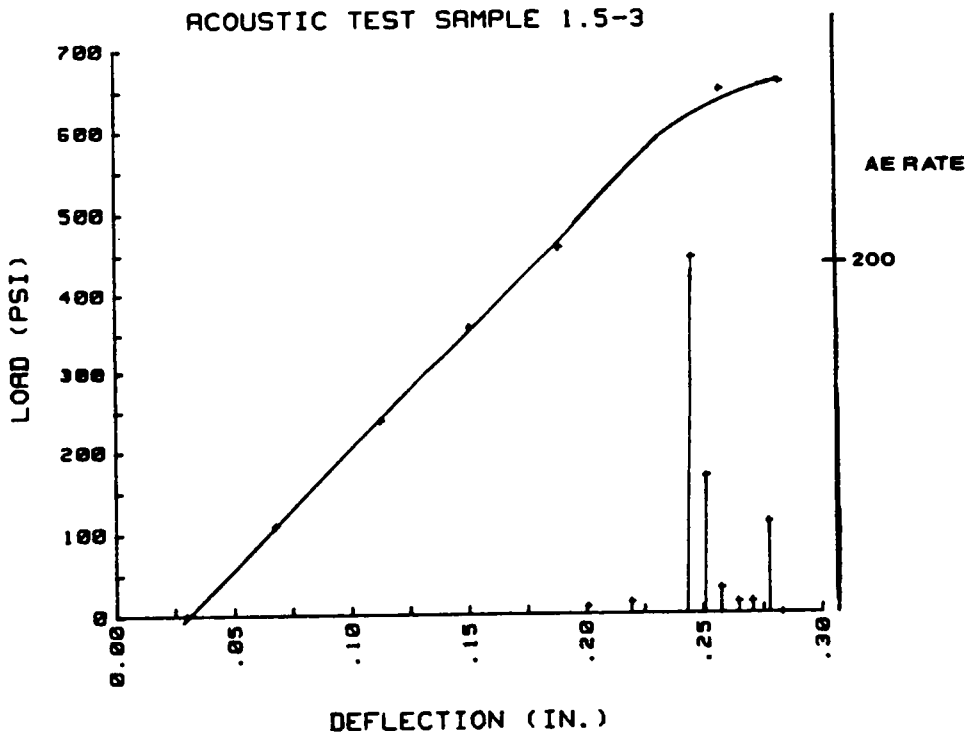

Figure 44. Load/deflection curve with the number of emissions per 10 second period superimposed. No visible cracking occurred until failure.

The load/deflection origin differs from zero because of the slight preload placed on the samples prior to the commencement of the test. The pattern is typical of that seen in nearly all of the tests. The rate of emissions increased at the point which was coincident with the onset of the non-linear portion of the curve. Using the green wafers, no visible cracks were seen until the samples failed catastrophically.

2. Discussion of the Results

The third point loading method was chosen because the maximum strain is concentrated at the outer surface of the sample which insures a failure pattern similar to surface checking will occur (Bodig and Jayne, 1982). The fiber stress at the surface under tensile stress was calculated using a flexure formula taken from ASTM Standard D-198 (1984). The values obtained for the failure strength were in general agreement with those of the strength tests. The sample failures were invariably within the gage length as would be expected for this type of loading if the equipment is proper and the tests were properly conducted.

The general magnitude of the acoustic emissions is relative and the value could be changed considerably simply by changing the threshold voltage adjustment. The nature of these tests was to identify some of the emission characteristics of the surface failure. As such, care was taken to adjust the equipment sensitivity to filter the gradually accumulating acoustic emissions and monitor only the large bursts above a threshold which are seen in the figure.

The general failure pattern is akin to that which occurs in brittle, glassy polymers such as polystyrene as illustrated in Figure 45. (Qien and Shu, 1987). Although microchecks are undoubtedly forming and some

elongation is occurring under stress, the advent of macroscopic failure is seen as a series of burst type emissions which occur just prior to catastrophic failure.

Although preliminary to further study, the results of these tests are encouraging. The advent of surface failure is clearly predictable under the conditions of the tests which, presumably, are somewhat similar to those which might occur when a green board begins to dry.

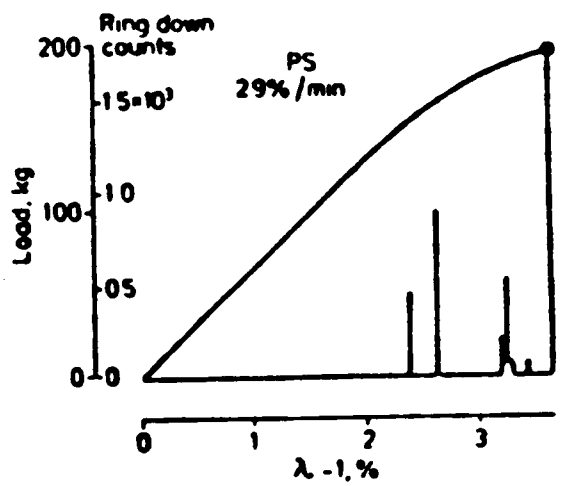

Figure 45. Load/deflection graph for polystyrene with the rate of emissions superimposed as reported by Qien and Shu, 1987.

I. The Computerized Simulation of Drying Stresses

1. Results of the simulation

In accord with other simulations, such as the model of Kawai (1980), the first step in modeling the development of stresses during drying is to predict the moisture distribution under various drying conditions.

Comparisons of the predicted versus actual moisture contents for three different drying conditions are illustrated in Figures 46-48. The positions noted on the figures refer to the first two wafers taken from a given surface.

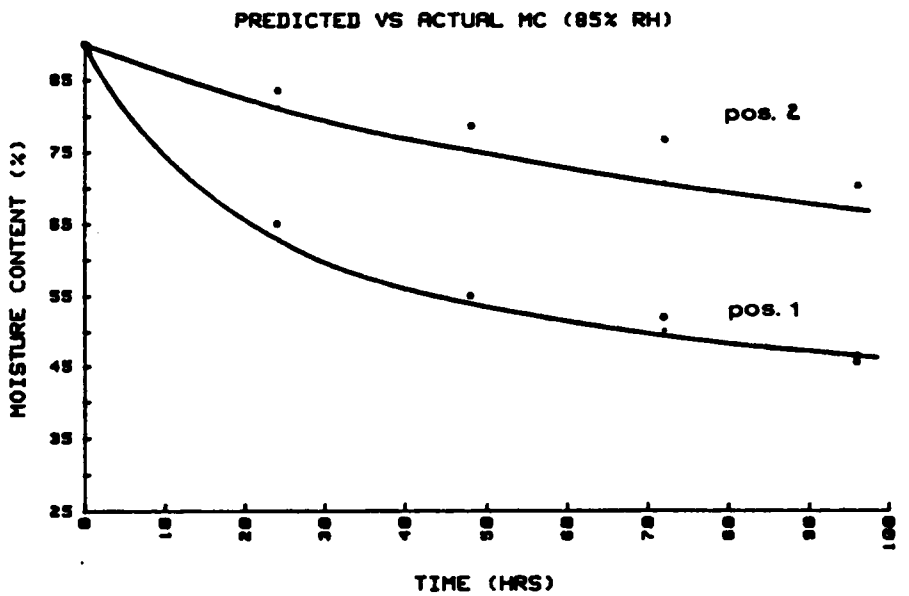

Figure 46. Predicted versus actual moisture contents for the 85 percent relative humidity condition. The solid lines are the predicted values.

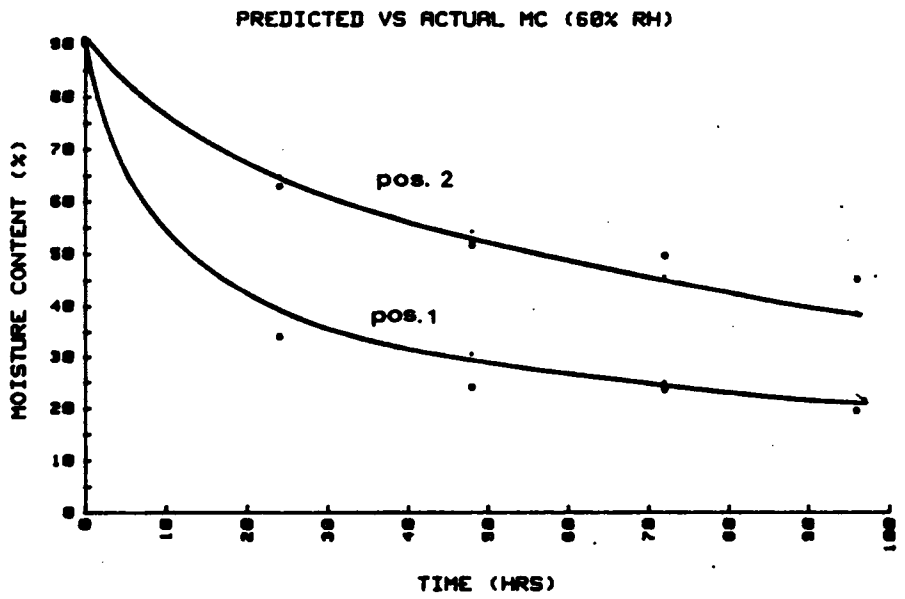

Figure 47. Predicted versus actual moisture contents for the 60 percent relative humidity condition. The solid lines are the predicted values.

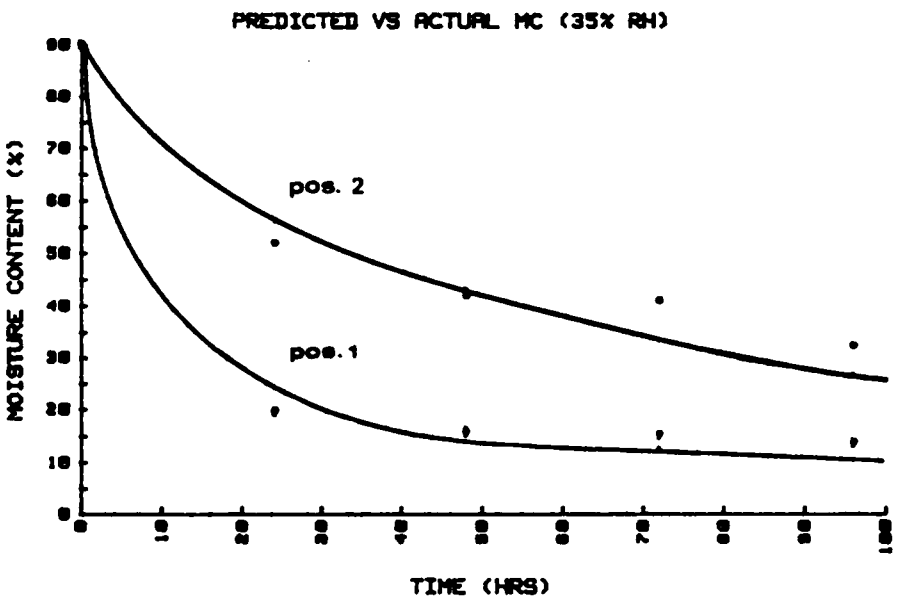

Figure 48. Predicted versus actual moisture contents for the 35 percent relative humidity condition. The solid lines are the predicted values.

As discussed in detail below, once the moisture distributions were determined for a given set of drying conditions, the regression equations relating strain to various drying parameters were used to predict the stresses during drying. Typical results are shown in Figures 49-51.

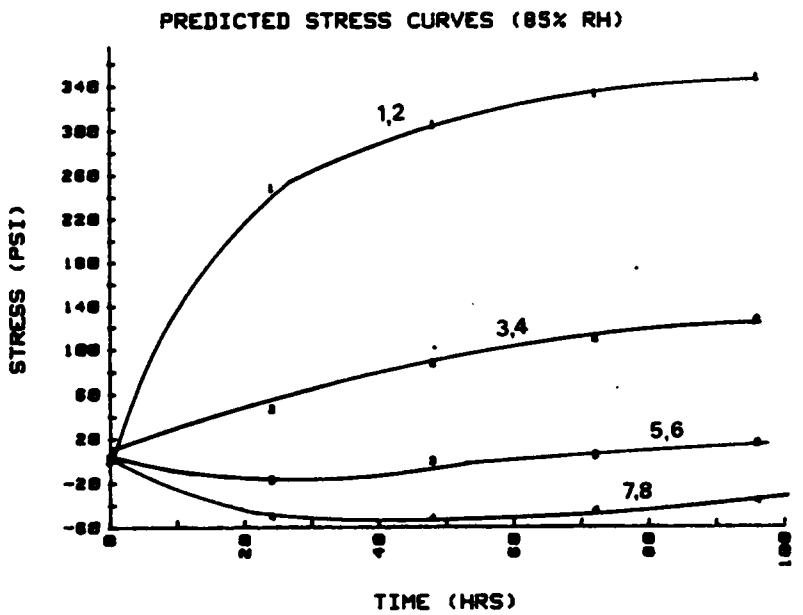

Figure 49. Predicted stress values for the 85 percent RH condition. The small numbers adjacent to the curves refer to the positions shown in Figure 17.

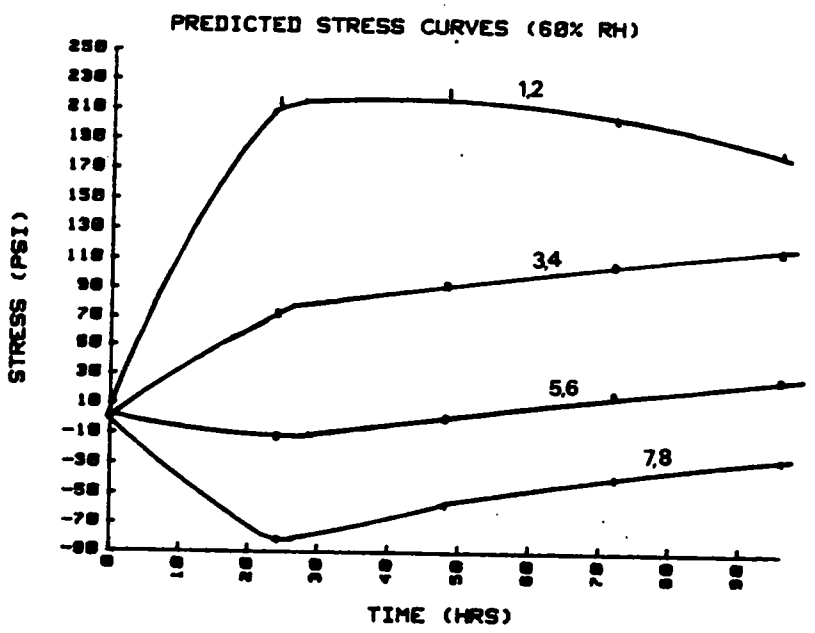

Figure 50. Predicted stress values for the 60 percent RH condition. The small numbers adjacent to the curves refer to the positions shown in Figure 17.

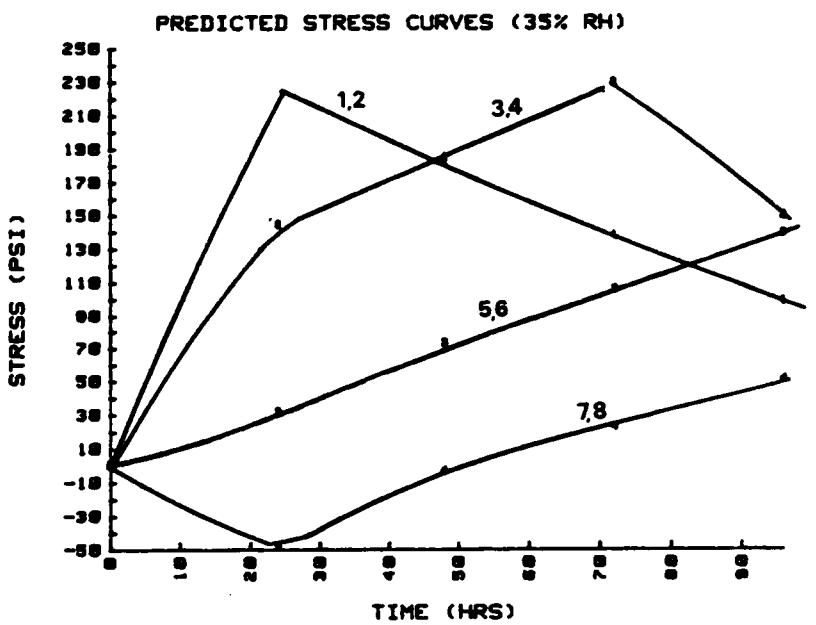

Figure 51. Predicted stress values for the 35 percent RH condition. The small numbers adjacent to the curves refer to the positions shown in Figure 17.

The actual output of the simulation uses Equation 15 to predict the liklihood of failure at various positions within the drying board. Typical output from the simulation is shown in Table 5.

Table 5. Typical output from the computerized simulation. The RH is 85 percent. MC is the moisture content, stress is in psi, the time is the number of hours since the beginning of drying, set is the mechano-sorptive creep in in/in, EL-STR is the elastic strain (in/in), POS is the distance from the surface and P.Fail is the probability of failure.

MC (%)	STRESS (PSI)	TIME (Hrs)	SET (in/in)	EL-STR (in/in)	POS	P FAIL (%)
89.29	-50.34	24	.026	-.000629	.857	<10
87.56	-19.71	24	.026	-.000276	.643	<10
81.52	46.97	24	.026	.00059	.429	<10
63.21	248.7	24	.026	.00292	.214	<10
87.08	-51.05	48	.026	-.000637	.857	<10
83.64	-2.777	48	.026	-8.06E-5	.643	<10
75.30	87.63	48	.026	.00106	.429	<10
55.44	305.3	48	.026	.00357	.214	<10

2. Discussion of the results.

The moisture gradients were determined using the Crank-Nicholson finite difference method discussed in the Methods and Materials section. The resulting system of equations was solved by inverting the left hand side coefficient matrix and multiplying the inverted matrix by the known

values on the right hand side. The result was a new set of moisture content values at each time step.

The transport coefficient was determined using Equation 13 which was resolved for each node each time a new moisture content value was determined. Using Equation 13, the predicted moisture content values were within about 3 percent of the measured values at all positions at the 85 percent relative humidity condition. For the more severe drying conditions (60 and 35 percent RH), the model predictions were much higher than the actual values. To account for this discrepancy, the transport coefficient was adjusted until the actual and predicted values were similar as shown in Figures 47 and 48. However, despite the adjustment, some problems remained particularly at the inner positions where the actual and predicted values differed by about 12 percent.

Mechano-sorptive creep was determined using Equations 18, 19 and 21 as well as the information provided in Figure 39. For all values of moisture content greater than 32 percent, the mechano-sorptive creep was considered constant at .026 in/in. In the 85 and 60 percent relative humidity ranges Equation 18 was used when the moisture contents were between 18-32 percent and Equation 19 was used for moisture content values less than 18 percent. For the 35 percent relative humidity range, Equation 21 was used at moisture contents less than 32 percent because using Equations 18 and 19 produced a considerable drop in stress at lower moisture contents.

The modulus for elastic strain was determined by increasing green modulus by 1.5 percent for every one percent drop in moisture content at all moisture content values less than 40 percent (Wood Handbook, 1987).

The green modulus was determined using the within gage length failure data from the strength tests performed at 110° F. The average value for the modulus was 8.67 x 10^4 psi. The modulus for the mechano-sorptive creep was based on Equation 12 developed by Oliver (1987). The ratio (e/ m) was assumed to be constant and equal to .00112 based on Equation 18. The value of the modulus was assumed to vary in accord with the modulus for elastic strain.

The overall strain at any position at a calculated moisture content is assumed to be the sum of the elastic strain and the mechano-sorptive creep strain. Once the moisture content at any given point is calculated, the elastic strain and its associated modulus are calculated. Then the mechano-sorptive creep and the mechano-sorptive creep modulus are determined at the same point. The total stress is determined by multiplying the strains by their moduli and summing. It is assumed that the mechano-sorptive strain always acts to reduce the total strain. That is, it always acts as a stress relieving mechanism.

The curves presented in Figures 49-51 are quite misleading because they indicate that the stress is lower under the more severe drying conditions. The confusion is the result of the regression equations for elastic strain (Table 3.) The equations were developed using the average moisture content of the .070 inch thick wafers and the overall elastic strain of the wafer. The strain situation changes considerably if the surface moisture contents and attendant strains are considered. To illustrate, suppose that the surface fibers immediately come to the equilibrium moisture content condition and the cells directly beneath the surface are still well above fiber saturation and relatively pli-

able. In this case, the true elastic strain restrained strain at the surface is closer to the magnitude of the unrestrained shrinkage than to the .0035 in/in strain of the thick wafer. If we assume that the restrained strain is a fraction of the total shrinkage potential and calculate the surface stress at various values of the moisture content curves, such as those shown in Figure 52, result.

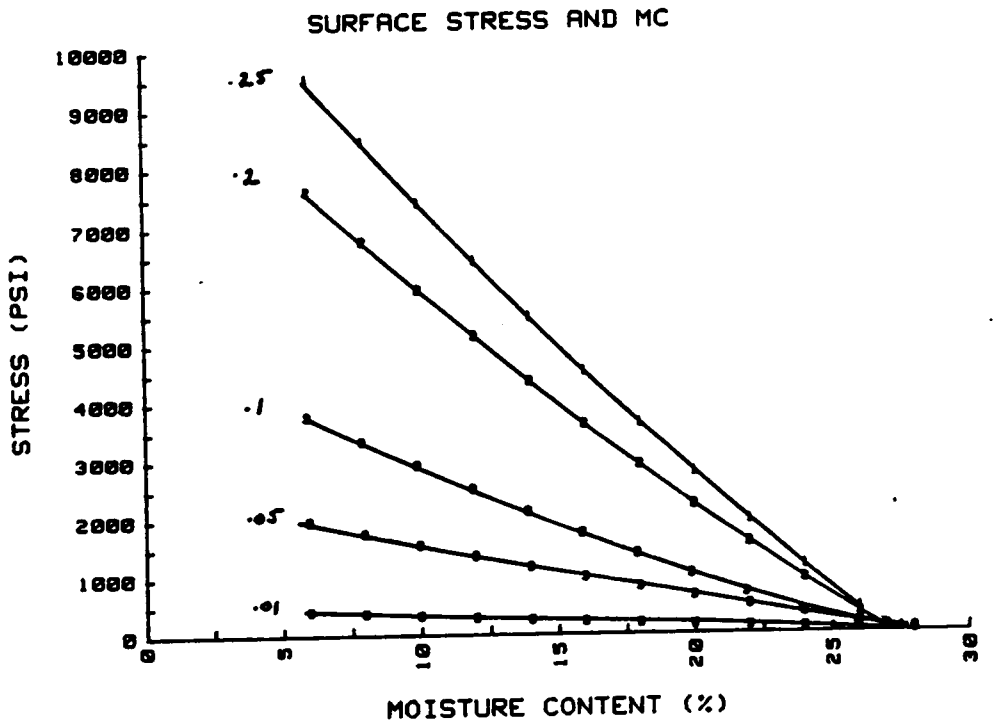

Figure 52. Surface stress calculations for various fractions of shrinkage potential. The small values next to the curves represent fractions of potential shrinkage. As an example, a value of .25 indicates that the strain used to calculate stress was .25 times the potential elastic strain at a given MC. No mechano-sorptive creep was included in the calculations.

The calculated stresses have increased considerably and indicate that the most severe stresses result from the lower equilibrium moisture content conditions. Although no data are available to substantiate the example given, it is clear that the stress gradient very close to the surface is critical to the development of surface checking. It is probable that preferential drying around the ray areas occurs. These cells then shrink in a relatively unrestrained manner and become somewhat brittle. As the cells away from the rays lose moisture and attempt to shrink, the stress causes failure to occur at the weakest point which is directly adjacent to the rays. The drying at the surface occurs relatively quickly and presents the shrinkage. Under mild conditions the entire surface dries more slowly and the steep gradients do not develop.

SUMMARY AND CONCLUSIONS

1. Moisture Gradient Tests

The results of the moisture profile tests clearly illustrate that develop quickly near the surface during drying. This is apparently true even under the mild conditions of 85 percent relative humidity and 110° F temperature, the mildest drying conditions used for this study. Although the profiles changed on a daily basis, the magnitude of the moisture loss was always greater for the more severe drying conditions.

The continuous profiles indicates that there is considerable mass flow from the center of the wood early in the drying process. This pattern led to the conclusion that no discontinuities exist and that Fick's law could be used to model the pattern.

The transport coefficients, which were determined using Egner's method, indicate that the drying rate slows considerably as fiber saturation is approached from above. The calculated magnitudes of the coefficients were in accord with the values found by other researchers.

2. Strain Measurements

The measurements of elastic strain followed the same patterns which were shown by McMillen (1955) for red oak. In general, the tensile elastic strains had a maximum magnitude of about .003 in/in and developed at the surface relatively quickly when compared to the smaller compressive strains at the interior. At the surfaces of the wood, the time span required to develop the maximum tensile strain was inversely related to the severity of the drying conditions. The maximum tensile strains at the 60 and 35 percent relative humidity conditions apparently developed within the first 24 hours of drying.

The mechano-sorptive creep tests using the wafer slicing methods and the loaded wafer method both led to the same results, that is, the magnitude of the creep is directly related to the change in moisture content. Under the desorption condition measured, the relationship between moisture content and creep is apparently linear at low moisture contents and becomes non-linear as fiber saturation is approached. Above fiber saturation, the mechano-sorptive creep was found to be constant and may have been the result of preferential drying of the wafers around the rays or to other reasons which were discussed in the text.

Perhaps the most surprising result from all of the tests centers on the magnitude of the mechano-sorptive creep which was approximately 25 times the maximum elastic strain. More specifically, when dried to 8 percent moisture content, the 4-inch long wafers were fully 1/4 inch longer than expected due to the plastic flow component. Clearly, the development of mechano-sorptive component is advantageous not only in decreasing failure potential but also in increasing wood volume.

The visco-elastic creep component is quite small in relation to the mechano-sorptive creep component. The magnitude of the visco-elastic component under the loading conditions and drying times used for this study was about the same as the elastic component as measured in the green condition.

3. Acoustic Measurements

Under third point flexural loading conditions where the maximum fiber strain is at the surface, the onset of checking in green wood can be predicted prior to the occurrence of visible checks. The pattern of acoustic emissions is similar to that found in brittle, glassy polymers

such as polystyrene.

4. Computerized Stress Simulation

Using the input parameters of mechano-sorptive creep and elastic strain, the general patterns of stress development can be predicted as stated in the original hypothesis under which this research was conducted. The patterns predicted clearly indicate that stress is a maximum at the surface. Due to the limitations in measurement in the slicing technique, the stresses which occur at the surface cannot be predicted using the model. However, using reasonable estimates of the elastic strain and moisture content near the surface, the magnitude of stress has been shown to rise sharply as the severity of drying conditions increases.

RECOMMENDATIONS FOR FURTHER STUDY

The general trends of stress development under different drying conditions have been predicted using the results of the strain measurements performed for this study. The magnitude of the mechano-sorptive creep component has been clearly shown to be large in relation to the other strains which were measured. However, because of the manner in which the tests were performed, no relationship between time and the development of mechano-sorptive creep could be determined. Presumably, the polymers of wood require some time to conform to any applied stress. Further, the ability to conform is probably a function of the temperature. The relationship of time and temperature to the development of mechano-sorptive creep merits further investigation.

An analogy comparing rubber-like elasticity to the development of mechano-sorptive creep was outlined in the Background section of this report. If the analogy is valid, then it may be expected the amount of creep is affected by the size of the sample and that there is a definite limit to the amount of creep which may occur. To speculate further, in tension perpendicular to the grain, one might suppose that the lignin component is responsible for the large magnitude of the creep and the cellulose crystallites probably limit the creep. A research program comparing the magnitudes of creep parallel and perpendicular to the grain under the same conditions may shed considerable light on the mechanisms of creep development. A study of size effects and creep limits could be an adjunct to this type of study.

Based on the results of the computerized simulation, it is clear that the magnitude of the stress at the surface is critical to the

development of surface checking. The wafer slicing technique is not adequate to determine the stress very close to the surface. It is suggested that an optical method, using either a grid or point type measurement might lead to a better understanding of stress development in the critical region.

With regard to drying practice, there are probably two methods which might avoid severe stress development. The first is follow the current practice of slow drying where the gradient is kept small. This allows sufficient time for the polymers to conform to the applied stress which is developing slowly near the surface. A second method and one which might lead to faster drying and improved quality would be to use the temperature effect to increase the ability of the polymers to conform to the applied stress. At first, very green wood could be heated to about 160° F under high humidity conditions. Then the humidity could be lowered and more rapid drying could be performed. The scheme is quite similar to one proposed by Torgeson (1951) for sweetgum after his studies of elastic strain development during drying.

The acoustic measurements clearly indicate that surface failure can be predicted prior to the onset of visible surface failure. However, separating the emissions which result from normal drying shrinkage from those which lead to macroscopic failure has not been done. The separation could probably be done using a wave form analysis method such as a Fourier transform. Once accomplished, the monitoring of surface stress development during the drying process would probably be a significant advance in process control.

REFERENCES

1. American Society For Testing and Materials. 1984. Standard Methods For Static Tests of Timber. ASTM D198-84. Phil. Pa.

2. Aklonis, J. W., J. McKnight and M. Shen. 1972. Introduction to Polymer Visco-elasticity. Wiley Interscience, New York.

3. Armstrong, L. D. and R. S. T. Kingston. 1962. The Effect of Moisture Content Changes on the Deformation of Wood Under Stress. Australian Jour. of Applied Sci. 13(4):257-276.

4. Armstrong, L. D. 1972. Deformation of Wood in Compression During Moisture Movement. Wood Science 5(2):81-86.

5. Ashworth, J. C. 1979. Design of Drying Schedules For Kiln-drying of Softwood Timber. Developments in Drying - Vol. 2. Hemisphere Press, New York.

6. Bello, E. D. 1976. The Effects of Temperature and Moisture Content on the Elastic and Residual Deformations in the Tangential Direction of Northern Red Oak (Quercus Rubra L.) and Aspen (Populus Tremuloides Michx.) The Pterocarpus 2(1):76-85.

7. Barrett, J. D. 1974. Effect of Size on Tension Perpendicular-to-grain Strength of Douglas-Fir. Wood and Fiber 6(2):126-143.

8. Bodig, J. and B. A. Jayne. 1982. Mechanics of Wood and Wood Composites. Van Nostrand Reinhold, New York. 712 pp.

9. Boyd. J. D. 1982. An Anatomical Explanation for Visco-elastic and Mechano-sorptive Creep in Wood, and the Effects of Loading Rate on Strength. New Perspectives in Wood Anatomy. Martinus Nijhoff/Dr. W. Junk Publishers. Pp 171-222.

10. Beery, W., G. Ifju, and T. E. McLain. 1983. Quantitative Wood Anatomy - Relating Anatomy to Transverse Tensile Strength. Wood and Fiber Science. 15(4):395-407.

11. Bramhall, G. 1976. Fick's Laws and Bound Water Diffusion. Wood Science, 8(3):153-161.

12. Carnahan, B., H. A. Luther and James O. Wilkes. 1969. Applied Numerical Methods. John Wiley and Sons, New York. Pp604.

13. Carslaw, H. S. and J. C. Jaeger. 1959. Conduction of Heat in Solids. Clarendon Press.

14. Cech, M. Y. 1964. Development of Drying Stresses During High Temperature Kiln-drying. Forest Products Journal. 14(2):69-76.

15. Christensen, G. N. 1962. The use of Small Specimens for Studying the Effect of Moisture Content Changes on the Deformation of Wood Under Load. Australian Jour. of Applied Sci. 13(4):242-256.

16. Comini, G. and R. W. Lewis. 1976. A Numerical Solution of Two-dimensional Problems Involving Heat and Mass Transfer. International Journal of Heat and Mass Transfer. 19(12):1387-1392.

17. Cuppett, D. G. 1966. Air Drying Practices in the Central Appalachians. U.S.D.A. Forest Service Research Paper NE-56.

18. Daniels, F. and R. A. Alberty. 1966. Physical Chemistry. John Wiley and Sons, New York. 767 pp.

19. Egner, K. 1934. Beitrage Zue Kenntnis der Feuchtigkeitsbewegung Im Holzern, Vor allem in Fichtenholz, wahrend der Trocknung unterhalb des Fasersattigungspunktes. Forschungsberichte Holz. Heft 2. 91pp Berlin. (Original not seen).

20. Erins, P. V., V. Cinite, M. Jakobsons and J. Gravitis. 1976. Wood as a Crosslinked, Multicomponent Polymer System. Applied Polymer Symposium No. 28. ACS. pp 1117-1138.

21. Fick, A. 1855. Uber Diffusion. Annelen Der Physik und Chemie; Von J. C. Poggendorf. 94:59-86.

22. Florey, P. J. 1953. Principles of Polymer Chemistry. Cornell Univ. Press. Ithaca, New York.

23. Fortes, M. and M. R. Okos. 1980. Drying Theories: Their Bases and Limitations as Applied to Foods and Grains. Advances in Drying -V. 1. Miller Freeman Press, New York.

24. Fujita, S. and K. Nakoto. 1965. Studies on the Drying Check. II. The Effects of the Tensile Load on the Deformation and Creep Failure. Mokuzai Gokkaiski. 11(6):236-239.

25. Gammon, G. L. 1971. Volume Loss and Grade Change of Hardwood Lumber During Air Drying. USDA Forest Service Research Paper NE-227.

26. Grossman, P. U. A. 1971. Use of Leicesters Model for Mechano-sorptive Deflection in Beams. Wood Science and Technology. V. 5. Pp. 232-235.

27. Grossman, P. U. A. 1976. Requirements for a Model that Exhibits Mechano-sorptive Behavior. Wood Science and Technology. V. 10. Pp. 163-168.

28. Hart, C. A. 1968. The Drying of Wood. The North Carolina Agric. Ext. Service Circular No.471. North Carolina Agric. Ext. Service, Raleigh, N. C.

29. Hawley, L. F. 1931. Wood Liquid Relations. U.S.D.A. Bull. No. 248. Washington, D.C.

30. Hill, R. L. 1967. The Creep Behavior of Individual Pulp Fibers under Tensile Stress. TAPPI 50(8):432-440.

31. Hisada, T. 1986. Creep and Set Behavior of Wood Relating to Kiln Drying. Bulletin of the Forestry and Forest Products Research Institute No. 335. 130pp (reprint)

32. Honeycutt, R., C. Skaar and W. Simpson. 1985. Use of Acoustic Emissions to Control Drying Rate of Red Oak. Forest Prod. Jour. 35(1) pp 48-50.

33. Hougan, O. A., H. A. McCauley and W. R. Marshall. 1940. Limitations of Diffusion Equations in Drying. Trans. AICHE 36(2):183-206.

34. Hunt, D. G. 1987. Creep Properties of Softwood. SERC Bulletin. 3(8):23.

35. Ivanov, Iu. M. 1941. The Limit of Plastic Flow in Wood, A New Theory of the Mechanical Strength of Wood. Moscow. (Translated from the Russian by H. Kipp). U.S. Forest Prod. Lab. Madison, WI Translation #111

36. Jentzen, C. A. 1964. Effect of Stress Applied During Drying on some Properties of Individual Pulp Fibers. Forest Prod. Journal. Sept. Pp. 387-392.

37. Johnson, J. A. 1978. Review of the Interaction of Mechanical Behavior with Moisture Movement in Wood. General Constitutive Relations for Wood and Wood-based Materials. Proceedings of a Symposium held at Syracuse Univ. July. Pp. 282-303.

38. Kaiser, J. 1950. Untersuchgen Uber Das Auftreten Gerauscher Beim Zugversuch. Ph.D. Thesis, Technische Hochschule, Munich (Original not seen).

39. Kawai, S. K. Nakato and T. Sadah. 1978. Moisture Movement in Wood Below the Fiber Saturation Point. M. Gakkaishi 24(5):272-280.

40. --, -----, -----. 1979. Computation of Drying Stresses Resulting from Moisture Gradients in Wood During Drying. I. M. Gakkaishi, 25(2) p. 103-110.

41. --, ----,----. 1979. Computation of Drying Stresses Resulting from Moisture Gradients in Wood During Drying II. M. Gakkaishi, 25(4) p. 272-279.

42. ------. 1980. Moisture Movement and Drying Stresses in Wood. Ph.D. Thesis. Kyoto University.

43. King, E. G. Jr. 1958. The Strain Behavior of Wood in Tension Parallel to the Grain. Forest Products Journal 8(11):330-334.

44. King, W. W. 1975. Air Drying Degrade Losses at Hardwood Sawmills in the Tennessee Valley. Southern Lumberman.

45. Leese, P. F. 1972. Osmotic Stress in Wood - Part I: The Analogy Between Thermal and Swelling Stress. Wood Science and Technology. V. 6. Pp. 204-214.

46. --, ----, and R. S. T. Kingston, 1972. Osmotic Stress in Wood -Part II: On the Computation of Drying Stresses in Wood. Wood Science and Technology. V. 6. Pp. 272-283.

47. Leicester, R. H. 1971. A Rheological Model for Mechano-Sorptive Creep of Beams. Wood Science and Tech. Vol. 5, pp. 211-220.

48. Lessard, R., D. E. Limbert, J. L. Pokoski, and J. L. Hill. 1982. A Stress Model for Lumber Drying Control. Jour. of Dynamic Systems, Measurement and Control. V. 104, Dec. Pp. 283-289.

49. Lewis, R. W., K. Morgan, H. R. Thomas and M. Strada. 1979. Drying Induced Stresses in Porous Bodies - An Elastovisco-plastic Model. Computer Met. in Appl. Mech. and Eng. Vol. 20, 291-301.

50. Loughborough, C. and H. Smith. 1946. U.S. Forest Products Laboratory Kiln Certification Manual. A.N.C. Bulletin No. 21.

51. Luikov, A. V. 1964. Heat and Mass Transfer in Capillary-Porous Bodies. Advances in Heat Transfer V. 1. Academic Press, New York.

52. ------. 1966. Heat and Mass Transfer in Capillary Porous Bodies. Pergamon Press, Oxford.

53. Maeglin, R. R. 1976. Natural Variation of Tissue Proportions and Vessel and Fiber Length in Mature Northern Red Oak. Silvae Genetica V. 25 Pp 122-126.

54. Markwardt, L. J. and W. G. Youngquist. 1956. Tension Test Methods for Wood, Wood-base Materials and Sandwich Constructions. Forest Products Laboratory Report No. 2055. U.S. Dept. of Agriculture.

55. Martley, J. F. 1926. Moisture Movement Through wood: The Steady State. Forest Prod. Res. Tech. Paper No. 2. Dept. of Sci. and Ind. Research. (Great Britain). London.

56. McMillen, J. 1955. Drying Stresses in Red Oak. Forest Products Journal. 5(1):71-76.

57. ------. 1956. Drying Stresses in Red Oak - Effect of Temperature. 5(8):230-241.

58. ------. 1968. Transverse Strains During Drying of 2-inch Ponderosa Pine. U.S. Forest Service Research Paper FPL 83. January.

59. ------, and Youngs, 1960. Stresses in Drying Lumber, unpublished FPL Report, U.S. Department of Agriculture, Madison, WI.

60. Miller, D. G. and P. George. 1974. A Method of Measuring Creep and Recovery due to Flexural Loads of Short Duration. Wood Science 7(2):153-159.

61. Morgan, K., R. W. Lewis and H. R. Thomas. 1980. Numerical Modeling of Drying Induced Stresses in Porous Materials. Drying 80 - Vol. 1, Pergamon Press. Pp. 451-460.

62. ------, K., H. R. Thomas and R. W. Lewis. 1980. Numerical Modeling of Stress Reversal in Timber Drying. Wood Science, 15(2):139-149.

63. Morrison, R. T. and R. N. Boyd. 1973. Organic Chemistry 3rd Ed. Allyn and Bacon, Boston.

64. Noguchi, M., Y. Kagawa and J. Katagiri. 1980. Detection of Acoustic Emissions During Hardwoods Drying. Mokuzai Gakkaishi 26(9):637-638.

65. ------, M., S. Kitayama, K. Satoyoshi and J. Umetsu. 1987. Feedback Control for Drying Zelkova Serrata Using In-Process Acoustic Emission Monitoring. Forest Products Journal 37(1):28-34.

66. Oliver, A. 1987. Personal communication.

67. Ott, L. 1984. An Introduction to Statistical Methods and Data Analysis. Second Edition. Duxbury Press, Boston. 775 pp.

68. Panshin, A. and C. DeZeeau. 1980. Textbook of Wood Technology. McGraw-Hill, New York. 722 pp.

69. Peck, E. C. 1945. A New Approach to the Formulation of Hardwood Dry-kiln Schedules. Southern Lumberman. 161(2033), Pp. 136-137.

70. Perry, C. C. and Lissner, H. R. 1962. The Strain Gage Primer. McGraw-Hill, New York.

71. Pollock, A. A. 1971. Acoustic Emission Methods of NDT. British Journal of NDE. V. 13, May. Pp. 85-89.

72. Porter, A., M. El-osta and D. Kusec. 1972. Prediction of Failure of Finger Joints Using Acoustic Emissions. Forest Prod. Journal. 22(9):74-82.

73. Qian, R. and X. Shu. 1987. Acoustic Emission of Polymers. In: Applied Polymer Analysis and Characterization. Hanser Publishers, New York.

74. Ranta-Maunus, A. 1975. The Visco-elasticity of Wood at Varying Moisture Content. Wood Science and Technology. V. 9. Pp. 189-205.

75. Reitz, R. C. 1950. Accelerating the Kiln Drying of Hardwoods. Southern Lumberman, 181(2262), Pp. 43.

76. Rosen, H. 1986. Personal communication.

77. Roth, F. 1895. Timber: An Elementary Discussion of the Characteristics and Properties of Wood. U.S. Dept. of Agriculture. Bull. 10. Washington, D.C.

78. Sales, C. 1984. Contribution A L'analyse Des Constraintes De Sechage Dans Le Bois. Ph.D Thesis. Institut National Polytechnique De Lorraine. (Original not seen).

79. Sato, K., M. Fushitani, and M. Noguchi. 1984. Discussion of Tensile Fracture of Wood using Acoustic Emissions. Mokuzai Gakkaishi 30(2):117-123.

80. Schaffer, E. 1972. Modeling and Creep of Wood in a Changing Moisture Environment. Wood and Fiber 3(4):232-235.

81. Schaffner, R. 1981. Fundamental Aspects of Timber Seasoning. MS Thesis. Univ. of Tasmania Research Report 81/1.

82. Schniewind, A. 1968. Recent Progress in the Study of the Rheology of Wood. Wood Science and Technology. V. 2 Pp188-206.

83. Skaar, C. 1954. Analysis of the Methods for Determining the Coefficient of Moisture Diffusion in Wood. Journal of the Forest Products Research Society, Dec., Pp. 403-410.

84. ------, --. 1972. Water in Wood. Syracuse University Press, Syracuse.

85. ------, W. Simpson, and R. Honeycutt. 1980. Use of Acoustic Emissions to Identify High Levels of Stress During Oak Lumber Drying. Forest Products Journal 30(2):21-22.

86. Sherwood, T. K. 1929. The Drying of Solids I. Indus. and Eng. Chem. 21:12-16.

87. Siau, J. 1984. Transport Processes in Wood. Springer-Verlag, New York. 245 pp.

88. Sliker, A. 1978. Strain as a Function of Stress, Stress Rate and Time at 90° to the Grain in Sugar Pine. Wood Science 10(4):208-219.

89. Stamm, A. J. 1946. Passage of Liquids, Vapors, and Dissolved Materials through Softwoods. U.S. Dept. Agric. Tech. Bull. No. 929. Washington.

90. ------. 1964. Wood and Cellulose Science. The Ronald Press. New York. 549 pp.

91. Stevens, R. R. 1972. Moisture Movement Above the Fiber Saturation Point in Loblolly Pine Sapwood. Ph.D. Thesis. State University of New York, Syracuse.

92. Szabo, T. and G. Ifju. 1970. Influence of Stress on Creep and Moisture Distribution in Wooden Beams under Sorption Conditions. Wood Science 2(3):159-167.

93. Takemura, T. 1972. On the Memory Effect of Wood During Drying. IV Prediction of Drying Stresses of a Board. M. Gakkaishi 18(3):105-113.

94. Tiemann, H. D. 1919. the Phenomena of Drying Wood. Jour. Franklin Institute. (188):27-50.

95. Torgeson, O. W. 1951. Schedules for the Kiln Drying of Wood. USDA Report FPL-1791. U.S. Department of Agriculture, Madison, WI.

96. Tuttle, F. 1925. A Mathematical Theory of the Drying of Wood. Jour. of the Franklin Institute. 200:609-614.

97. Ugolev, B. N. 1959. Internal Stresses in Wood Caused by Drying. U.S. Dept. of Commerce Clearing House for Federal Scientific and Technical Information.

98. ------. 1976. General Laws of Wood Deformation and Rheological Properties of Hardwoods. Wood Sci. and Technology V. 10 Pp. 169-181.

99. USDA Forest Service, Forest Products Lab. 1987. Wood Handbook. USDA Agric. Handbk.* 72. Madison, WI.

100. Vanek, M. 1987. Kiln Drying Control by Means of Drying Stresses (Different Methods). Abstract of a Paper Presented at the International Conference on Stress Development and Degrade During Wood Drying. Skelleftea, Sweden. Sept. 28 - Oct. 2.

101. Voight, H., O. Krischer and H. Schauss. 1940. Die Feuchtigkeitsbewegung bei der Verdunstrocknung von Holz. Holz als Roh und Werkstoff. 3:305-321.

102. Wengert, E. M. 1977. Some Considerations in Modeling and Measuring Moisture Flow in Wood. Wood Science, 10(1):49-52.

104. Wiley, A. T. and E. T. Choong. 1975. An Analysis of Free Water Flow During Drying in Softwoods. Wood Science 7(4):310-318.

105. Wannier, G. H. 1966. Statistical Physics. Dover, New York.

106. Weller, J. 1987. Die Erfasung von Trocknungsspannungren wahrend der Kammertrockung von Schnittholz. Ph.D. Thesis. Univ. of Hamburg.

107. Wilkes, G. A. 1986. Polymer Structure and Morphology. Notes from a class taken at the Virginia Polytechnic Inst. and State Univ. Blacksburg, VA.

108. Youngs, R. L. 1957. The Perpendicular to Grain Mechanical Properties of Red Oak as Related to Temperature, Moisture Content and Time. USDA Report FPL-2079. U.S. Department of Agriculture, Madison, WI.

109. ------ and C. B. Norris. 1958. A Method of Calculating Internal Stresses in Drying Wood. USDA Report FPL-2133. U.S. Department of Agriculture, Madison, WI.

APPENDIX 1.

This Appendix contains the program for the computerized simulation which calculates stresses which result from drying. The program was written for a Hewlett-Packard 9836 computer.

```
10    ! PROGRAM FICK- CALCULATES THE SOLUTION TO FICK'S SECOND
NK-NICOLSON IMPLICIT FINITE DIFFERENCE METHOD.
20    !  INPUT THE INITIAL VALUES OF THE PARAMETERS
30    INPUT "INPUT THE THICKNESS OF THE BOARD IN INCHES",Th
40    INPUT "INPUT THE GREEN MOISTURE CONTENT (IN PERCENT)",Ugn
50    INPUT "INPUT THE EMC CONDITION",Uemc
60    INPUT "INPUT THE TIME STEP, IN HOURS",Dtau
70    INPUT "INPUT THE NUMBER OF NODES",M
80    INPUT "INPUT THE RH OF THE AMBIENT",Rh
90    Th=1.5
100 ! Ugn=90
110 ! Uemc=10
120 ! Dtau=12
130   Dtau=3600*Dtau
140 ! M=4
150   ALLOCATE A(M-1,M-1),Ai(M-1,M-1),Ukn(M-1),D(M-1),T(M),U(M)
),Ss(M),Elstr(M),Str(M),Sg(M)  ! SET UP THE MATRICES OF UNKNOWN
160 ! Rh=60
170   Loc=Th/(2*M-1)   ! LOCATION IN SPECIMEN
180   Dx=Th*2.54/(2*M-1)   ! CAL THE X INCREMENT IN CM
190   Ra=Dtau/(Dx*Dx)   ! Ra STANDS FOR RATIO
200   Tau=Dtau     ! SET THE INITIAL TIME
210   FOR I=0 TO M-1      ! INITIALIZE MOISTURE MATRIX
220   U(I)=Ugn
230   NEXT I
240   PRINT " POSIT    MC      STRESS   TIME (HRS)    SET
 FAIL"
250   U(M)=Uemc     ! SET UPPER BDY CONDITION
260   !*******************************************************
270   !*
280   !*               CALCULATE THE TRANSPORT COEFFICIENTS
290   !*
300   !*******************************************************
310   FOR I=0 TO M-1
320   !******* RH>75******************
330 ! ***************************
340   IF Rh>75 THEN T(I)=(.756*10^(-5)*U(I)^3-.00054*U(I)^2+.02
6)  ! COMBINED D FROM ALL TESTS
350 ! **************RH FROM 45 TO 75**************************
360 !*******************************************************
370   IF Rh>45 AND Rh<74.99 THEN T(I)=2.8*(.756*10^(-5)*U(I)^3-
*U(I)+.84)/(1*10^6)  ! COMBINED D  FROM ALL TESTS WITH MOD.
380 ! IF Rh>45 AND Rh<74.999 THEN T(I)=2.5*(1.12+.003*U(I)-.000
U(I)^3)/1.E+6   ! D FROM THE 60% RH TESTS
390 !****************** RH < 45*****************************
```

```
400 !*****************************************************
410   IF Rh<44.99 THEN T(I)=3*(.756*10^(-5)*U(I)^3-.00054*U(I)^
1*10^6)     ! COMBINED D  FROM ALL TESTS
420 ! IF Rh<44.99 THEN T(I)=3.0*(1.278-.017*U(I)+1.58E-3*U(I)^2
1.E+6  ! D DETERMINED FROM RH VS MC CURVE AT 35% RH
440   NEXT I
450   !********* SURFACE TRANSPORT COEFFICIENTS***************
460   !*****************************************************
470   !*****************************************************
480   IF Rh>75 THEN T(M)=(.756*10^(-5)*Uemc^3-.00054*Uemc^2+.02
6)   ! COMBINED D  FOR SURFACE
490   !************SURFACE 45 TO 75 % RH*********************
500   !*****************************************************
510   IF Rh>45 AND Rh<74.99 THEN T(M)=5.9*(.756*10^(-5)*Uemc^3-
*Uemc+.84)/(1*10^6)    ! COMBINED D  FOR SURFACE
520 ! IF Rh>45 AND Rh<74.999 THEN T(M)=5.3*(1.12+.003*Uemc-.000
Uemc^3)/1.E+6   ! SURFACE D FROM THE 60% RH TESTS
530 !************* SURFACE < 45% RH************************
540 !***********************************************
550 ! IF Rh<44.99 THEN T(M)=9*(.756*10^(-5)*Uemc^3-.00054*Uemc^
1*10^6)     ! COMBINED D  FOR SURFACE
560   IF Rh<44.99 THEN T(M)=11*(1.278-.017*Uemc+1.58E-3*Uemc^2-
.E+6
590 ! *****************************************************
600 ! ******************SET UP RHS MATRIX *****************
610    FOR I=1 TO M-1
620   S=2*(T(I-1)*T(I))/(T(I-1)+T(I))  ! S AND B ARE THE HARMON
630   B=2*(T(I)*T(I+1))/(T(I)+T(I+1))
640    D(I)=Ra*S*U(I-1)+U(I)*(2-Ra*S-Ra*B)+Ra*B*U(I+1)
650    D(0)=Ra*U(1)*2*B+U(0)*(2-2*Ra*B) ! INNERMOST NODE
660    NEXT I
670  ! ********* SET UP THE LHS COEFFICIENT MATRIX  A(I,J)****
680   FOR I=1 TO M-1
690   FOR J=1 TO M-1
700   S=2*(T(I-1)*T(I))/(T(I-1)+T(I))  ! S AND B ARE THE HARMON
710   B=2*(T(I+1)*T(I))/(T(I+1)+T(I))  ! S AND B ARE THE HARMON
720   IF J=I THEN A(I,J)=2+Ra*S+Ra*B  ! MAIN DIAGONAL
730   IF J=I-1 THEN A(I,J)=-Ra*S
740   IF J=I+1 THEN A(I,J)=-Ra*B
750   NEXT J
760   NEXT I
770   A(0,0)=2*(1+Ra*B)  ! SPECIAL COEFFICIENTS FOR THE BOUNDAR
780   A(0,1)=-Ra*2*B
790   A(1,0)=-Ra*(T(0)+T(1))/2
870   !***********************************************
```

```
880   ! ********INVERT MATRIX A AND MULTIPLY IT BY D**********
890   ! ****THESE OPERATIONS DETERMINE THE NEW MC VALUES ******
900   MAT Ai= INV(A)
910   MAT Ukn= Ai*D
920   FOR I=0 TO M-1
930   Ukn(I)=DROUND(Ukn(I),4)   !  REDUCE THE NUMBER OF DIGITS
940   NEXT I
1020 ! ***** PUT NEW VALUES INTO THE MOISTURE MATRIX*********
1030 ! *********THEN DISPLAY THE NEW VALUES***************
1040  FOR I=0 TO M-1
1050  U(I)=DROUND(Ukn(I),4)
1060  NEXT I
1140  !**********************MODULUS CALCULATIONS**************
1150  ! THE CALCULATIONS ASSUME A 1.5 PERCENT CHANGE FOR EACH 0
 IN MC BELOW 40% MC
1160  Eg=8.67E+4  ! GREEN MODULUS VALUE
1170  FOR I=0 TO M
1180  IF U(I)>40 THEN E(I)=Eg
1190  IF U(I)<39.99 THEN E(I)=Eg*(1+(40-U(I))/100*1.5)
1200  IF U(I)>32 THEN Eset(I)=E(G)/.6*.00112  ! MODULUS FOR SET
1210  IF U(I)<32 THEN Eset(I)=E(I)/.6*.00112    ! MODULUS FOR S
1240  NEXT I
1250  ! ***************** CALCULATE THE SET STRAIN**************
1260  !*********************************************************
1270  FOR I=0 TO M
1280  IF U(I)>32. THEN Ss(I)=.026
1290  IF U(I)<32. AND U(I)>18. THEN Ss(I)=.066-.00112*U(I)
1300  IF U(I)<17.999 THEN Ss(I)=.088-.00332*U(I)
1310! IF U(I)<31.999 THEN Ss(I)=.084-.003*U(I)+.48*10^(-4)*(U(I
ION FOR RH OF < 45%
1330  NEXT I
1350  !***************** CALCULATE THE ELASTIC STRAIN*************
1360  !*********************************************************
1370  FOR I=0 TO M
1400  IF Rh>65 THEN Elstr(I)=.0128+1.76E-3*I*.335/(M)-1.13E-5*T
(I)-.0974*Ss(I)
1430  IF Rh<64.999 AND Rh>45.001 THEN Elstr(I)=.00628-7.34E-3*(
6E-6*Tau/3600-3.89E-5*U(I)-5.69E-2*Ss(I)
1440  IF Rh<45. THEN Elstr(I)=7.7E-3-1.07E-2*(M-I)*.335/M+2.52E
-5*U(I)-.102*Ss(I)
1460  NEXT I
1480  !************************** CALCULATE THE STRESS*********
1490  !*********************************************************
1500  FOR I=0 TO M-1
1520  IF Elstr(I)>0 THEN Str(I)=Elstr(I)*E(I)-Eset(I)*Ss(I)
```

```
1530  IF Elstr(I)<0 THEN Str(I)=Elstr(I)*E(I)+Eset(I)*Ss(I)
1540  PRINT I,U(I),DROUND(Str(I),4),Tau,DROUND(Ss(I),3),DROUND(
D((M-I)*Loc,3),"< 10 "
1550  NEXT I
1560   PAUSE
1570 !******INCREMENT THE TIME***********
1580   Tau=Tau+Dtau
1590  GOTO 250
1600   END
```

The vita has been removed from the scanned document